METEOR Berichte 06

Mid-Atlantic Expedition 2006

Cruise No. 68, Leg 1

Fluid geochemistry, biology and geological setting of hydrothermal systems at the southern MAR (4°S - 10°S) (MAR-SÜD III)

27 April – 2 June 2006, Bridgetown (Barbados) – Recife (Brazil)

A. Koschinsky, A. Billings, C. Devey, N. Dubilier, A. Duester, D. Edge, D. Garbe-Schönberg, C. German, O. Giere, R. Keir, K. Lackschewitz, H.A. Mai, H. Marbler, J. Mawick, B. Melchert, C. Mertens, W.-T. Ochsenhirt, M. Peters, S. Sander, O. Schmale, W. Schmidt, R. Seifert, C. Seiter, U. Stöber, I. Suck, M. Walter, S. Weber, D. Yoerger, M. Zarrouk, F. Zielinski

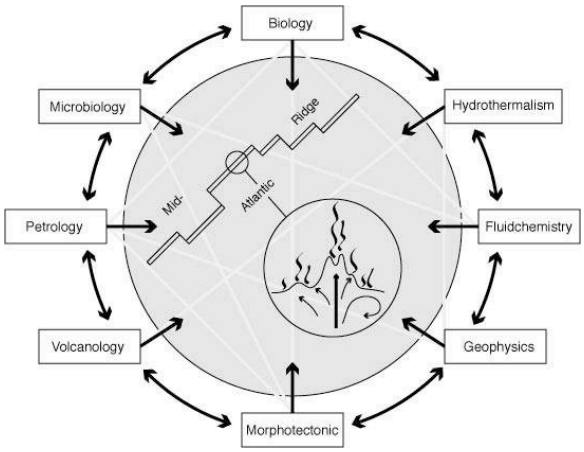

Project Leader: Andrea Koschinsky

Leitstelle Meteor
Institut für Meereskunde der Universität Hamburg

2006

Content

Summary of Cruise M68/1 (April 27 – June 2, 2006)

Following the investigations performed during previous cruises, the goal of cruise M68/1 was to continue the detailed interdisciplinary work at the selected hydrothermal vent sites on the southern Mid-Atlantic Ridge (MAR). This included mapping and exploration for additional hydrothermal vent systems using CTD and the AUV ABE (WHOI), estimating hydrothermal fluxes of heat and chemical compounds, and sampling of hydrothermal vent fluids, associated vent fauna, host rock and sulfide samples using the ROV Quest (MARUM). The three target areas are the following:

(1) 5°S, where two hot vent fields (Turtle Pits and Red Lion) and a diffuse-flow mussel field (Wideawake) had been found and sampled in 2005 (cruises CD169 and M64/1),
(2) 8°S (Nibelungen) where a hydrothermal plume had been detected during cruise M62/5 in 2004, but the hydrothermal source had not been found,
(3) 9°S where a diffuse vent field with young mussel populations named Lilliput was located during cruise M64/1.

In the 5°S area, all known vent fields were revisited and sampled for comparison with the 2005 data. The young, post-eruptive vent field at Turtle Pits was still extremely hot, and the highest temperature ever measured so far in a hydrothermal fluid (407°C) was recorded. Based on the AUV dives, another field was detected (Comfortless Cove), located between Turtle Pits and Red Lion, with the hot smoker "Sisters Peak" (399°C) and two diffuse vent sites, one of them ("Golden Valley") showing very high mussel coverage.

In the 9°S area the AUV detected signals for several hydrothermally active sites, one of them being the known Lilliput mussel field at 9°33'S. The other sites were also all low-temperature sites with diffuse flow and populations with young mussels. This field is driven by volcanic activity, as the 5°S area, and many lava flow structures were observed. At one site, lava columns and hollow lava structures had formed in a former lava lake.

In the Nibelungen field at 8°18'S, a very complex current pattern complicated the search for the source of the extensive plume, which changed its intensity and location on short time scales. Finally, the AUV and ROV dives detected a large smoking crater resembling the craters observed in the Logatchev field at 15°N, which we named "Drachenschlund". Many extinct smokers were found in the vicinity, but no other hot vent field. The fluid chemistry clearly indicates reactions with mantle rocks, similar to the Logatchev field. The absence of hydrothermal fauna around the crater was striking.

In summary, seven new vent fields could be located and sampled during cruise M68/1, which was possible due to the very effective combination of CTD, AUV and ROV deployments. Further indications for hydrothermal activity at 5°S, 8°10'S and 7°57'S could not be followed up due to time constraints. Generally, the fauna at the 5°S and 9°S sites resembles the fauna from the northern MAR biogeographic province and is dominated by high abundances of the mussel Bathymodiolus and shrimps.

Zusammenfassung der Fahrt M68/1 (27. April – 2. Juni 2006)

Im Anschluss an Untersuchungen vorangegangener Fahrten war das Ziel der Forschungsfahrt M68/1 die Fortsetzung der detaillierten interdisziplinären Arbeiten an ausgewählten hydrothermalen Feldern des südlichen Mittelatlantischen Rückens (MAR). Dies beinhaltete Kartierungen, die Exploration weiterer Hydrothermalsystems mittels Einsatz von CTD und dem AUV (WHOI), die Abschätzung hydrothermaler Flüsse von Wärme und chemischen Komponenten, und die Beprobung von Hydrothermalfluiden, assoziierter Vent-Fauna, Wirtsgesteinen und Sulfiden mit Hilfe des ROV Quest (MARUM). Die drei Zielgebiete waren die folgenden:

(4) 5°S, wo zwei heiße Ventfelder (Turtle Pits und Red Lion) und ein Muschelfeld mit diffusem Fluidfluss (Wideawake) in 2005 gefunden und beprobt wurden (Fahrten CD169 und M64/1),
(5) 8°S (Nibelungen), wo eine hydrothermale Wolke in der Wassersäule während der Fahrt M62/5 in 2004 lokalisiert wurde, aber die hydrothermale Quelle am Meeresboden nicht gefunden werden konnte,
(6) 9°S, wo ein diffuses Fluidfeld mit jungen Muschelpopulationen (genannt Lilliput) während der Fahrt M64/1 entdeckt wurde.

In dem Gebiet bei 5°S wurden alle bekannten Felder wieder kartiert und beprobt zum Vergleich mit den Daten aus 2005. Das junge post-eruptive Feld Turtle Pits war noch immer extrem heiß, und die höchsten jemals in einem Ventfluid gemessenen Temperaturen wurden aufgezeichnet (407°C). Auf der Basis der AUV-Tauchgänge wurde ein weiteres Feld zwischen Turtle Pits und Red Lion entdeckt (Comfortless Cove), das einen heißen Smoker (Sisters Peak, 399°C) und zwei diffuse aktive Stellen beinhaltet, wobei ein diffuses Feld (Golden Valley) durch extrem hohe Muscheldichten auffiel.

Im Gebiet bei 9°S zeichnete das AUV Signale für verschiedene hydrothermal aktive Bereiche auf, von denen eines das bekannte Lilliput-Feld bei 9°33'S war. Alle anderen Stellen zeigten sich ebenfalls als niedrigtemperierte Systeme mit diffusem Fluidfluß und Populationen mit jungen Muschen. Dieses Gebiet ist ebenso wie das bei 5°S durch vulkanische Aktivität angetrieben, und zahlreiche Lavafluss-Strukturen wurden beobachtet. An einer Stelle zeigten Lavasäulen und hohle Lavagewölbestrukturen einen ehemaligen Lavasee auf.

Im Nibelungen-Feld bei 8°18'S erschwerten sehr komplexe Strömungsverhältnisse die Suche nach der Quelle der ausgedehnten Wolke in der Wassersäule, welche ihre Intensität und Lage in kurzen Zeitabständen veränderte. Auf der Basis der Daten der AUV-Tauchgänge konnte schließlich während eines ROV-Tauchgangs ein tiefer großer rauchender Krater (genannt „Drachenschlund") lokalisiert werden, ähnlich der rauchenden Krater im Logatchev-Feld bei 15°N. Viele erloschene Schornsteine charakterisieren die Umgebung, aber kein anderer heißer Vent wurde gefunden. Die Fluidchemie zeigt deutlich Reaktionen mit Mantelgeesteinen an, was wiederum die Ähnlichkeit mit dem Logatchev-Feld bestätigte. Auffällig war das Fehlen jeglicher hydrothermaler Fauna in der Umgebung des Kraters.

Zusammengefaßt wurden während der Forschungsfahrt M68/1 zusätzlich zu den bekannten Feldern sieben neue hydrothermal aktive Stellen im Bereich 5-9°S lokalisiert und

beprobt. Diese erfolgreiche Exploration war möglich durch die sehr effektive Kombination von CTD-, AUV- und ROV-Einsätzen. Weiteren Anzeichen für hydrothermale Aktivität bei 5°S, 8°10'S und 7°57'S konnte aus Zeitgründen nicht weiter nachgegangen werden. Generell lässt sich sagen, dass die Fauna in den Feldern bei 5°S und 9°S den Faunenverbreitungen am nördlichen MAR ähnelt und dominiert wird durch die hohe Anzahl an Bathymodiulus-Muscheln und Garnelen.

1.1 Participants

Name	Discipline	Institution
Koschinsky, Andrea, Prof. Dr.	*Chief Scientist*	IUB
Billings, Andrew	AUV	WHOI
Devey, Colin, Prof. Dr.	Geology, Petrology	IFM-GEOMAR
Dubilier, Nicole, Dr.	Hydrothermal Symbioses	MPI Bremen
Duester, Alan	AUV	WHOI
Edge, David	ROV	NOC
Garbe-Schönberg, Dieter, Dr.	Fluid Chemistry	Univ. Kiel
German, Chris, Dr.	AUV, photo mapping	WHOI
Giere, Olav, Prof. Dr.	Zoology	MPI Bremen
Keir, Robin, Dr.	Gases (Methane)	IFM-GEOMAR
Lackschewitz, Klas, Dr.	Documentation ROV	IFM-GEOMAR
Mai Hoang, Anh	ROV	MARUM
Marbler, Herwig, Dr.	ROV	IUB
Mawick, Jule	Fluid Chemistry	IUB
Melchert, Bernd	Bathymetry	IFM-GEOMAR
Mertens, Christian, Dr.	Physical Oceanography	Univ. Bremen
Peters, Marc	Sulfur Isotopes	Univ. Münster
Sander, Sylvia, Dr.	Fluid Chemistry	IUB/Univ. Otago
Schmale, Oliver	Gases (Methane)	IFM-GEOMAR
Schmidt, Werner	ROV	MARUM
Seifert, Richard, Dr.	Gases (Hydrogen)	Univ. Hamburg
Seiter, Christian	ROV	MARUM
Stöber, Uwe	Physical Oceanography	Univ. Bremen
Suck, Inken	ROV	MARUM/Fielax
Walter, Maren, Dr.	Physical Oceanography	Univ. Bremen
Weber, Stefan	Gases (Hydrogern)	Univ. Hamburg
Yoerger, Dana, Dr.	AUV	WHOI
Zarrouk, Marcel	ROV	MARUM
Zielinski, Frank	Hydrothermal Symbioses	MPI Bremen
Ochsenhirt, Wolf-Thilo	Weather Technique	DWD

Participating Institutions

International University Bremen IUB
School of Engineering and Science
P.O. Box 752561
D-28725 Bremen, Germany

Max-Planck Institut für Marine Mikrobiologie
Celsiusstr. 1
D-28359 Bremen, Germany

Leibniz-Institut für Meereswissenschaften
IFM-GEOMAR
Wischhofstr. 1-3
D-24148 Kiel, Germany

MARUM Zentrum für Marine Umweltwisenschaften
Universität Bremen
Leobener Str.
D-28359 Bremen, Germany

Christian-Albrechts-Universität Kiel
Institut für Geowissenschaften
Ludewig-Meyn-Str. 10
D-24118 Kiel, Germany

FIELAX GmbH
Schifferstr. 10-14
D-27568 Bremerhaven

Universität Hamburg
Institut für Biogeochemie und Meereschemie
Bundesstr. 55
D-20146 Hamburg, Germany

Woods Hole Oceanographic Institution WHOI
Woods Hole, MA 02543-1050
USA

Universität Bremen
Institut für Umweltphysik
PF 330440
D-28334 Bremen, Germany

University of Otago
Department of Chemistry
P.O. Box 56
Dunedin, New Zealand

National Oceanography Centre NOC
European Way
Southampton SOI 4 3ZH
United Kingdom

Westfälische Wilhelms-Universität Münster
Geologisch-Paläontologisches Institut
Corrensstr. 24
D-48149 Münster, Germany

1.2 Research Program

Following the investigations performed during and subsequent to cruises M62/5, CD169 and M64/1 it was of prime importance during cruise M68/1 to continue the detailed interdisciplinary work at the selected vent sites on the southern Mid-Atlantic Ridge (MAR). This includes mapping and exploration for additional hydrothermal vent systems on a regional scale and sampling of hydrothermal vent fluids, associated vent fauna (both macro- and microbiology), host rock and sulphide samples.

Our goals were:

(1) Locating and characterising the vents for the 4°48'S, 8°10´S, 8°18´S and 9°33´S hydrothermal plumes (Fig. 1), where the hot vent sources have not yet been found;
(2) Quantifying the hydrothermal fluxes (heat, gases, metals) and the role of mixing for plume dispersal and distribution of hydrothermal fluids and gases;
(3) Assessing the origin and dispersal of vent fauna and variability of the communities linked to the physico-geochemical environment;
(4) Determining the factors controlling the composition and temporal variability of hydrothermal fluids and the microbial communities they support.

The work plan included detection and mapping of the hydrothermal plumes by CTD and turbidity sensors and localization of the hydrothermal emanation sources using the AUV ABE (WHOI). ABE dives consisted of three phases, first looking for the largest hydrothermal signal in the neutrally buoyant plume, then searching for the interception of the rising plume, and in the third phase a detailed sensor and photo mapping of the active area was carried out.

Bathymetric mapping was carried out with the multibeam system of RV Meteor, and high-resolution mapping of the AUV. The ROV Quest (MARUM, Univ. Bremen) was deployed in parallel and subsequent to the AUV discoveries in the known and newly discovered fields to sample rocks, sulfides, fluids and animals. Sample recoveries were complemented by onboard measurements of chemical compounds in the fluids, microbial experiments, and preparation of animal samples.

1.3 Narrative of the Cruise

(A. Koschinsky)

Cruise M68/1 began at 09:00 a.m. on April 27, sailing from Bridgetown, Barbados. The transit to the first working area at 5°S on the Mid-Atlantic Ridge (MAR) took 12 ½ days, due to strong head-wind and swell. The long transit time was being used by the interdisciplinary scientific team, composed of geologists, oceanographers, geochemists and biologists, supported by the technical teams of the ROV Quest (MARUM, Univ. Bremen) and the AUV ABE (Woods Hole Oceanographic Institution) to equip the labs and coordinate its activities. Besides the preparations for the deployment of the equipment, the transit time was also a much-appreciated opportunity for a scientific exchange between the different working groups and disciplines. We carried out a little hydrothermalism workshop covering four afternoons, during which scientists presented the background of their work. In addition, the ROV and AUV teams provided us with a detailed insight into how the equipment functions and the possibilities that their devices offer.

On the way to our first working area close to 5°S, 12°W we released so-called ARGO-Floats, which we were asked to deploy by NOAA in Miami, at 45°W, 40°W and 35°W. When the weather improved we tested several pieces of equipment. An ROV test dive to 1000m worked perfectly and a CTD deployment to 100m too. As this was the first time that the Autonomous Underwater Vehicle (AUV) „ABE“ was on board Meteor, the crew practiced deployment with the crane and, after a short manoeuvre on the surface, recovery of the vehicle.

During the night of May 9/10 we finally arrived in our first working area at 5°S, first deploying three transponders as preparation for the first dive of the AUV ABE, which followed immediately after a CTD station. A complete AUV survey for the exploration of hydrothermal vents consists of three phases. During phase 1, the wide head of the hydrothermal plume is mapped on a larger scale (at 200-300 m above the seafloor), using the CTD, redox and turbidity sensor data to locate the center of the hydrothermal plume. In Phase 2, based on the data from phase 1, the seafloor is mapped at high resolution from 50 m above the seafloor with a survey line spacing which should allow the rising stem of the plume to be intercepted. As the rising plume has a limited width, this information already enables a good location of the active vent site. In the 3rd phase, a photo survey of a limited area directly around the rising stem is carried out from 5 m above the seafloor, providing information about the smoker structures and faunal abundances. This information can then be used to prepare a ROV dive in detail. With this combination of the two devices, which can be deployed in parallel, we achieved an optimum use of the ROV and precious ship time.

The first AUV dive covered the vent fields Turtle Pits, Red Lion and Wideawake, known from the cruises CD-169 and M64/1 in 2005, and also included sites southwest and east of these fields, where we had detected hydrothermal signals in the water column last year. In parallel, the first ROV dive in the Wideawake mussel field and the Turtle Pits hot vent field started in the morning of May 10. After a total dive time of 12 hours without technical problems, the ROV brought mussel samples, hot fluids and rock samples on board. The nights were also filled with intense hydrographic investigations of the area to gain more information about how the hydrothermal plumes are spreading in the water column and hence about the regional input of hydrothermal material to the oceans. Numerous plume signals at different sites were recorded. In the morning of May 11 the ROV started its second dive, targeted at the Red Lion field with its four very different smokers.

With the ROV working perfectly, May 12th saw the 3rd dive in a row to finish the program in Wideawake and Turtle Pits. Besides the successful search for the rare Calyptogena clam, the largest success of this dive was the measurement of the hottest vent fluid found so far, with 407°C, at the Turtle Pits vent. Sampling of rocks with the ROV was complemented by three volcanite wax corer stations.

While the ROV was still finishing sampling in the known vent fields at 5°S, the AUV ABE had already found several new locations with indications of hydrothermal input in an area between the hot vent fields Turtle Pits and Red Lion, and at other sites displaying anomalies in turbidity, temperature and redox potential. Additionally, the photo mapping with ABE had recorded clear indications of hydrothermalism. During the 4th dive of the ROV on May 14 we found a 12 meter-high chimney emanating 399°C hot fluid and black smoke. The site was called “Sisters Peak”. The ROV continued its way according to the data of the AUV dive evaluation and in the afternoon it reached a fissure with intense colonization of mussels and other animals,

which we named "Golden Valley". In the evening, the ROV reached the 3rd hydrothermally active site, which was characterized by high turbidity of the water ("Foggy Corner") – probably caused by bacteria. This new locations became the starting point for ROV dive no. 5 the following morning. It is also a low-temperature diffuse source, however it differs in its appearance and colonization from the previously discovered mussel valley, which was also revisited to sample mussels and fluids. The remaining time was dedicated to the hot smoker Sister Peaks.

As further work in the 5°S area, a number of CTD stations were carried out. North and south of the 5°S area 2 hydrographic profiles were carried out (CTD/LADCP/130 He samples). For the purpose of long-term observation of the background current and for the precise determination of tidal amplitudes and phases, a current meter mooring was deployed in the area, which will remain there for one year. Deploying the CTD/MAPR combination from a drifting ship (Tow-yo) produced 3 high-resolution transects of temperature anomalies and turbidity both along and across the axis of the valley. Plume anomalies were detected in several density layers and could partly be assigned to the known vent fields. Several weaker signals lie south of the known vents and indicate the presence of further (possibly diffuse) hydrothermal sources.

After 6 very successful working days we had a transit of 25 hours to the next target area at 9°33'S. This site is much shallower (1500 m) than the 3000 m deep sites at 5°S. A diffuse hydrothermal field, which was called Lilliput during its discovery cruise M64/1 in 2005 because of the high abundance of very young mussel populations, was already known. Four dredges and one wax corer station retrieved volcanic rock from this area. While the AUV was searching for signals of active hydrothermal venting around the Lilliput field, the ROV had to stay on deck for a day. A complicated problem in the winch for the A-frame made a deployment of the ROV impossible. After the repair, the ROV descended immediately at 5 p.m. on May 18 for its 6th dive. This dive started in a diffuse site that we had observed during an OFOS track in 2005 and continued over a bizarre underwater landscape consisting of lava pillars, lava domes and wide caves (we called the place "Roman City") and finally led us to a diffuse-flow mussel field ("Limtoc") just south of the Main Lilliput site. The photo mapping and sensor records of the AUV 5 m above the seafloor revealed further strong signals of hydrothermal activity, which were followed on May 19 during the 7th ROV dive. Besides the known Main Lilliput site, more diffuse active emanation sites north of Lilliput were discovered and sampled. In addition to the common mussels, shrimps and crabs, also dense accumulations of hydrozoans (giving the site the name "Candelabrum Meadow"), gorgonians and some tube-forming worms could be observed. Even though we did not find any high-temperature field in the area at 9°33' S, which had been expected based on a clear anomaly of gases and metals about 300-400 m above the seafloor, we could still consider this leg of the expedition with its diverse occurrences of widespread low-temperature hydrothermal activity very successful.

After 7 hours of transit from the Lilliput area to the Nibelungen field at 8°18'S the first station on May 19 was a CTD station destined to confirm the hydrothermal plume that was found here during cruise M62/5 in December 2004. This area, which had already been investigated during this former cruise with extensive CTD work and ROV deployments, is characterized by very complex current patterns and temporal variability of the location and intensity of the hydrothermal plume. Therefore, it had not been possible to detect the exact location of the vent site and the whole area had been named "Cheating Bay". The CTD station data could

immediately confirm the existence of the plume at the expected water depth 300 m above the seafloor, and the coordinates for the first dive of AUV ABE could be set. The third AUV dive finally revealed the source of the plume: a black smoker in a large field of otherwise dead chimneys. Two CTD tow-yo tracks confirmed the strong temporal variability of plume dispersion in Cheating Bay: during one station, the plume signal was clearly visible east of the now known position of the source, another time west of it.

Now that the location of the Nibelungen field was identified, the increasing winds and strong swell made the deployment of the ROV impossible. Finally on May 24 the weather had improved. After only 20 minutes on the bottom Quest had already found the source of the strong redox, temperature and turbidity anomalies that ABE had located: “Drachenschlund” (Dragon Throat). This vent does not represent a chimney structure, but is a four meter deep crater with a diameter of about half a meter, from which an enormous volume of black smoke emanates at high velocity. This made sampling of the fluids and temperature measurements very difficult, but still shipboard analysis of the fluid samples gained above the crater throat could immediately prove to us that Nibelungen is a vent influenced by serpentinization processes. In addition, a few serpentinized breccias could be sampled at the crater wall of Drachenschlund during the ROV dives. In contrast, 1 dredge and 5 volcanite wax have sampled only basaltic rocks and glass fragments.

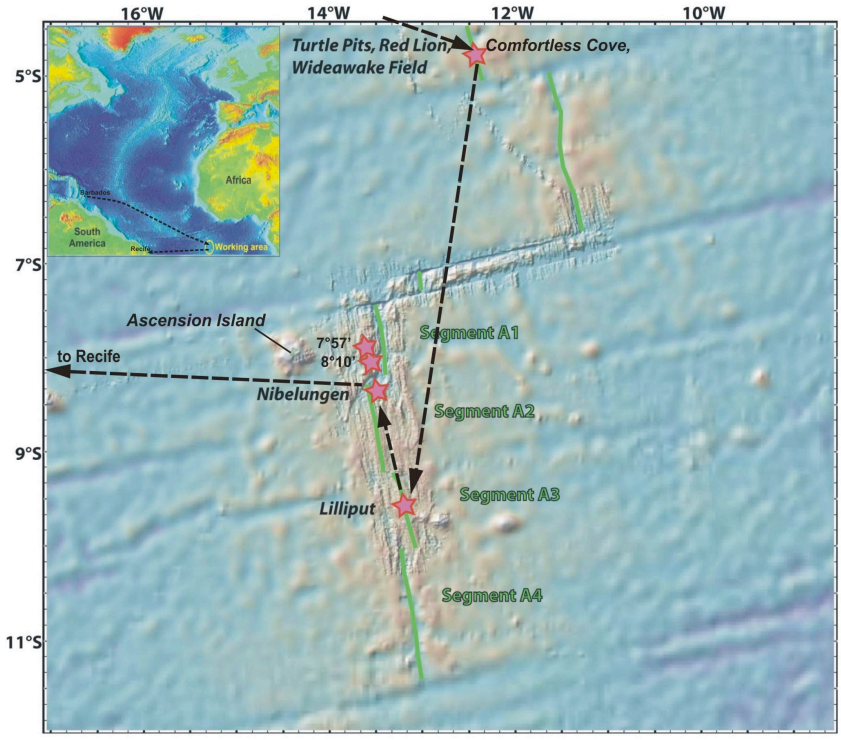

Fig. 1.1: Cruise track and working areas of cruise M68/1.

As the ROV was only deployed again after the location of the Nibelungen field was known, the intermediate time was used by a CTD tow-yo and one dredge for preparing another target area at 7°57’S for AUV dives. This area in the A1 segment close to Ascension had shown turbidity and temperature anomalies during CTD stations and TOBI sidescan sonar deployments of former cruises. These anomalies apparently originated from terrace structures at the western

rift valley, close to the center of the segment – a geological situation similar to the Logatchev field at 15°N on the MAR. The Tow-yo data of the oceanography team could indeed identify a distinct plume with its maximum turbidity anomaly lying directly above terraces cut into the valley walls. The AUV dive phase 1 localized the hydrothermal signals, whereas a dredge along the slope recovered hydrothermal breccia, so that the 2nd dive phase of ABE could be prepared. However, as this dive did not result in the clear localization of the hydrothermal source, as we had hoped for, we stopped work in this area for the rest of this cruise, because station work time was coming to its end and a further search did not appear useful. Instead, the station work was finished with a dredge in the Nibelungen field, a CTD station at 8°10'S and an ROV dive in the Lilliput mussel field at 9°33'S, where again mussels were recovered for experiments with the symbiotic bacteria and where fluid and lava samples were taken from the area with the lava columns.

1.4 Preliminary Results

1.4.1 Geology of the Working Area

A general description of the geologic situation of the working areas was given in the cruise reports of the former cruises M62/5 and M64/1. More detailed information on geologic features of the areas at 5°S, 8°S, and 9°S is given in chapter 1.4.3.2 "Description of the ROV dives" of this report.

1.4.2 AUV Dives

1.4.2.1 Technical Description of the AUV

(C. German, D. Yoerger, A. Billings, A. Duester)

Overview

The *Autonomous Benthic Explorer* (*ABE*) is a fully autonomous underwater vehicle used for exploring the deep ocean up to depths of 4500 meters. *ABE* produces bathymetric and magnetic maps of the seafloor and has also been used for near-seabed oceanographic investigations, to quantify hydrothermal vent fluxes. Most recently, *ABE* has been used to locate, map, and photograph deep sea vent sites following preliminary work by towed and lowered instruments. *ABE* has taken digital bottom photographs in a variety of deep sea terrains, including the first autonomous surveys of an active hydrothermal vent site. By the end of M68/1, ABE has completed 181 dives in the deep ocean over 16 cruises, covering more than 3000 km of survey tracks at an average survey depth of deeper than 2000 meters.

Vehicle Characteristics

ABE is a three body, open frame vehicle that utilizes glass balls as flotation in two free-flooded upper pods while the single, lower housing is host to the batteries that power the vehicle and all of its electronics. This separation of buoyancy and payload gives a large righting moment which simplifies control and allows the vertical and lateral thrust propellers to be located inside the protected space between the three, faired bodies. ABE has five thrusters allowing it to move in any direction. It can travel forward at a cruising speed of 0.6m/sec but one of ABE's most unique characteristics is that it can also hover and reverse – characteristics that are particularly

valuable in the hostile and rugged terrain routinely encountered when investigating the deep seafloor. The navigation system onboard ABE consists of two proven and complementary navigation systems. For general use, ABE uses long "baseline" transponders, identical to those used by the research submersible *Alvin* and ROV Jason, and these allow deep seafloor surveys over distances of ca.5 kilometers to be carried out. In addition, however, ABE also carries an acoustic doppler velocity log (DVL) which provides short-range, high-precision navigation. With these navigation systems, ABE has the ability to follow tracklines with a repeatability of order 10m line-spacing or better.

Standard Sensors on ABE

The sensors on board ABE consist of a number of vehicle attitude sensors such as depth, altitude, heading, pitch and roll. In addition, ABE carries a suite of dedicated science-specific sensors. These include:

- a SIMRAD SM2000 200kHz multibeam sonar, rated to 3000m
- an Imagenex 675kHz scanning sonar, rated to ≥4500m
- a 3-component Develco fluxgate magnetometer, rated to ≥4500m
- 2 SeaBird 9/11+ CTD systems, rated to ≥4500m
- SeaPoint optical backscatter sensor (OBS) rated to ≥4500m
- a digital still camera imaging system, rated to ≥4500m

NB: for M68/1 an Eh sensor was also interfaced to the AUV through an on-going collaboration between the *ABE* group and Dr Koichi Nakamura (Japan).

All data are stored on the vehicle and retrieved upon recovery.

How ABE Works

ABE operates autonomously from the support research vessel. It has no tether, and is controlled in real-time by onboard computers using its own rechargeable batteries for all power. Upon launch, ABE descends to the seafloor through the use of a descent weight which is released after safe arrival at the seafloor. Throughout any dive, ABE uses acoustic long- baseline transponder navigation together, when close enough to the seafloor, with bottom-lock acoustic doppler measurements to determine its position and velocity over the seabed. ABE descends at 15-20m/minute following a controlled spiral trajectory to ensure that it reaches the desired starting point while consuming minimal energy. After reaching the seafloor and performing a series of checks, ABE releases its descent weight to become neutrally buoyant and begins its pre-programmed survey. A dive can consist of any mix of water column investigations (e.g. hydrothermal plume surveys) at constant water depths, seafloor geophysical investigations at fixed heights above the seafloor (anywhere from 50-200m off depending on the application: e.g. magnetics, high-resolution bathymetric mapping) and digital photography at a height of just 5 meters above the seafloor. ABE usually surveys until either it reaches the end of its programmed survey or its batteries are depleted (typically between 20-30km along track and 15-30 hours of survey time, depending on sensor payload, survey type, and terrain). At the end of its dive, ABE releases two ascent weights to become positively buoyant and return to the surface at 15-20m/minute.

Three Phases of Hydrothermal Exploration

Precise navigation, robust control, and coregistered sensors permit ABE to characterize the seafloor and the near-bottom environment on the meter-scale through complementary sensing modalities. Consequently, three different phases of data acquisition can be used for hydrothermal exploration.

Phase I: non-buoyant plume surveys. Using previously collected MAPR and/or CTD tow-yo data, the ABE vehicle is pre-programmed to fly a survey pattern that traverses the seafloor at a fixed depth (order 200m above the seabed) with ca. 300m line spacing, to map out the core and distribution of a non-buoyant hydrothermal plume (key sensors: CTD, E_h, optical backscatter).

Phase II: seafloor mapping and buoyant-plume interception. Using information from Phase I, a ca. 1km^2 area is chosen for more detailed analysis. This comprises high-resolution multibeam mapping from 50m above the seabed. At this height, 30m-spaced lines also ensure interception of any rising buoyant plumes allowing sources of high-temperature hydrothermal vents to be located (key sensors: Simrad SM2000, CTD, E_h, optical backscatter and vertical displacement of the vehicle by the rising plume).

Phase III: bottom-photography of vents and vent-communities. Once a buoyant plume has been intercepted the source of venting is known to within ±100m. The final phase, therefore, is to conduct systematic photo-mapping of an area order 200m x 200m, at 5m above the seabed, to precisely locate vents and areas of diffuse flow (key sensors: Digital Still Camera, CTD, E_h, optical backscatter and vertical displacement of the vehicle by rising plumes.)

1.4.2.2 First Results of AUV Dives

Overview

During cruise M68/1, ABE was deployed on 11 successful dives in 4 research areas. There were 4 dives at 5°S, 2 dives in the Lilliput Area, 3 dives at Nibelungen and 2 in the centre of the A1 segment near 8°S. A final, 12th, scheduled dive – which would have been a Phase III dive in A1 segment was cancelled to allow time for a last ROV dive at Lilliput at the end of the cruise.

5°S Area

Four dives were completed at 5°S, ABE dives 171-173 were dedicated to exploration for, and location, of new hydrothermal fields. Dive 174 was a time-series repeat photo-survey of the Turtle Pits and Wideawake areas that had first been photo-mosaiced by ABE in March 2005 and had revealed fresh glassy lavas apparently over-flowing already-established Wideawake diffuse-flow vent communities.

ABE 171 Summary:

Launch: 2006/05/10 07:02	Recovery: 2006/05/11 06:16
Survey start: 2006/05/10 11:14	Survey end: 2006/05/11 03:27
Survey distance: 31.70 km	Ave survey depth: 2793 m

ABE171 was a Phase 1 dive. We obtained Eh and backscatter hits at two potentially new sites as well as over Red Lion and Turtle Pits. The dive was planned with the depth alternating on each trackline between 2750 and 2850 meters. For the first block of lines in the west, the vehicle paused during the depth changes, so each line was run at the desired depth. The lines to the east did not include the appropriate pause during the depth change, so the vehicle changed depth over about the first half of each line. Eh signals showed the locations of the Red Lion, Turtle Pits, and Wideawake fields discovered by ABE in 2005 (CD169) as well additional signals which were used to target further ABE missions and successful location of new vent sites found during ABE173.

ABE 172 Summary:

Launch: 2006/05/12 09:14	Recovery: 2006/05/13 01:33
Survey start: 2006/05/12 12:38	Survey end: 2006/05/12 22:28
Survey distance: 16.36 km	Ave survey depth: 2926 m

ABE172 was a Phase 2 dive, originally planned in two blocks. We terminated the dive after the first block. The dive was progressing slower than expected and we determined it would not get to the prime search area in the second block before depleting its batteries. The vehicle started in the SW corner, so it was driving with or against the current. When the vehicle timed out on the first two tracks driving to the SE, it was driving into the current. The current then rotated about 90 degrees, and we saw no more timeouts. Plots of Eh sensor data showed that the only substantial hits were in the SW corner at about the same place where the vehicle timed out on SE-bound tracklines. No T or optical backscatter anomalies accompanied this Eh hits: diffuse flow?

ABE 173 Summary:

Launch: 2006/05/13 15:54	Recovery: 2006/05/14 09:27
Survey start: 2006/05/13 18:49	Survey end: 2006/05/14 06:01
Survey distance: 15.68 km	Ave survey depth: 2961 m

ABE173 did a combined Phase 2 and Phase 3 survey. The dive succeeded in locating three vent sites which were visited later the same day by the ROV. These vents were determined from Eh, optical backscatter, and temperature data. By this measure the dive was extremely successful, but a programming error prevented the SM2000 from running and resulted in the camera quitting early, soon after photographing the black smoker site Sisters Peak. Despite this disappointment, the camera did run through the first several vent sites and gave good pictures showing diffuse flow, mussels, shrimp, and an active black smoker. At least as important was the fact that the water column data were sufficient to accomplish the primary goal of the dive – to guide the ROV to the vent sites. Fig 1.2 shows the Phase 3 (T1) temperature measurements that were used to target all three vents visited by the ROV.

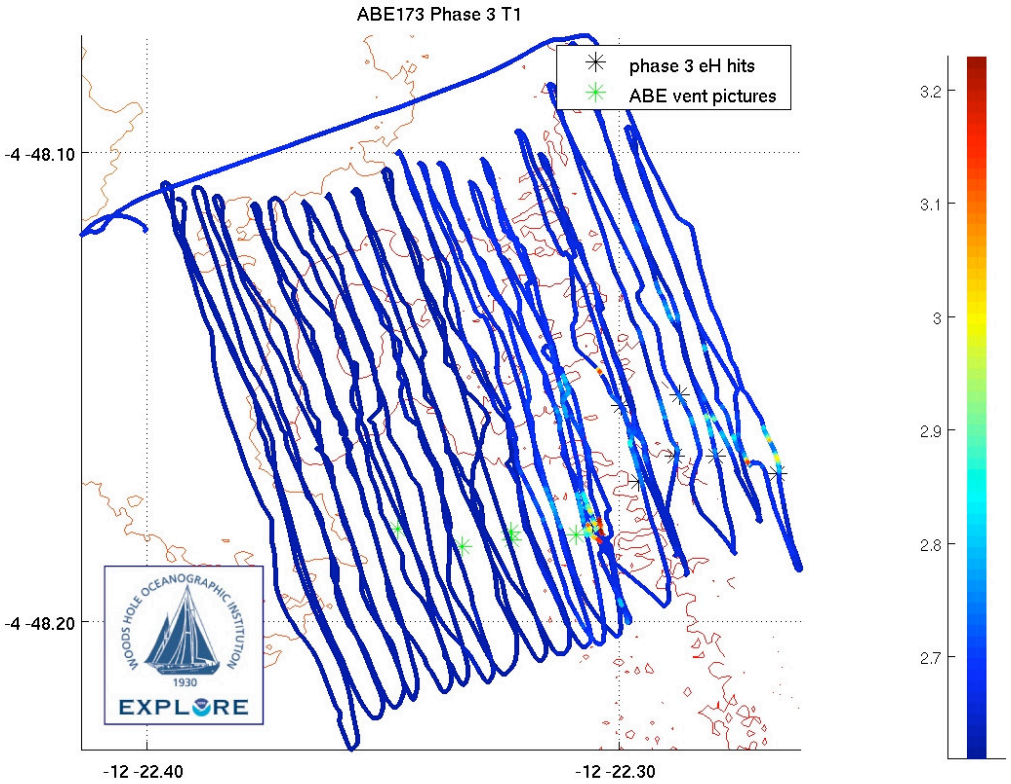

Fig. 1.2: Phase 3 (T1) temperature measurements recorded during the ABE173 dive.

ABE 174 Summary:

Launch: 2006/05/14 23:21	Recovery: 2006/05/15 10:16
Survey start: 2006/05/15 02:04	Survey end: 2006/05/15 07:12
Survey distance: 6.51 km	Ave survey depth: 2966 m

ABE174 was a phase 3 dive designed to repeat the survey we made on ABE154 at the Turtle Pits and Wideawake sites. The dive went well and all 5740 photos were recorded properly. The vehicle had two collisions with structures in Turtle Pits. In addition to the areas covered in ABE154, we also added a block to the east and a cross track block over the initial Wideawake survey area. Fig. 1.3 shows the real-time and post-processed navigation tracks and, hence, the positions from which photo-mosaic images have been obtained.

The Turtle Pits block is to the northwest, the main Wideawake block is in the center, and the extension of the Wideawake survey lies to the east. The vehicle held the 5 meter track spacing fairly well except when flying over the big structures in Turtle Pits. The crooked track in the center of the Turtle Pits block is the line over the big spires. The vehicle made it over the large spire without a collision but collided squarely with the next structure even though the downlooking sensors measured ranges that were too short, and the vehicle was backing off as the collision occurred. Happily, the vehicle suffered no apparent damage, just a large black mark on its nose.

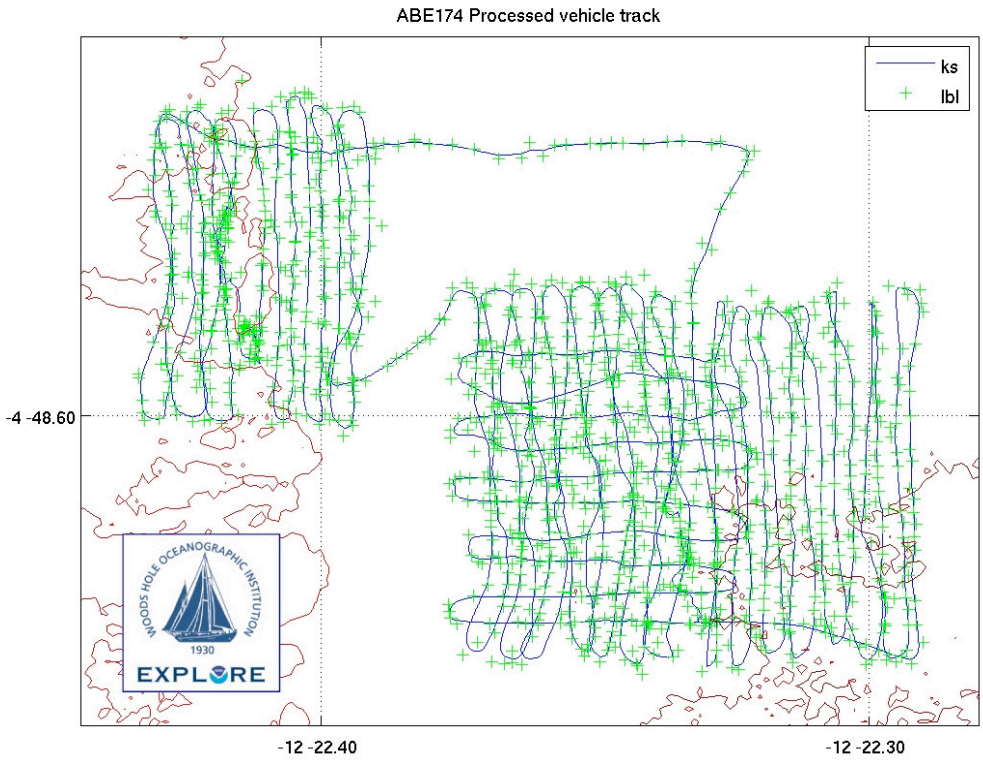

Fig. 1.3: Real-time and post-processed navigation tracks for the ABE174 dive.

Lilliput Area, 9°30'S

Two dives were completed in this area. First, a Phase II dive was conducted to carry out high-resolution bathymetric mapping of the OFOS and Lilliput Sites and to continue exploration and mapping north along the neovolcanic axis. Based on those results a further Phase III dive was chosen which identified a new diffuse flow field "Candelabrum Meadows" and a large extinct hydrothermal deposit in the very NE of our survey.

ABE 175 Summary:

Launch: 2006/05/17 06:55	Recovery: 2006/05/18 02:01
Survey start: 2006/05/17 08:40	Survey end: 2006/05/17 23:49
Survey distance: 28.28 km	Ave survey depth: 1436 m

ABE 175 made a successful phase 2 survey at Lilliput. Fig. 1.4 shows the Eh data for the run superimposed on the new SM2000 bathymetry. At least three solid hits were detected.

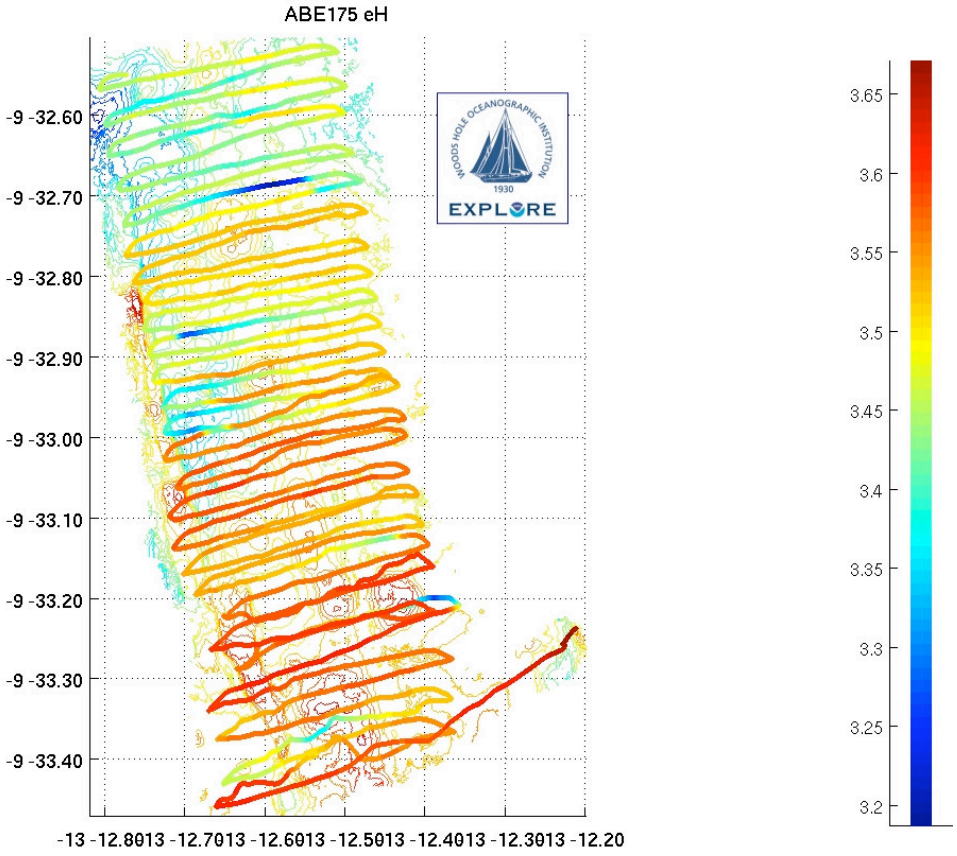

Fig. 1.4: Eh data for the ABE175 run superimposed on the new SM2000 bathymetry.

ABE 176 Summary:

Launch: 2006/05/18 19:50	Recovery: 2006/05/19 07:56
Survey start: 2006/05/18 21:44	Survey end: 2006/05/19 06:15
Survey distance: 9.18 km	Ave survey depth: 1487 m

ABE176 was a phase 3 dive at Lilliput. The vehicle located at least three vent sites. One was marked by strong temperature, Eh, and optical backscatter signals, the other two had much lower signatures but were clearly apparent in bottom photographs. The vehicle took 5000 pictures which showed a variety of vent animals and diffuse flow. The area featured a prominent mound about 25 meters high that was heavily fissured. ABE was able to fly over this feature without a problem. Fig. 1.5 shows the temperature (T1) data, superposed on the SM2000 multibeam bathymetry, that was used to locate, and visit with the ROV, the diffuse flow site “Candelabrum Meadows”. Lesser anomalies in the North East coincide with a large “extinct” hydrothermal field.

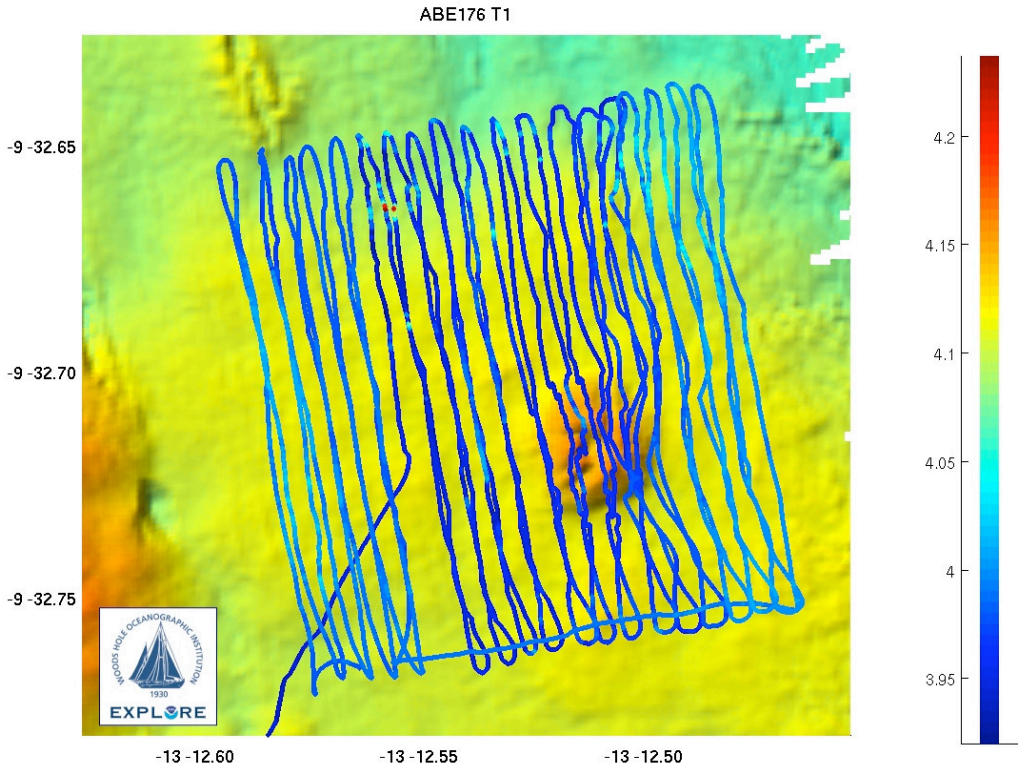

Fig. 1.5: Temperature (T1) data for the ABE176 dive, superposed on the SM2000 multibeam bathymetry.

Nibelungen Area, 8°18'S

Three dives were dedicated to this area to explore for, locate and photograph the new "Drachenschlund" black smoker vent.

ABE 177 Summary:

Launch: 2006/05/20 15:34 Recovery: 2006/05/21 09:52
Survey start: 2006/05/20 20:03 Survey end: 2006/05/21 06:53
Survey distance: 22.34 km Ave survey depth: 2697 m

ABE177 was the Phase 1 dive at the Nibelungen site. The dive was conducted at a constant depth of 2700 meters centred on previously located CTD plume signals. The dive recorded significant Eh anomalies in mid-water toward the centre of our survey but approximately 400m West of where the Drachnschlund vent was eventually detected. In fact, the vehicle flew directly over the vent site while converging onto its connector line after rising to survey height on ABE 177 but saw little indication of the vent.

ABE 178 Summary:

Launch: 2006/05/21 18:45 Recovery: 2006/05/22 15:04

Survey start: 2006/05/21 21:21 Survey end: 2006/05/22 11:29
Survey distance: 21.74 km Ave survey depth: 2844 m

ABE178 was a phase 2 dive at Nibelungen. The dive succeeded in locating the vent, but we were a little lucky. The main survey area showed no substantial hits on Eh, backscatter, or temperature. But on the connector line from the landing spot to the start of the first line, the vehicle got solid hits on all sensors. In hindsight, the survey block should have been moved more to the east. Fig. 1.6 shows the Eh data superimposed on the multibeam bathymetry. Eh, backscatter and temperature all showed strong hits at the very beginning of the survey over the Drachenschlund site.

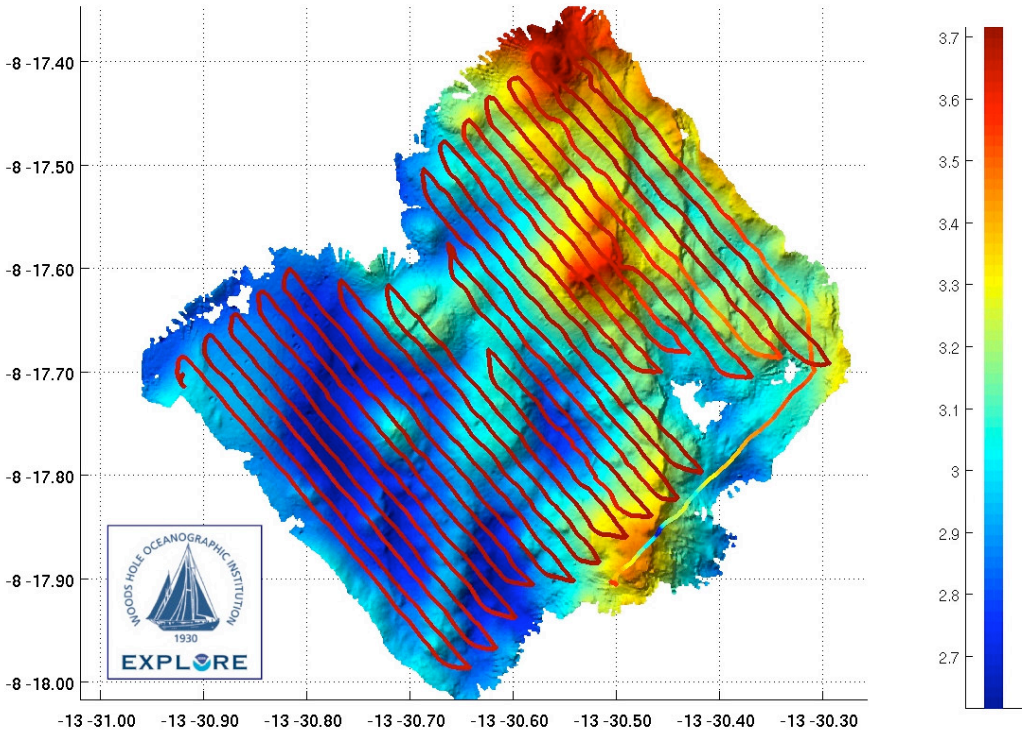

Fig 1.6: Eh data superimposed on the multibeam bathymetry for the ABE178 dive.

ABE 179 Summary:

Launch: 2006/05/22 20:49 Recovery:2006/05/23 10:23
Survey start: 2006/05/23 00:06 Survey end: 2006/05/23 06:58
Survey distance: 3.18 km Ave survey depth: 2860 m

ABE179 was a very successful “truncated” phase 3 survey at Nibelungen. The vehicle passed directly over a black smoker that was named Drachenschlund (Dragon's Throat). The site was very rugged: over 200 meter tracklines the vehicle changed depth by 90 meters on one side of the rise and 40 meters on the other side. The vehicle had trouble when attempting to descend the steep slope on the 2nd through 5th eastbound tracklines. When it reached the sharp drop-off, the vehicle would reduce forward thrust to maintain the proper distance from the seafloor, at which

point the current would force the vehicle back. So the vehicle would get stuck at the cliff edge, confirmed in ABE's photographs. The ROV pilots reported similar problems in attempting to fly down to the east from the crest of the hill.

Fortunately, ABE managed to get over the drop-off on the line that really counted. ABE flew over the edge of the smoker field on the eastbound descending line, then flew directly over the smoker on the return ascent. Fig. 1.7 shows the temperature (T2) data for the run.

There is only one significant hit, directly above the Drachenschlund vent even though Eh and backscatter anomalies were also observed along the cliff-top where the vehicle stalled, to the south west. Although ABE photographed additional extinct chimneys – and more were found with the ROV on subsequent dives – it seems likely that there is only one high-temperature fluid flow source at this site – the Drachenschlund vent, itself.

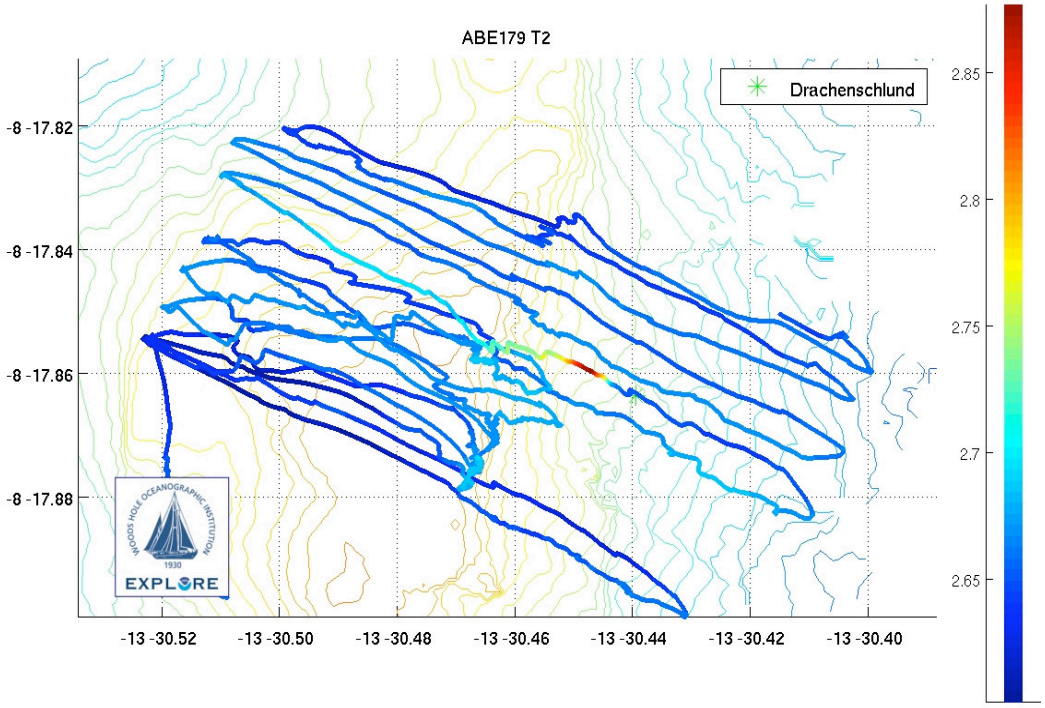

Fig. 1.7: Temperature (T2) data for the ABE 179 run.

A1 Segment, 7°57'S

Two final ABE dives were conducted, centered at 7°57'S where previous observations of particle-rich plume anomalies from CTD profiles and TOBI/MAPR data were confirmed by CTD tow-yo during this expedition. Although only minimal water column work had been conducted, it was possible to continue ABE exploration by close coordination with the ROV team who were simultaneously investigating the Drachenschlund vent located by ABE during dives 177-179.

ABE 180 Summary:

Launch: 2006/05/24 07:00 Recovery: 2006/05/25 05:44
Survey start: 2006/05/24 09:28 Survey end: 2006/05/25 02:59

Survey distance: 35.21 km Ave survey depth: 2601 m

ABE180 was a phase 1 dive at the 8S site. It provided some weak clues, which we followed up in ABE181 with no conclusive result. The dive took place over a shelf cut into a very steep cliff – the A1 segment's western rift-valley wall. The shelf was split in two parts. The survey lines were conducted at previously reported plume height (2600m) and planned to align at their western end with the 2700 contour. Lines were aligned East-West and designed to span the entire target depth range on the seafloor, 2700-2900m.

From Eh records, the two most significant hits were shortly after leaving the mooring and then when crossing back near the landing spot, but the magnitude of these hits was rather small.

ABE 181 Summary:

Launch: 2006/05/26 05:59 Recovery: 2006/05/27 02:12
Survey start: 2006/05/26 08:30 Survey end: 2006/05/26 23:11
Survey distance: 21.06 km Ave survey depth: 2787 m

ABE181 was a phase 2 survey at the 8S site. It did not find any plausible sources for the significant plume anomalies found in the CTD tow-yo.

In the SE corner of our survey the vehicle stalled for long periods. Clearly, driving along a steeply dropping edge should be avoided in the future. Better to drive off the edge, despite the problems encountered in ABE 179, and then approach the cliff at the floor level, climbing the cliff to proceed. We saw little if any significant plume activity on any of the sensors. The SM2000 bathymetry for the area, previously hidden in shadow in TOBI sidescan reveals an area that is flat with low backscatter. There is a rise toward the drop-off, then the steep drop-off itself. Unfortunately, survey lines timed out when approaching our prime target area from ABE 180 in the SE corner of the plateau.

1.4.3 ROV deployments

1.4.3.1 Technical Description of the ROV

(C. Seiter, D. Edge, H. A. Mai, H. Marbler, W. Schmidt, I. Suck, M. Zarrouk)

During M68-1, the remotely operated vehicle (ROV) "QUEST4000m" was used aboard R/V METEOR on its 9th cruise mission. "QUEST4000m" is operated by and installed at MARUM, Center for Marine Environmental Sciences at the University of Bremen, Germany. Designed and built by Schilling Robotics, Davis, USA, "QUEST4000m" is the fifth model of Schilling Robotics's electrical work class ROV QUEST series, but modified and specially adapted to the operational use in water depths down to 4000 m for MARUM.

Besides the "QUEST4000m" vehicle, the system includes a full control and handling periphery consisting of 20' control van, 20' workshop van, MacArtney Cormac electrically-driven storage winch with 5000 m of 17.6 mm NSW umbilical, and two specially designed transportation vans for the 16 t winch and the 3.3 t vehicle. With an overall weight of 45 t, the QUEST system is well adapted for use on R/V METEOR. The ROV is installed on the aft deck

of R/V METEOR, from where launch and recovery of the vehicle are done with a custom build launch and recovery system (LARS), installed to the A-frame of R/V METEOR.

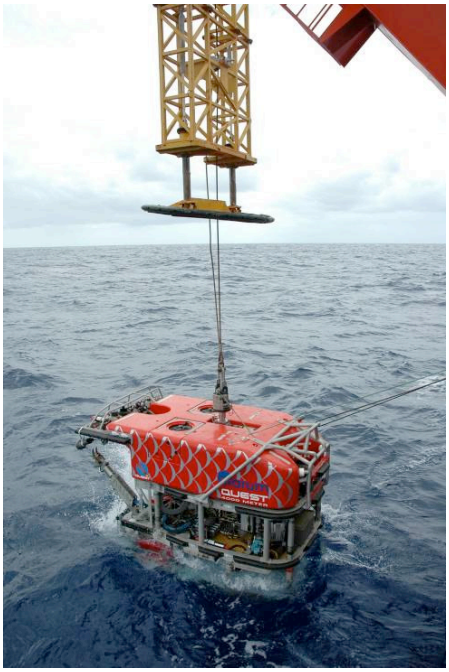

Fig. 1.8: MARUM ROV “QUEST4000m” deployed from the A-frame mounted launch and recovery system (LARS) behind the stern of R/V METEOR.

The free-flying ROV "QUEST4000m" is equipped with an RDI 1200 Hz Doppler Velocity Log (DVL), which, in combination with 60 kW electrical propulsion power from seven electric ring thrusters in the latest “Houken-Arts” design and auto control functions (i.e. “Stationkeep”) provides a relative positioning accuracy of the vehicle within decimeters. When combined with the ship’s hull-mounted IXSEA Posidonia USBL positioning system an absolute GPS positioning accuracy within 10-15 m could be obtained during cruise M68-1. The analogue software tool DVLNav with display of vehicle, ship, and bathymetry allows highly efficient cooperation between pilots and ship’s bridge staff and safe vehicle-umbilical-ship-system handling. All relative and absolute vehicle positioning data, as well as heading and relative movement data, are time coded and stored in a real-time database system (DAVIS-ROV).

The "QUEST4000m" telemetry and power supply system SeaNet with its two vehicle installed HUBs provides the capacity of using up to 16 video and 60 RS-232 data channels. The data transfer and communication - control data to the vehicle as well as sensor, diagnostics, and video data from the vehicle - is done via one single mode optical fiber and can be observed and controlled during operation. SeaNet telemetry also provides a convenient implementation and quick handling of third party equipment on the vehicle. The topside control system allows transparent access to all RS-232 and video channels, and via TCP/IP from control van network/database to ship’s net work real-time data distribution to nearly all laboratories on the ship is possible. Sensor data interpretation and processing is then practicable during dive operation, regardless of the original raw-data format and hardware interface.

The basic "QUEST4000m" vehicle set up includes on port side a 5-function manipulator (“Rigmaster”) and on starboard side a 7-function master arm controlled slave manipulator

("Orion") for task requiring sampling tools and devices. Two hydraulically driven toolskid-mounted drawers with boxes and/or custom built mounting frames provide the accessability and storage of these tools and devices, as well as of samples.

Fig. 1.9, left: "QUEST4000m" front view (from top to bottom): upper porch with lights, strobes, sonar, beacon finder, InsitePacific AURORAs, and USBL transducers; upper pan&tilt with light, DSPL Seacam6500, and lasers; lower pan&tilt with InsitePacific PEGASUS and SCORPIO, and light; Orion manipulator on left, Rigmaster manipulator on right; two forward lateral thrusters (FS, FP)on behind; on toolskid from left to right suction hose for rotary sampler, KIPS fluid sampling nozzle and high temperature sensor, InsitePacific ATLAS, tool/sample box with three Niskin bottles; lower porch with grating

Fig. 1.9, right: "QUEST4000m" aft view (from top to bottom): synthactic foam block with aft guard; thruster vertical aft (VA) in suction pump function with suction hose adapter; two aft lateral thrusters (AS, AP) with high power lights transformer and two compensators; toolskid with rotary sampler in the middle and KIPS pump and valve pack to the right

The vehicle front side installed light suite including various 10 W high-intensity discharge lights (HID), two 400 W HMI Daylights, 150 W dimmable and 500 W non dimmable incandescent lights illuminates the area in front of the vehicle up to a range of about 10 m depending on water turbidity. Within this range, detailed photo shooting and camera filming is possible with the vehicle's upper pan & tilt - mounted color zoom video camera DSPL Seacam 6500, the lower pan & tilt - mounted color zoom video camera InsitePacific PEGASUS and the 3.3 Megapixel digital still camera Insite Pacific SCORPIO with two strobes installed on the front porch, and the near-bottom on drawer mounted InsitePacific ATLAS, a broadcast quality 870 TVL 3CCD video camera. In addition, the set up contains up to three small InsitePacific AURORAs, wide-angle fix-focus color cameras for tool and device handling observation tasks. All camera signals are distributed in the control van for digital video time coded recording, to the pilot's head up display for navigating, and to a ship's laboratory for most efficient cooperation between pilots, observers and scientists in the laboratory. Pan & tilt data of both upper and lower units are stored time-coded in the real-time database.

Further equipment installed on the vehicle front includes two 532nm 5mW lasers for dimension measuring, a Sea & Sun CTD with additional turbidity and high temperature sensor, an Sonardyne ROV HOMER acoustic beacon finder for site marking and/or positioning, and a Kongsberg 625 Hz scanning sonar for mapping and also safety reasons in steep and dangerous environments. CTD sensor data are time-coded stored in the real-time database.

Post-cruise data archival will be hosted by the information system PANGAEA at the World Data Center for Marine Environmental Sciences (WDC-MARE), operated by MARUM and the Foundation Alfred Wegener Institute for Polar and Marine Research (AWI), Bremerhaven.

During cruise M68-1, "QUEST4000m" performed 11 dives including one dive for LAR training and system stability testing. All dives were planned in cooperation with the science team and were based on a combination of the results of the Woods Hole Oceanographic Institute (WHOI) autonomous underwater vehicle (AUV) ABE phase 1-3 survey flights, CTD station results (Oceanography Institute, University of Bremen), and on results from previous cruises, i.e. M62-5 and M64-1. A total dive time of 108 hrs 13 min including 67 hrs 32 min bottom time was achieved with highly efficient operational quality.

Table 1.1 gives a short overview of the M68-1 station numbers, Marum ROV "QUEST4000m" dive numbers, sites visited, maximum dive depth and all LAR and bottom start and end times. For detailed descriptions of the single ROV dives see chapter 1.4.3.2.

Table 1.1: Overview about M68-1 station and Marum dive numbers, sites, and all LAR and bottom start and end times.

M68-1 Station #	Marum Dive #	Date	Site	Depth (m)	Time Launch	Time Start (Bottom)	Time End (Bottom)	Time on Deck	Bottom Time	Total Dive Time
	85	05.05.06	Test Dive	920	15:30			17:30		**02:00**
03ROV	86	10.05.06	Wideawake/ Turtle Pits	3000	12:30	14:21	22:20	00:38	**07:59**	**12:08**
07ROV	87	11.05.06	Red Lion	3000	10:15	12:30	21:00	23:22	**08:30**	**13:07**
12ROV	88	12.05.06	Turtle Pits/ Wideawake	3000	11:10	13:02	21:33	23:53	**08:31**	**12:43**
20ROV	89	14.05.06	Comfortless Cove	3000	11:02	12:58	21:15	00:15	**08:17**	**13:13**
24ROV	90	15.05.06	Comfortless Cove	3000	14:55	17:10	23:11	01:00	**06:01**	**10:05**
39ROV	91	18.05.06	Roman City/ Limtoc	1500	18:15	19:22	23:58	01:11	**04:36**	**06:56**
41ROV	92	19.05.06	Lilliput / Candelabrum Meadow	1495	15:00	16:06	22:44	00:13	**06:38**	**09:13**
63ROV	93	24.05.06	Nibelungen	2900	13:50	15:45	22:28	01:50	**06:43**	**12:00**
69ROV	94	26.05.06	Nibelungen	2900	13:40	15:33	21:45	00:05	**06:12**	**10:25**
70ROV	95	27.05.06	Roman City / Limtoc	1500	13:42	14:50	19:55	22:05	**04:05**	**08:23**

The following scientific tools and devices were used on "QUEST4000m" during the above - mentioned dives for obtaining biological, geological, sediment, and fluid-geochemical samples.

All tools were primarily handled or released with the 7-function "Orion" slave manipulator, if necessary supported by the 5-function "Rigmaster" manipulator:

- fine mashed nets with and without lid for mussels, clams, polychaetes, and sediment samples
- KIPS fluid nozzle and high temperature sensor on a T-handle for fluid samples and in-situ T monitoringHe-sample tubes for fluid samples, pressure keepingMicroCat CTD on a spool for measuring oceanographic parameters in and above hot vent plumes
- suction gun with rotary sampler for sediment, glass, gravel, and biological samples
- Niskin bottles for fluid samples
- fine cotton sack for particle sampling above hot vents
- buoyant markers with ground weight for marking new hydrothermal sites
- metal scoops for sediment and biology samples

On two dives, an ADCP from the Oceanography Institute, University of Bremen was mounted on the ROV in place of the rotary sampler. ADCP, rotary sampler/suction pump, and KIPS valve and pump, were topside software controlled.

1.4.3.2. Description of the ROV Dives

(C. Devey, K. Lackschewitz, B. Melchert)

Wideawake and Turtle Pits (Stations 3ROV (dive 86) and 12ROV (dive 88))

Both dives aimed at sampling fluids, rocks and biology in the Turtle Pits high temperature field and the Wideawake diffuse flow area. During the first dive we were able to take co-located biological and fluid samples (with temperatures around 18°C) at a Wideawake vent (Fig. 1.10), and sample the fresh lava flow which marks the eastern margin of the field (and apparently overlies a low-temperature vent at Wideawake, see Fig. 1.11). This fresh lava appears to have more sediment cover this year than last, based on photo comparisons. The second dive (12ROV) also retrieved one specimen of *Calyptogena* clam. The sampling at Turtle Pits consisted of collection of water samples (using both KIPS, Niskin bottles and helium tubes) from the high temperature vents, including one sample during 12ROV which gave the highest temperature yet recorded worldwide on a spreading axis vent of 408.5°C. Collection of sulphide samples at the hot vents was also achieved – no mussel samples could be collected at Turtle Pits, the fresh lava visible on the ABE pictures from 2005 was also no longer accessible, presumably covered with chimney debris in the last year. Photo-mosaicing of the largest chimney at Turtle Pits, "Southern Tower", shows how quickly these structures grow. Since May 2005 the Tower has risen by 4m!

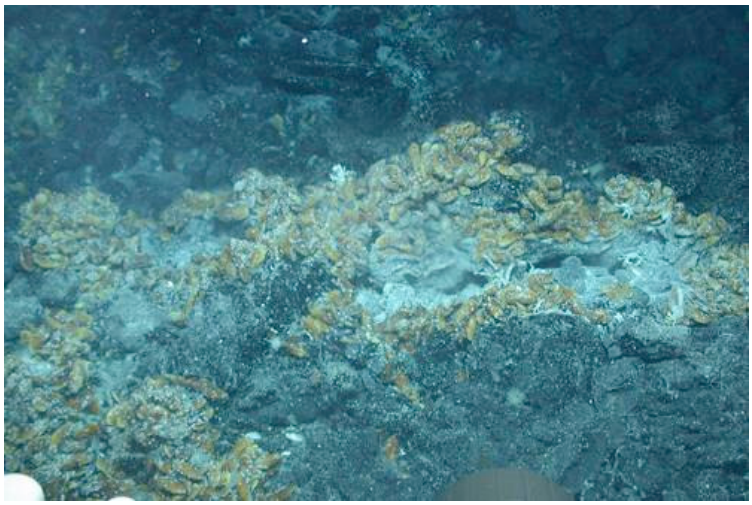

Fig. 1.10: The Wideawake vent sampled for fluids and biology during 3ROV.

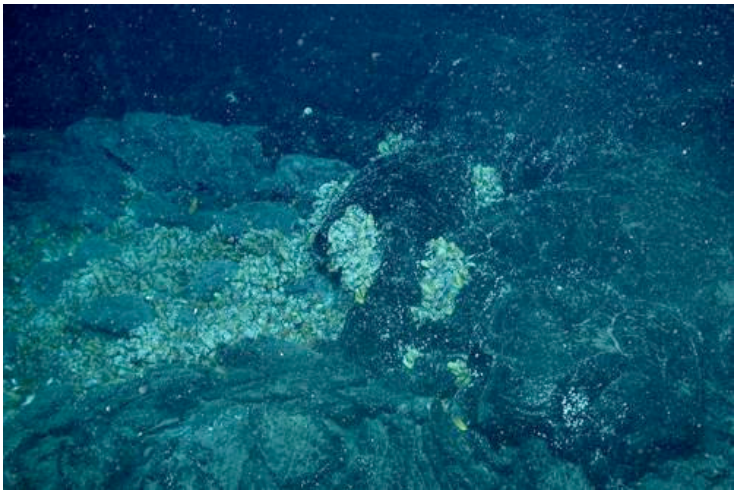

Fig. 1.11: Fresh lava apparently covering part of a Wideawake vent, mussels have started to settle on the fresh lava.

Red Lion Hydrothermal Field (Station 7ROV (dive 87))

The Red Lion hydrothermal field was discovered and sampled in 2005 during the RV Charles Darwin cruise 169 and the RV Meteor cruise M64/1. During M68/1 we visited this field again in order to document any changes in the structure of the chimneys and in the biological activity and to continue our time-series experiments. The Red Lion hydrothermal field is characterized by 4 active chimneys called Shrimp Farm, Zuckerhut (Sugarhead), Mephisto and Tannenbaum. During dive 87 (station 7ROV), we surveyed the relative positions of these structures using USBL (Posidonia) and DVL navigation on the ROV. We determined the Posidonia position of Shrimp Farm (4°47.827 S/12°22.604 W, 3047 m waterdepth) and measured the position of the other three smokers relative to this (see Fig. 1.12, below).

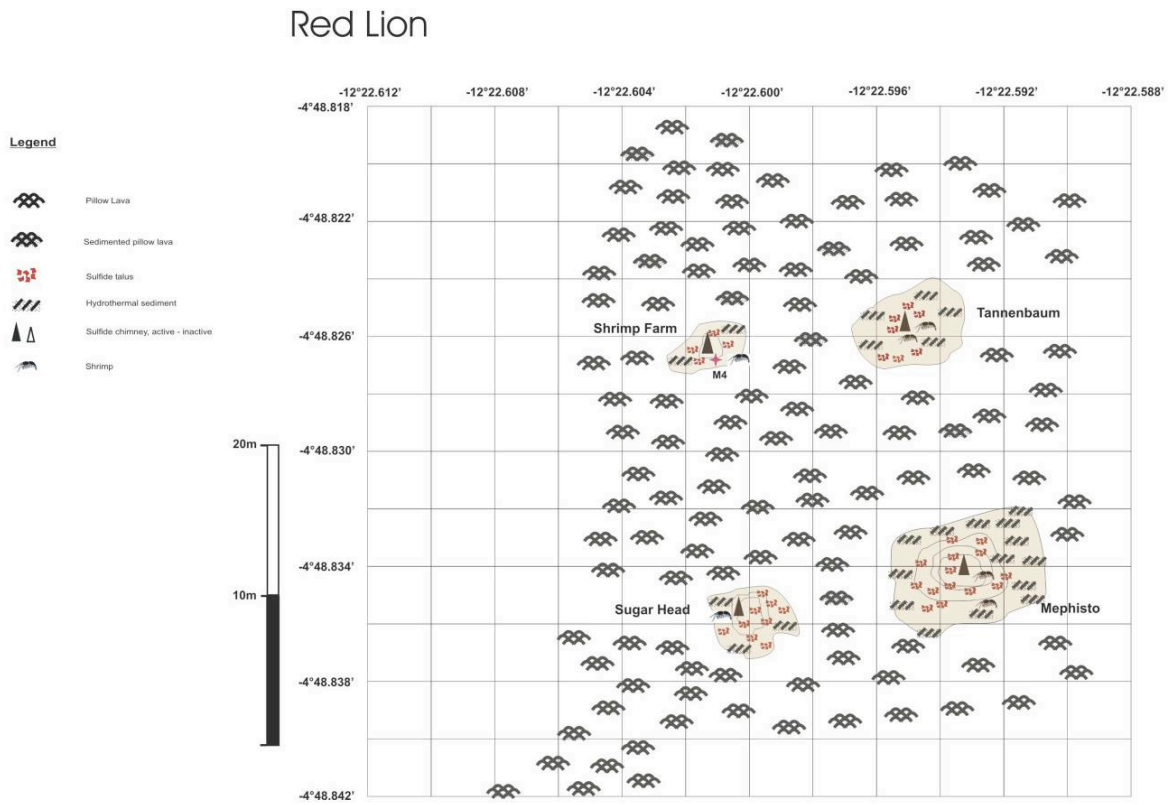

Fig. 1.12: Map of Red Lion field based on measurements made during station 7ROV.

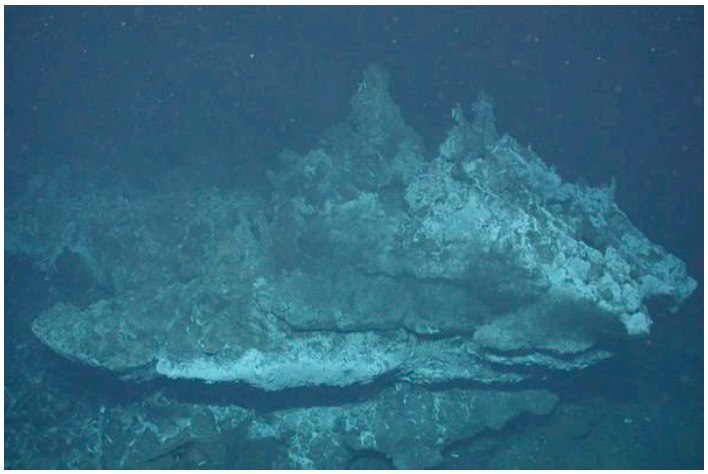

Fig.1.13: Showing chimney "Shrimp Farm" with only a few shrimps during M68/1 (2006).

In comparison to the M64/1 expedition the shrimp coverage has drastically decreased at the Shrimp Farm smoker, whereas Mephisto had more extensive shrimp colonization this year (Fig.s 1.13 and 1.14). We sampled a net with shrimps, a sulfide sample and fluid samples from the high temperature vents at Mephisto. During fluid sampling we recorded a constant temperature of 345°C whereas the maximum temperature measured was 380°C. A second sulfide sample was taken at the base of Tannenbaum.

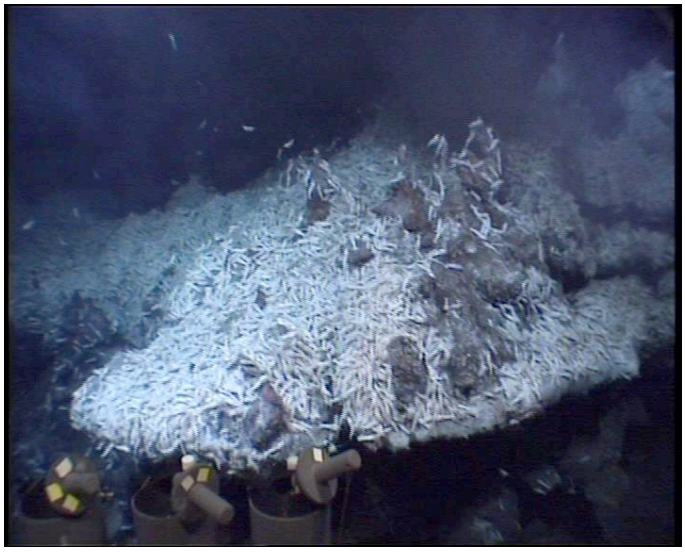

Fig.1.14: Showing chimney "Shrimp Farm" covered with shrimps during M64/1 (2005).

The New Vent Field "Comfortless Cove" (Stations 20ROV (dive 89) and 24ROV (dive 90))
Based on an ABE survey, the ROV started dive 89 at 4°48.13'S/12°22.35'W where the Eh-sensor of ABE measured 3 distinct anomalies. The area is characterized by a mound consisting of pillows (Fig. 1.15).

The area with the highest Eh-anomaly is related to a 12.8 m high smoker with two spires (named „Sisters Peak") approximately 70 m southeast of the mound (4°48.188'S/12°22.301'W, 2996 m; Fig. 1.15 and 1.16). The east spire of this smoker is inactive, whereas the west spire is venting intensely. Temperature measurements revealed exit temperatures of up to 399°C. The base of the chimney is colonized by mussels, crabs and shrimps which were sampled for taxonomic studies. A sulfide pile at the eastern base of the chimney is covered by a very fresh and probably young lava flow.

We found an intensely-colonized mussel field („Golden Valley", see Fig. 1.17) in a N-S oriented fissure somewhat north and east of Sisters Peak. We placed "Marker 6" (4°48.166'S/12°22.267'W, 2981 m) at this site. On ROV dive 90 we took biological and fluid samples and measured a temperature of 3.6°C between the mussels. Another diffusely-venting field lies approximately 50 m to the northwest of Golden Valley, almost along strike from Sisters Peak. The size of the field is 10 * 20 m and is characterized by lots of mussel patches and a diffuse venting with temperatures of up to 5°C. The cloudy water which characterized this area led us to name it "Foggy Corner". Here, we placed "Marker 7" (4°48.159'S/12°22.306'W) and sampled diffuse fluids.

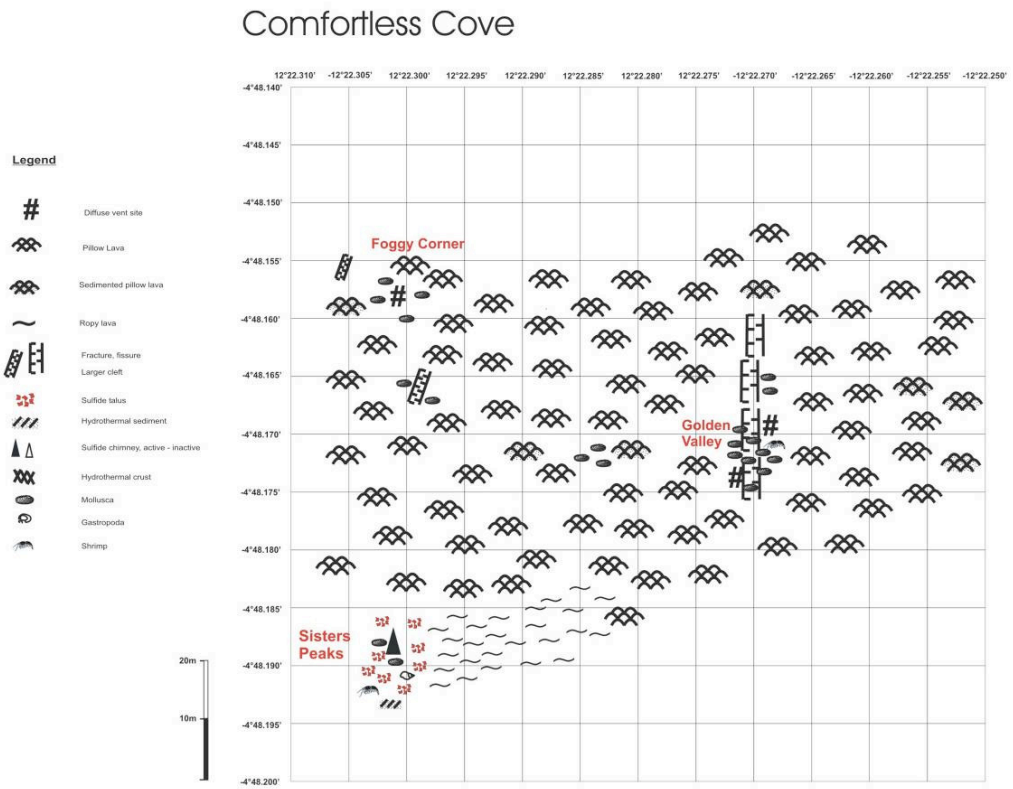

Fig. 1.15: Map of region around Comfortless Cove area compiled on the basis of ROV observations.

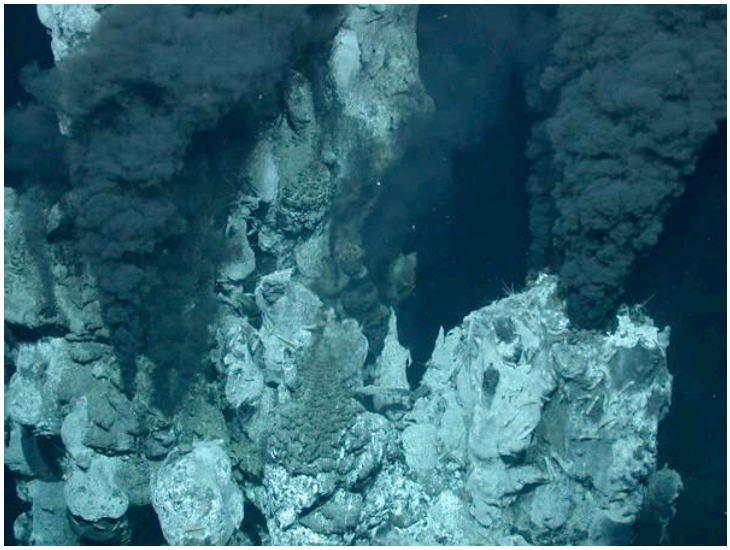

Fig. 1.16: High-temperature chimneys at Sisters Peak.

Fig. 1.17: Dense population of *Bathymodiolus* in the Golden Valley.

Diffuse Vent Fields of the Lilliput hydrothermal field (Stations 39ROV (dive 91), 41ROV (dive 92) and 70ROV (dive 95))

Three AUV and two ROV dives were dedicated to the area of the Lilliput hydrothermal field. The AUV deployments yielded several additional targets located both north and south of of the Main Lilliput site. The ROV dives then studied these, with station 39ROV (dive 91) going south and 41ROV (dive 92) revisiting Main Lilliput and exploring the area to the north.

The area is characterised by evidence for two distinct types of hydrothermal activity;

(a) large mounds of orange-coloured, presumably Fe-rich hydrothermal sediments at which we found no evidence for present-day venting (Fig. 1.18)

(b) diffuse venting (e.g. Fig. 1.19) apparently sometimes associated with high-porosity lava-sheet fields showing columns and roof-collapse (Fig 1.20).

Fig. 1.18: Extinct hydrothermal mound.

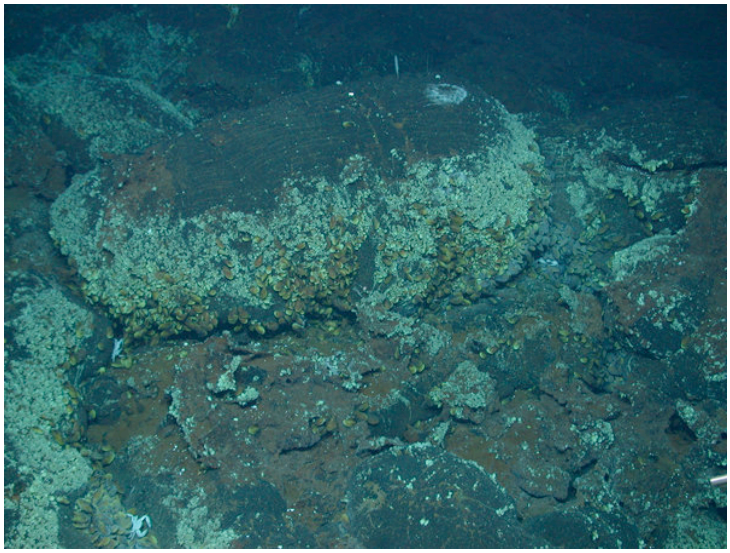

Fig 1.19: Mussel field south of Main Lilliput site.

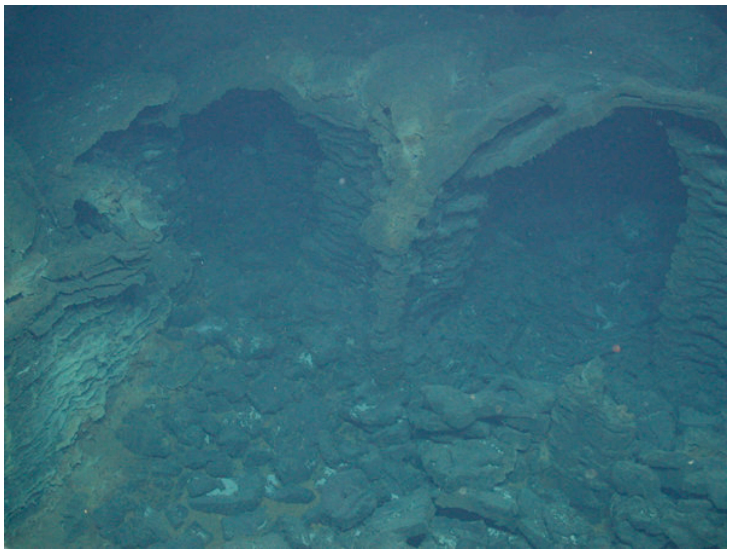

Fig. 1.20: Lava drainout roof-and-column structure of Roman Ruins, columns have hydrothermal flow.

The Main Lilliput site is an example of this type of venting. Fig. 1.21 shows a detailed bathymetric map of the area around the Lilliput field from the ABE SM2000 sonar together with the TOBI sidescan image and the tracks of ROV dives carried out there during M68-1.

The Main Lilliput site itself is characterized by red-orange Fe-oxide-rich hydrothermal deposits which we sampled successfully at the site of the M64/1 “Marker A” (9°32.845’S/13°12.546’W, 1496m). Close to the deposits several mussel patches with mostly juvenile mussels, some crabs and a few shrimps are concentrated.

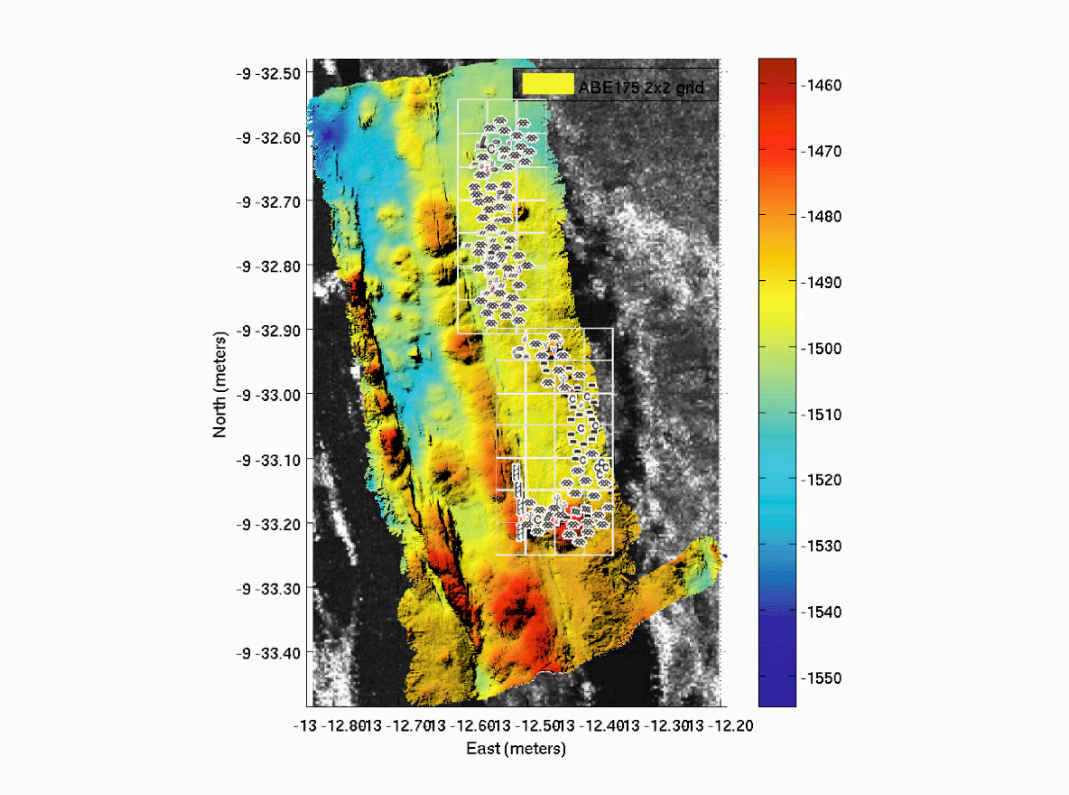

Fig. 1.21: TOBI-side scan imagery, ABE SM2000 bathymetry and ROV-based seafloor observations in the area of the Lilliput hydrothermal field.

Fig. 1.22: Fissure with lava tongues flowing downwards.

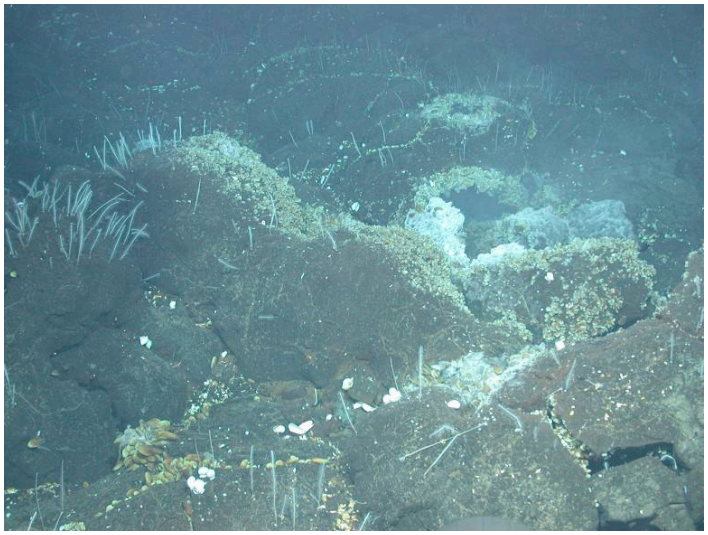

Fig. 1.23: The diffuse venting field “Candelabrum Meadow”.

Shimmering water is visible above some of the mussel patches. During our fluid sampling program at one of these sites we measured temperatures up to 4.8°C (backround temperature is 4.0°C). Approximately 200m NNW of the Main Lilliput site (at 9°32.675’S/13°12.562’W, 1501m) we found another diffuse venting field (Lustrog) based on the results of the AUV deployment. The field is characterized by mussel colonies and some collapsed pillows with venting of milky water in some places. Temperature measurements gave values of up to 6.6°C.

A fifth diffuse venting field lies approximately 70m ENE of Lustrog (9°32.653’S/13°12.552’W). The area between both these fields shows a broad fissure where downward flowing lava tongues indicate this fissure as their eruption source (Fig.1.22) The third diffuse venting field shows abundant hydrozoans of the species *Candelabrum* growing on top of the pillows (Fig. 1.23) leading us to call it “Candelabrum Meadow”. During the fluid sampling we measured a temperature of up to 7°C.

The Nibelungen Hydrothermal Field (Stations 62 ROV (dive 93) and 69 ROV (dive 94))

During the Meteor cruise M62/5 in 2004, we found strong evidence for hydrothermal activity on a topographic high that rises to 2900 m depth from the rift valley floor at 3500 m between 8°17’ S and 8°19’ S to the East of the tip of ridge segment A2 (named Cheating Bay). High methane concentrations (up to 115 nmol/l) together with layers of increased light scattering peaking at 2700m depth in the vicinity of 8°18’S, 13°31’W indicated the presence of venting in this area, although black smokers were not directly observed (Devey et al., 2005). During cruise M68/1 we discovered the Nibelungen vent site with the AUV “ABE” by Eh- and photo-mapping at the eastern side of Cheating Bay (see chapter AUV).

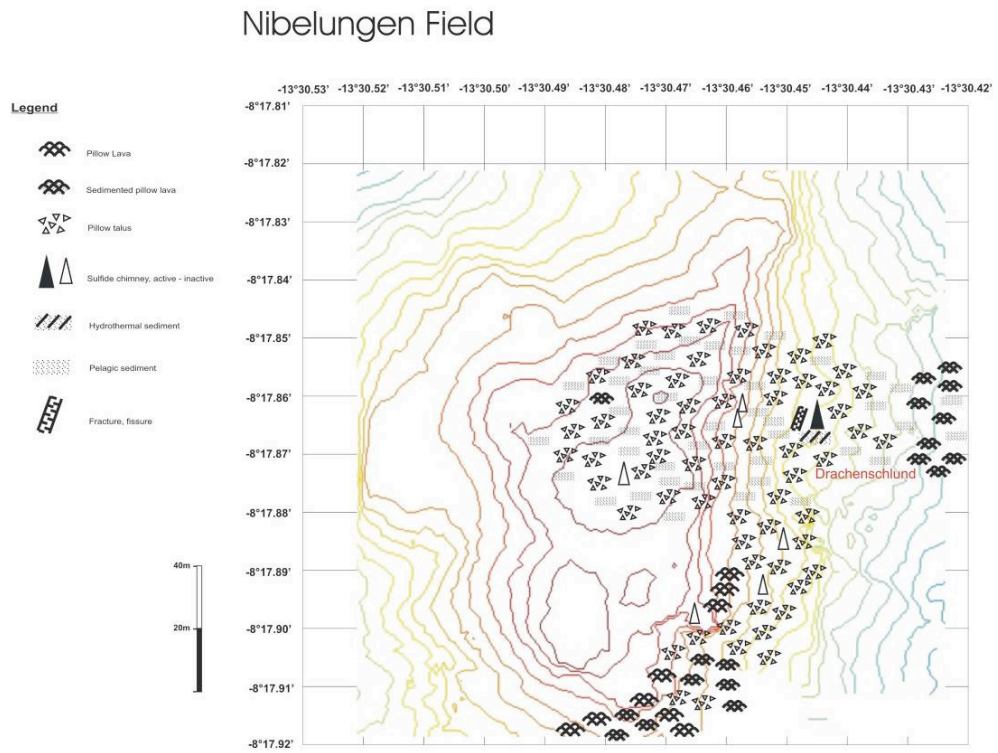

Fig. 1.24: Map of the area of the Nibelungen vent site.

The following dive of the ROV "Quest" (station 62ROV) revealed active and inactive vent sites along a steep slope at 2905 m water depth (see Fig. 1.24). The only active vent site (located at 8°17.853'S, 13°30.443'W) is characterised by a 4-5 m wide crater where intense flow of hydrothermal fluid produced a black smoker from an estimated 0.5 m wide hole (Fig. 1.25). Although it was difficult to come close to the hole we sampled hot fluids about 1m above the seafloor at constant temperatures of 90°C. The highest measured temperature was 175°C. The 4 m high crater wall consists of talus of basaltic and serpentinized clasts and breccias. The fauna was sparse, consisting of anemones and polychaetes which we sampled during dives 62 and 69. We named this smoking crater "Drachenschlund". On top of the northern crater rim we placed a marker (#9). At both sides of the crater several extinct groups of chimney spires are located (Fig. 1.26).

During dive 69ROV we mapped the southern extent of the Nibelungen field. Several extinct chimneys were found along the 2900 m contour line of the slope almost as far south as the southeastern edge of the hill (8°17.898'S, 13°30.468'W). The south-easternmost corner of the hill shows broken pillow shells out of which the last lava remnants have drained (Fig. 1.27) and abundant small lava tubes (Fig. 1.28). The slope below the 2900 m contour line is characterized by sediment and a lot of talus material. Above this line the slope consists mainly of pillow lavas.

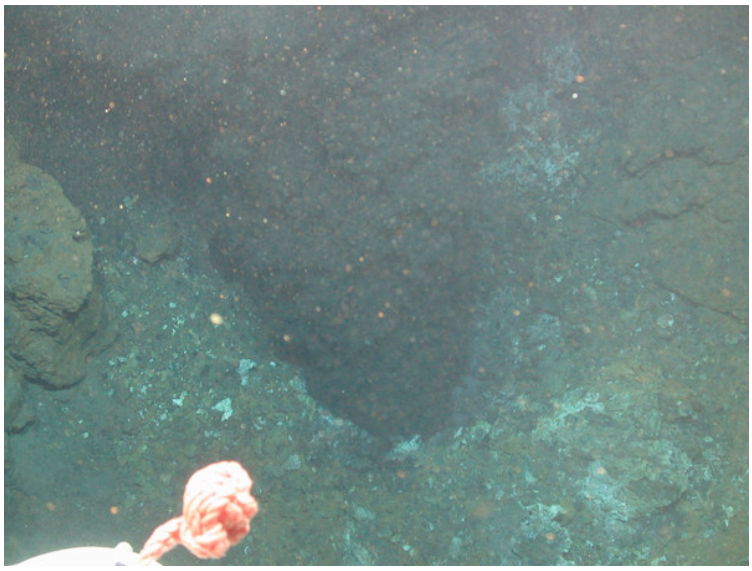

Fig. 1.25: Active smoking crater site “Drachenschlund” at the Nibelungen Field.

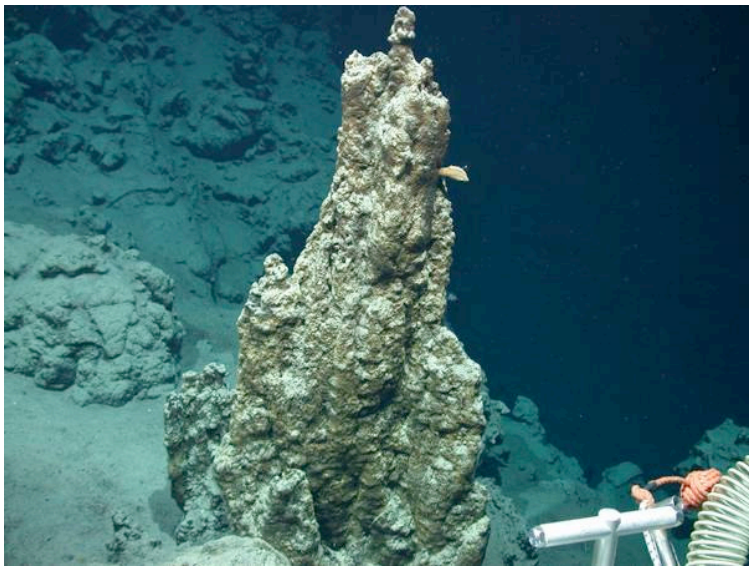

Fig. 1.26: Inactive chimney spire on a steep slope at the Nibelungen Field.

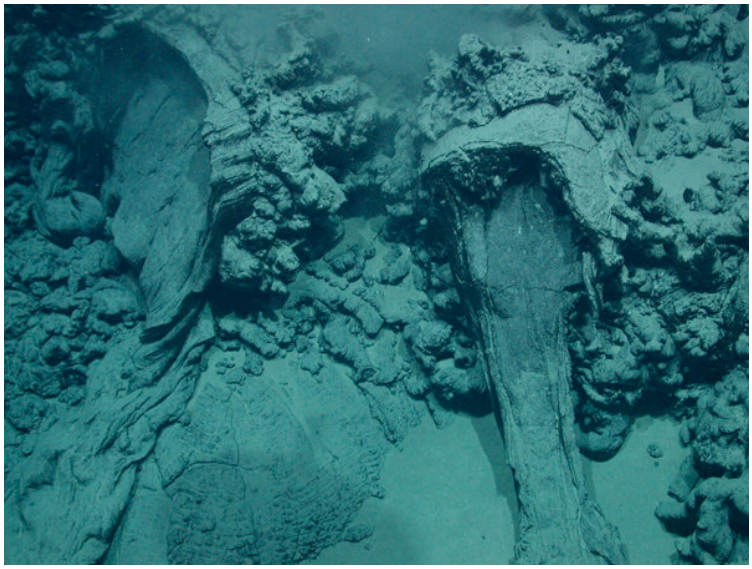

Fig.1.27: Broken pillow shells out of which the last lava remnants have drained.

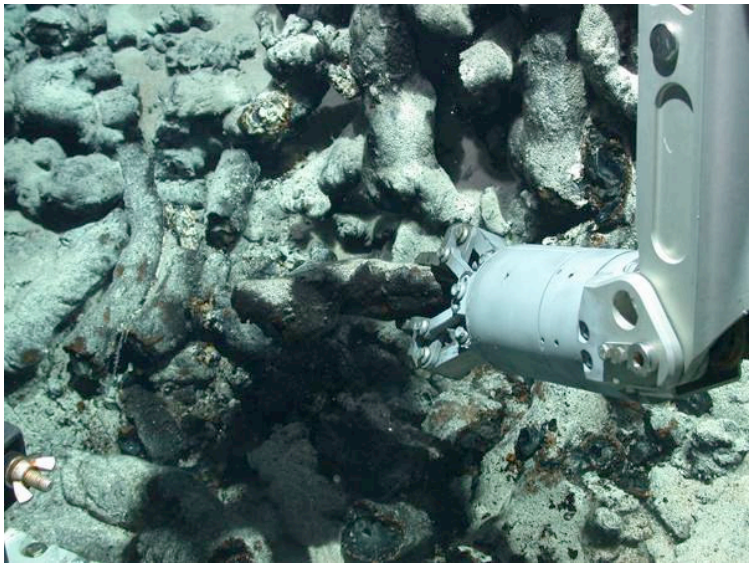

Fig.1.28: Small lava buds on the southeast corner of the Nibelungen massif.

1.4.4 Description of Rocks and Hydrothermal Precipitates

(K.S. Lackschewitz, C.W. Devey, S. Petersen)

During cruise M68/1 a total of 8 ROV dives, 10 wax corers and 3 dredge stations recovered geological samples from hydrothermal fields and the ocean crust between 5°S and 10°S along the slow-spreading Mid-Atlantic Ridge. The samples consist of fresh to altered basalts, sulfides, Fe-oxyhydroxides and serpentinized breccias. More information on all the successful sampling stations is given in Table 1.2.

Table 1.2: Rocks and hydrothermal precipitates

No.	Date / time	Lat / Long	Depth	comment
3ROV-6B	10.05.06/17:28	Wideawake 4°48.640'S/ 12°22.363'W	2980 m	Sparsely plagioclase-phyric lava crust with glass
3ROV-7B	10.05.06/17:37	Wideawake 4°48.640'S/12°22.363'W	2980 m	Sparsely plagioclase-phyric lava crust with glass
3ROV-8	10.05.06/17:28	Wideawake 4°48.620'S/ 12°22.345'W	2984 m	volcanic glass chips
6VSR	11.05.06/08:57	4°47.82'S/ 12°22.62'W	3036 m	Few pieces of fresh volcanic glass
7ROV-1	11.05.06/14:32	Red Lion 4°47.826'S/ 12°22.595'W	3046 m	chimney outer wall fragment from base of Tannenbaum
7ROV-6	11.05.06/18:42	Red Lion 4°47.834'S/ 12°22.593'W	3045 m	Outer thin wall of a high-temp. chimney from base of Mephisto
7ROV-7	11.05.06/18:52	Red Lion 4°47.834'S/ 12°22.593'W	3045 m	Altered sulfide rubble from base of Mephisto
7ROV-8	11.05.06/18:55	Red Lion 4°47.834'S/ 12°22.593'W	3045 m	Altered sulfide rubble from base of Mephisto
12ROV-1	12.05.06/13:49	Turtle Pits 4°48.576'S/ 12°22.418'W	2994 m	massive sulfide from base of Two Boats
12ROV-2	12.05.06/15:28	Turtle Pits 4°48.576'S/ 12°22.414'W	2985 m	beehive rubble from Southern Tower
12ROV-3B	12.05.06/17:43	Wideawake 4°48.6'S/ 12°22.3'W	2980 m	Glassy lava crust
12ROV-9B	12.05.06/21:26	Wideawake 4°48.6S/ 12°22.3'W	2980 m	sheet lava with glass crust
14VSR	13.05.06/15:22	4°48.10'S/12°22.38'W	2989 m	Small volcanic glass chips
20ROV-1A	14.05.06/15:30	Comfortless Cove 4°48.188'S/12°22.301'W	2996 m	Altered chimney fragments from base of Sisters Peak
20ROV-2	14.05.06/17:00	Comfortless Cove 4°48.188'S/12°22.301'W	2996 m	Chimney outer wall fragment from base of Sisters Peak
20ROV-3A, -B	14.05.06/17:05	Comfortless Cove 4°48.188'S/12°22.301'W	2996 m	3A: Massive sulfide with a 0.5 cm Fe-oxide crust from base of Sisters Peak 3B: Lava flow from base of Sisters Peak overflowing sulfides
28DS-1 to -3	17.05.06/12:23	9°32.79'S/13°12.25'W	1441 m	Old pillow segments with mm-thick Mn-crust
30VSR	17.05.06/21:54	9°33.90'S/13°12.30'W	1456 m	A few volcanic glass chips
31VSR	17.05.06/22:45	9°33.70'S/13°12.41'W	1476 m	Fresh volcanic glass chips
33VSR	18.05.06/00:44	9°33.09'S/ 13°12.55'W	1479 m	A few volcanic glass chips
36VSR	18.05.06/9:42	9°31.94'S/13°12.78'W	1477 m	200g volcanic glass chips
39ROV-1	18.05.06/21:38	Roman City 9°33.148'S/13°12.420'W	1486 m	red FeO(OH) mud
39ROV-2	18.05.06/21:43	Roman City 9°33.148'S/13°12.420'W	1486 m	aphyric basalt
39ROV-6A	18.05.06/23:55	Limtoc 9°32.956'S/ 13°12.524'W	1494 m	volcanic glass crust
39ROV-7B	18.05.06/23:56	Limtoc 9°32.956'S/ 13°12.524'W	1494 m	FeO(OH) crust
41ROV-1	19.05.06/17:11	Lilliput 9°32.845'S/ 13°12.546'W	1495 m	red FeO(OH) mud
41ROV-14	19.05.06/22:40	9°32.639'S/ 13°12.490'W	1496 m	volcanic glass
46VSR	21.05.06/12:45	8°17.31'S/ 13°35.82'W	2904 m	Sheet flow fragment with glass
54VSR	22.05.06/14:36	8°15.80'S/ 13°31.10'W	3211 m	Soft white sediment
57VSR	23.05.06/4:45	8°21.06'S/ 13°35.00'W	2807 m	Some glass above cloth
58VSR	23.05.06/6:40	8°22.48'S/ 13°35.07'W	2774 m	Almost empty, some glass on outside
62ROV-1	24.05.06/17:48	Nibelungen 8°17.884'S/ 13°30.451'W	2906 m	inactive chimney fragment
62ROV-2	24.05.06/18:45	Nibelungen 8°17.858'S/ 13°30.358'W	2906 m	inactive chimney fragment
62ROV-6	24.05.06/20:57	Nibelungen 8°17.853'S/ 13°30.443'W	2903 m	serpentinzed breccia from Drachenschlund crater
62ROV-11	24.05.06/22:15	Nibelungen 8°17.853'S/ 13°30.443'W	2903 m	breccia of altered basalts from Drachenschlund crater
66DS-1 to -8	25.05.06/23:03	7°57.14'S/ 13°27.72'W	3034 m	Several massive basalt and pillow pieces, some with glass
69ROV-1	26.05.06/17:00	Nibelungen 8°17.916'S/ 13°30.482'W	2878 m	Lava tube
69ROV-2A	26.05.06/20:10	Nibelungen 8°17.916'S/ 13°30.438'W	2898 m	strongly altered wall rock
70ROV-4	27.05.06/18:00	Roman City 9°33.094'S/ 13°12.410'W	1495 m	Lava piece from Roman City
71DS-1 to -4	28.05.06/05:40	Nibelungen 8°17.83'S/ 13°30.51'W	2854 m	Pillow buds and a hydrothermal crust with Mn-coating (-2)

During the stations 3ROV (dive #86) and 12ROV (dive #88), fresh lava crusts and volcanic glass were recovered from the Wideawake diffuse flow area. The stations were also targeted at the high-temperature chimneys of the Turtle Pits hydrothermal field. One sample is a typical piece from a massive sulfide mound forming the base of the "Two Boat" chimney and is characterized by recrystallized chalcopyrite, pyrite ± h~~a~~ematite, magnetite(?) and anhydrite. Another sample is rubble of a beehive structure from the "Southern Tower" consisting of chalcopyrite, sphalerite and pyrrhotite. 7ROV recovered several sulfide samples from the "Red Lion" hydrothermal field. Sample 7ROV-1 was taken from the base of "Tannenbaum", comprising of recrystallized marcasite, pyrite and sphalerite, whereas samples 7ROV-2 to –4 were taken from base of "Mephisto" and are characterized by marcasite, chalcopyrite, sphalerite, wurzite and pyrite.

During station 20ROV (dive #89) outer chimney wall fragments were sampled from the base of the high-temperature chimney "Sisters Peak" at the newly-discovered Comfortless Cove hydrothermal field (see Fig. 1.29). These chimney fragments consist of an outer pyrite-marcasite crust followed by pyrrhotite-sphalerite and an inner zone of chalcopyrite. In addition, we recovered a piece of a relatively fresh lava flow covering a sulfide pile at the eastern base of the chimney.

During two ROV stations (39ROV, dive #91; 41ROV, dive #92) hydrothermal Fe-oxyhydroxide-rich crusts and mud were sampled from three diffuse venting hydrothermal sites (Roman City, Limtoc, and Main Lilliput) at the Lilliput hydrothermal field around 9°33 (see Fig. 1.29). During both dives we also sampled a basalt, a glass crust and volcanic glass chips. At station 70ROV (dive 95) a lava piece from top of the "Roman City" roof was recovered (see Fig. 1.29).

Geological sampling during stations 62ROV (dive #93) and 69ROV (dive #94) at the Nibelungen hydrothermal field recovered sulfide samples from inactive chimneys, lava fragments, as well as serpentinized and basaltic breccias, from the „Drachenschlund" smoking crater.

Three dredges at 7°57'S (station 66DS), 8°18'S (station 71DS), and 9°32'S (station 66DS) recovered old pillow segments with a 1mm Mn-crust, pillow buds with a mm-thick glass crust and basalt fragments with glass crusts, respectively.

At 9 wax core stations we recovered varying amounts of volcanic glass.

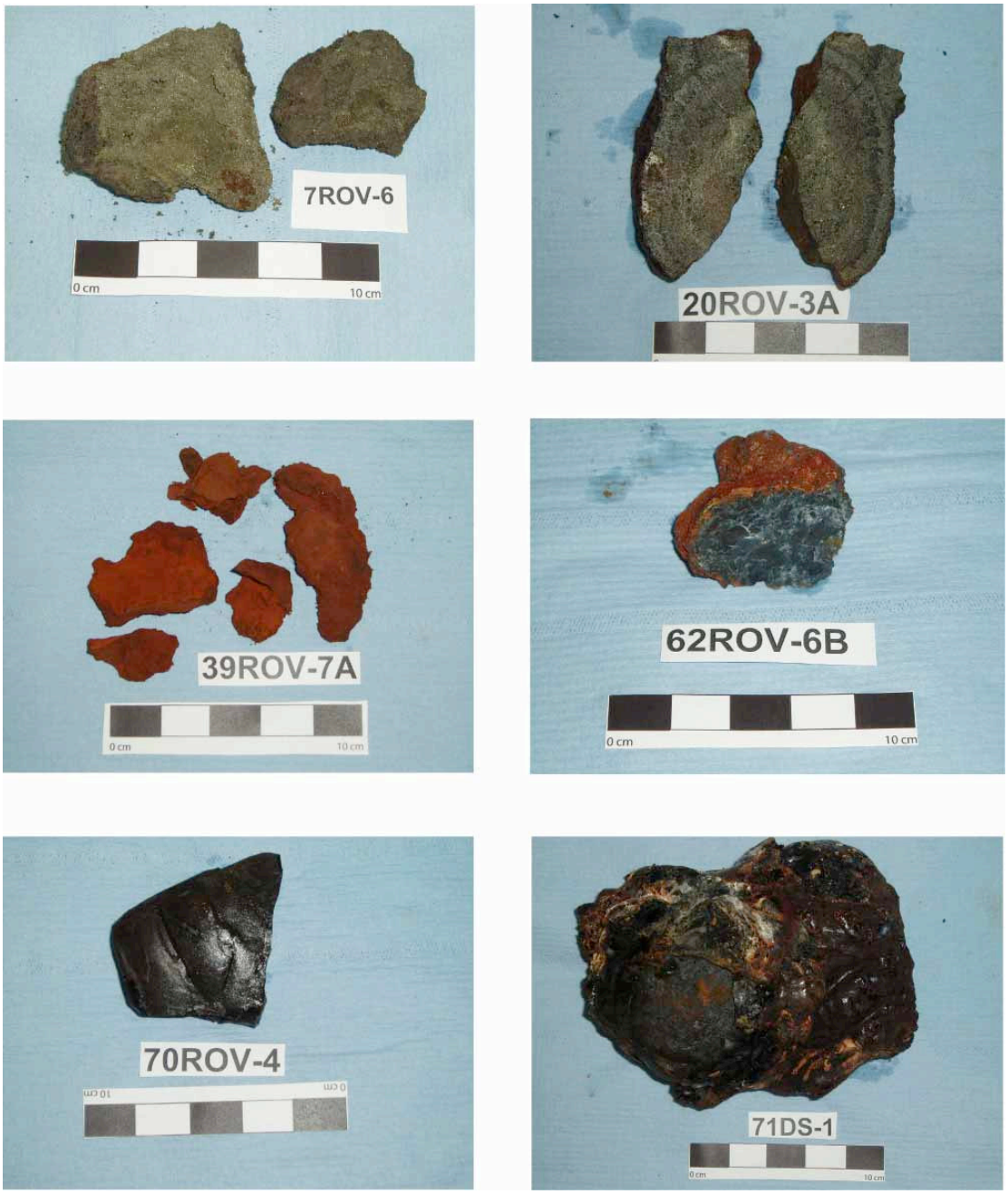

Fig. 1.29: Geological samples recovered during ROV and dredge (DS) stations: 7ROV-6: High-temperature chimney wall fragment from the Red Lion hydrothermal field (base of "Mephisto" chimney); 20ROV-3A: complete chimney wall from the Comfortless Cove hydrothermal field (base of "Sisters Peak" chimney); 39ROV-7A: Fe-oxyhydroxide crust from Limtoc low-temperature hydrothermal site; 62ROV-6B: altered serpentinized breccia from the Nibelungen hydrothermal field (from the rim of the "Drachenschlund" crater): 70ROV-4: Lava piece from top of the "Roman City" roof; 71DS-1: Pillow bud from the eastern flank of the Nibelungen hydrothermal field.

1.4.5 Hydrography (CTD, MAPR & Lowered ADCP)

(M. Walter, C. Mertens, U. Stöber)

During the Meteor cruise M68/1, the temperature, salinity, turbidity and velocity field of the near field of several hydrothermal plumes were mapped to describe the general hydrography in the target areas and study the spreading of the plumes. For the same purpose, water samples were taken for water and gas chemistry analysis (see section on water chemistry/gases). A hydrothermal plume in the local background stratification should be marked by negative anomalies in temperature and salinity as well as an increase in turbidity. In addition to the plume mapping, the temperature and density field, as well as the vertical shear of the horizontal velocity field, will be analyzed to determine the strength and distribution of vertical mixing processes in the water column in the rift valley environment.

1.4.5.1 Instrumentation and Methods

CTD

During the M68/1 cruise a total of 27 conductivity-temperature-depth (CTD) casts was carried out using a Sea-Bird Electronics, Inc. SBE 911plus system additionally equipped with a Wet Labs LSS backscatter sensor (E. Baker, NOAA/PMEL) and a redox potential/Eh probe (R. Seifert).

The CTD sensors were calibrated at Sea-Bird Electronics in September 2004. The underwater unit was attached to a SBE 32 carousel water sampler with 22 Niskin bottles. Two bottles were left out for the lowered ADCP system, hence a maximum of 22 bottles was used.

The complete system worked properly throughout the entire cruise.

Salinity samples, typically two to five per cast, were analysed onboard using a Guildline Autosal 7 salinometer. The salinometry was severely hampered by a malfunction of the salinometer, which drifted unpredictably during the measurements. An attempt to correct for the drift was made by doing repeated standardizations and removing a linear trend from the measurements. An offset in salinity was removed from the CTD data by means of comparison with the M62/5 salinities in the deep water, the pressure dependence was determined by the salinometry. However, the resulting accuracy in salinity was considerably reduced compared to other cruises and is expected to be better than at least 0.005 in salinity. The salinity data set is therefore preliminary; a final data set will be produced after re-analyzing the salinity samples at home in the lab.

LADCP

All the hydrographic stations were accompanied by current measurements with a lowered acoustic Doppler current profiler (LADCP) system attached to the CTD and water sampling carousel. Two RDI 300 kHz Workhorse Monitor instruments were used in the setup in a synchronized Master-and-Slave mode, with the upward looking (SN 1973) as Slave and the downward looking (SN 2161) as Master. For 4 of the stations, only a single (downward looking) instrument was used. During three of those stations (64 CTD, 67 CTD & 72 CTD), the second instrument was prepared for or used in an ROV experiment; in the case of the 4th profile (1 CTD), a software failure prevented the Slave instrument from working. The instruments were powered by an external battery supply, consisting of 35 commercial quality 1.5V batteries

assembled in a pressure resistant Aanderaa housing. The system was set to a ping rate of 1 ping/s and a bin length (= vertical resolution) of 10 m in the Master-and-Slave mode.

An inverse method incorporating the bottom track velocities was used for the post processing of the raw data. This resulted in high quality velocity profiles, even for profiles with very weak current velocities (<0.05 m/s) and zero mean. The overall performance of the two instruments was very good: The range of each instrument was typically 150 m in the upper parts of the water column and 60 to 70 m at depth larger than 1500 m. Thus, the total range of the package reached from 150 to 300 m. With lowering and heaving velocities of 1 m/s of the instrument package, this range amounted from 100 to over 200 shear estimates per depth bin in the deep water, and more in the shallow layers, depending on the abundance of backscatterers. For the cast with the single instrument, the reduction of range lead to a decrease of shear estimates per bin, but as the water depth did not exceed 3000 m and the abundance of backscatterers was high, the resulting current data were still of good quality.

MAPR

Four Miniature Autonomous Plume Recorder (MAPR, courtesy of Dr. E. Baker, NOAA/PMEL) were used in addition to the CTD package for plume mapping. MAPR are self-contained instruments, which record data at pre-set time intervals from temperature (thermistor mounted in a titanium probe, resolution 0.001°C), pressure (0 - 6000 psi gauge sensor, resolution 0.2 psi), and nephelometer (Sea Tech Light Backscatter Sensor, LBSS) sensors. The instruments were attached to the hydrographic wire at distances between 50 and 200m from the CTD to extend the mapping range of towed yo-yo CTD casts, thus optimizing horizontal resolution and vertical range of the mapping.

Three of the instruments were working fine throughout the cruise; the forth instrument showed some erratic behavior and unrealistic high backscatter signals.

Helium

For measurements of the He concentrations and isotopic signature, water samples were taken from Niskin bottles of the rosette (258 samples in total) and the ROV (5 samples) and sealed head space free and gas tight in copper tubes (sample volume 40 ml). Special containers for sampling vent fluid (developed and tested in the frame of the SPP) were used by the ROV pilots. The sampling containers can keep a pressure of more than 3·107 Pa and avoid phase separation of vent fluids and gases. He isotope measurements will be performed at the IUP, section of Oceanography, at the University of Bremen with a fully automated UHV mass spectrometric system. The sample preparation includes gas extraction in a controlled high vacuum system. He and Ne are separated from permanent gases in a cryo system at 25 K. A split of the sample is analyzed for ^{4}He, ^{20}Ne and ^{22}Ne with a quadrupole mass spectrometer. At 14 K He is separated from Ne and released into the sector field mass spectrometer for analysis of ^{3}He and ^{4}He. The facility achieves about ± 0.2 % precision for $^{3}He/^{4}He$ ratios, and ± 0.5 % or better for helium and neon concentrations (for details see Sültenfuß et al. 2006).

The primordial components of helium isotopes are ideal tracers for large-scale distribution of vent fluids in the water column also in the South Atlantic (Rüth et al. 2000). Samples of this cruise should provide a picture of a more regional distribution of dispersing vent fluids in the

water column leading to an estimate of its volume. $CH_4/^3He$ ratios separate CH_4 of hydrothermal fluids from other sources.

ROV Experiment
During two of the ROV dives (24 ROV & 69 ROV), one of the ADCPs was mounted on the frame of the ROV to measure vertical velocities of the rising plume of the Sisters Peak and Drachenschlund smokers, respectively. Additionally, a pumped MicroCat (Sea-Bird Electronics, Conductivity and Temperature Recorder SBE 37-SMP) which measures temperature, salinity and pressure at high precision (absolute precision $\Delta T = 0.002°C$, $\Delta C = 0.0003S/m$, $\Delta p = 0.1\%$ of the max. range) , was lowered into the plume to monitor coinciding temperature fluctuations.

Mooring
A current meter mooring was equipped with 3 Aanderaa Recording Current Meter RCM 11 which measure acoustically current speed ($\Delta V = 0.0015m/s$) and direction ($\Delta° = 5°$). All instruments carry a temperature sensor ($\Delta T = 0.05°C$), two of them are fitted with a pressure gauge ($\Delta p=0.25\%$ of the max. range).

vmADCP
Additionally, shipboard ADCP (75 kHz Ocean Surveyor) data were recorded on the transit across the equator from the rim of the Brasil trading zone at 1°N to the working area at 5°S on request of P. Brand (PI M68/2).

FLOATs
Four ARGO floats (R.J. Roddy, NOAA/AOML) were launched during the transits to and from the working area crossing 45°W, 40°W, 35°W, and 17°W latitude.

1.4.5.2. First results

5° S area (Turtle Pits, Red Lion and Comfortless Cove fields)
The work in the 5°S area comprised 12 hydrographic stations in total. Two hydrographic sections with 3 profiles each (CTD/LADCP/Water sampling/130 Helium samples) were carried out north (8 CTD, 9 CTD, & 10 CTD) and south (16 CTD, 17 CTD, & 18 CTD) of the 5°S area. The local topography is closed to the sides below a water depth of 2500 m, hence these two sections form a box where measurements of the current field and the stratification allow to calculate fluxes of volume, heat and helium into and out of the vent field area.

The area was dominated by along-valley northward currents with a slight westward component, which were modulated in strength with a tidal frequency. The average current velocity below a depth of 2500 m was 5 cm/s, with maxima of more than 15 cm/s. The strongest currents were orientated northward (Fig. 1.31). The volume transport associated with the flow amounts to 0.25 Sv (10^6 m^3/s) across the section north of the vent sites.

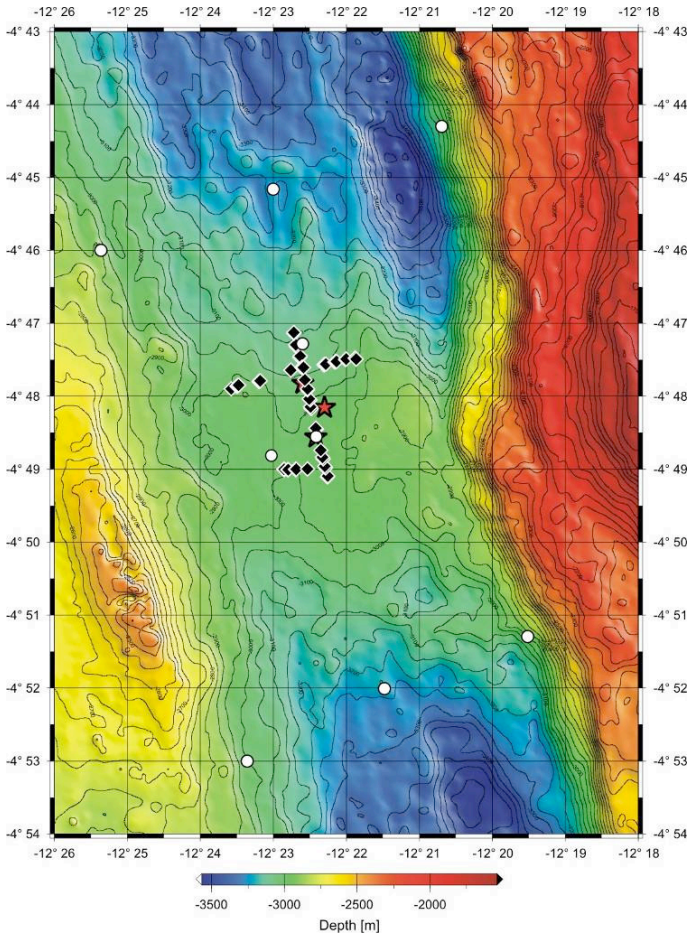

Fig. 1.30: Map of the 5°S working area. Red stars denote the vent sites, white dots classical CTD/LADCP stations and black diamonds water samples during tow-yo casts. Map by O. Schmale.

For an accurate determination of the background flow field and for the precise determination of tidal amplitudes and phases, a one-year current meter mooring was deployed at the sill of the valley, in the center of the vent fields at 12°22.5'S, 4°48.2'S.

A detailed mapping of the hydrothermal plumes, both along and across the axis of the valley, was accomplished with 3 towed transects of a CTD/MAPR combination (Tow-yos, 13 CTD, 19 CTD, and 22 CTD), where up to four MAPR were mounted in a distance from 50 to 200 m above the CTD on the cable.

The horizontal and vertical extent of the plumes in the water column could be detected by the observation of several parameters as potential temperature ($\Delta\Theta$), backscatter (Δntu), and redox potential (Eh).

The along-valley tow-yo track (13 CTD) crossed the latitudes of the three sites Turtle Pits, Comfortless Cove, and Red Lion (Figs. 1.30, 1.32), and shows clearly the different temperature anomalies in the effluent layers of the plumes of Turtle Pits and Red Lion (Comfortless Cove is located further east of the track than the other two, and not as easily identifiable as the other two), which are shifted to the north from the sources, coinciding with the dominant flow direction. Weaker signals upstream of the known vent sites indicate the possible presence of yet

unknown (possibly diffusive) vent sites. The maximum (negative) temperature anomalies exceeded 1/100K on this transect.

The across-valley tow-yos show that the plume is focused in the centre of the valley, and has a lateral extent of less than one kilometer (Fig. 1.33).

The density field in the 5°S area is dominated by the flow over the sill in the axial valley. Downstream of the sill, the isopycnals (and hence the plume anomalies) deepen and the water column stretches as a result.

Further work in this area consisted of one profile at Turtle Pits (4 CTD), Red Lion (5 CTD), and the location of a turbidity anomaly detected by ABE a year before (1 CTD), respectively, to determine the amplitude of the anomalies and the density range of the effluent layer close to the sources.

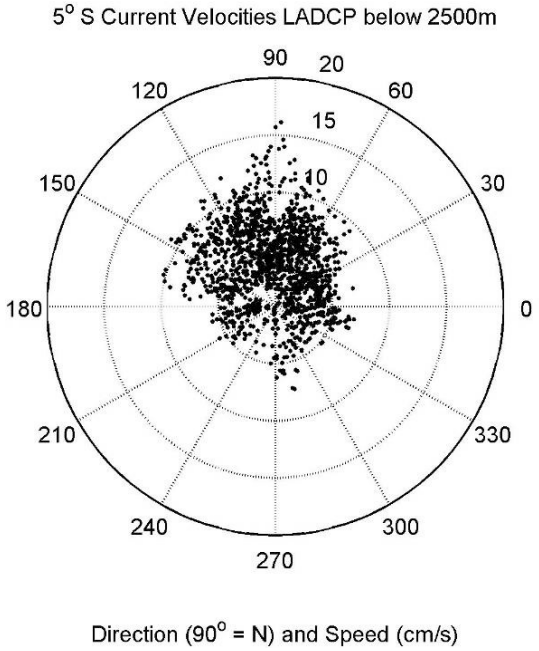

Fig. 1.31: Scatter plot of amplitude and direction of the currents measured below 2500 m water depth in the 5°S area. Most of the data points have a northward component, i.e. fall into the E-N-W segment of the diagram (N=90°). The amplitude of these deep currents (distance from the centre of the plot) ranges from a few centimeters to more than 15 cm/s.

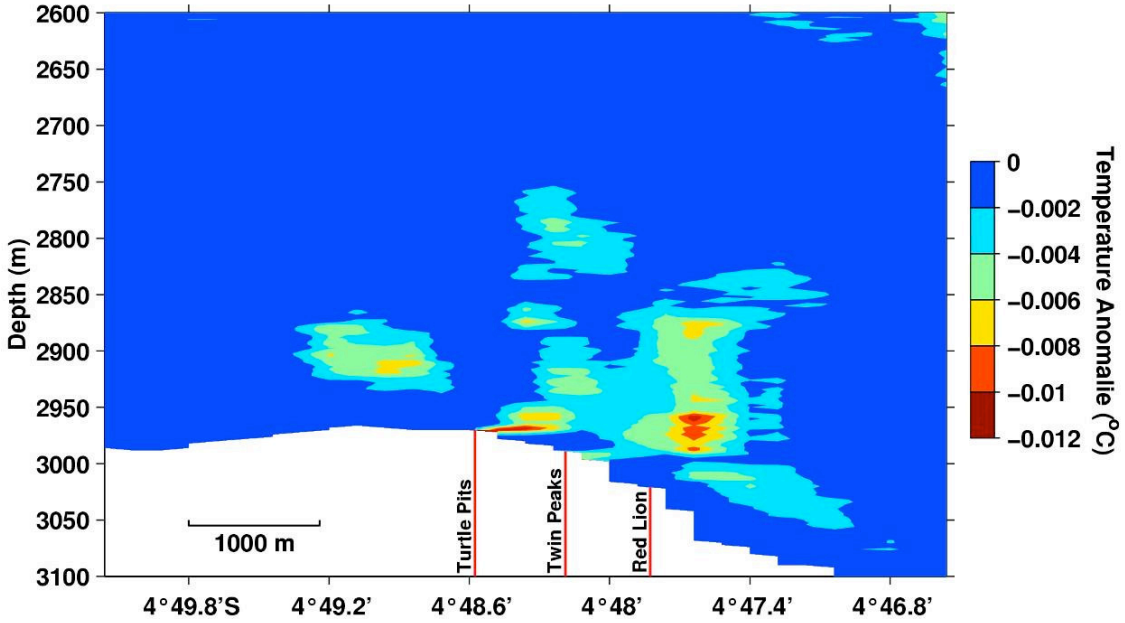

Fig. 1.32: Anomalies of potential temperature Θ along a south-north orientated tow-yo track (13 CTD) across the 5° S vent sites. The positions of the hydrothermal sites Turtle Pits, Comfortless Cove and Red Lion are marked in red. Currents are predominantly northward; the temperature anomaly south of Turtle Pits is thus upstream of the known vents and could not be clearly assigned to a source.

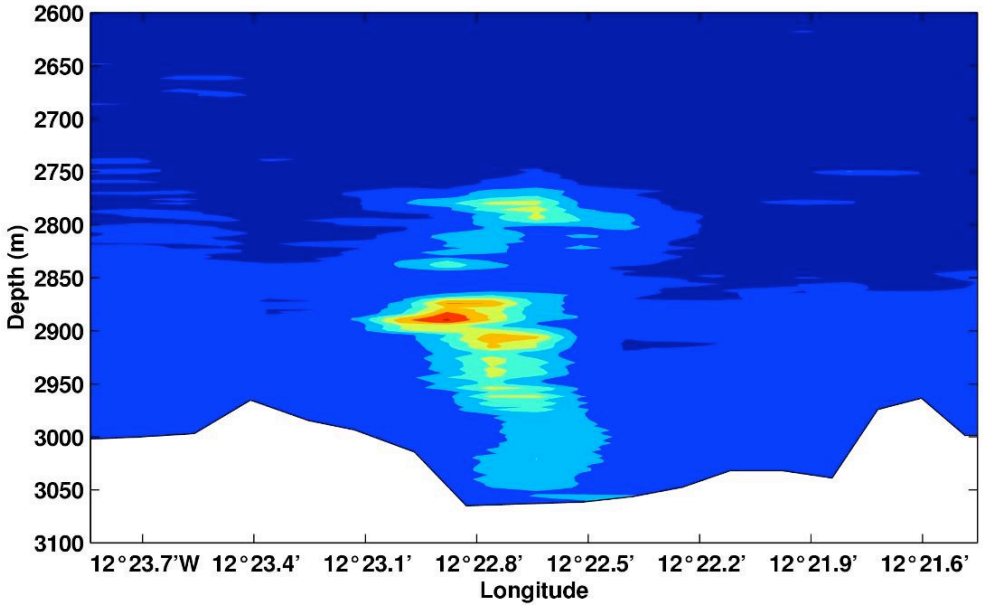

Fig. 1.33: Backscatter signal along a west-to-east orientated tow-yo track north of the 5° S vent sites (22 CTD). The lateral extent of the core plume signal is < 1km. Data from the CTD nephelometer in Δntu relative to background.

9° S area (Lilliput)

Since the 9°33´S site is quite shallow (1500 m), hydrothermal anomalies in the water column are difficult to observe. Hydrothermal fluids in shallower areas have lower maximum temperatures and lower metal contents and hence often carry no turbidity signal; on the other hand, the background variability of temperature is high in this depth range because it is situated between the shallow Antarctic Intermediate Water and the upper North Atlantic Deep Water (cf. Fig. 1.35).

The hydrographic work at the site was therefore restricted to a profile directly at the Lilliput field (27 CTD), which showed only minor anomalies in turbidity and redox potential close to the seafloor.

Additionally, a series of 3 stations (29 CTD, 34 CTD, & 37 CTD) was carried out from the spreading axis out to the east to study the far field plume spreading and dilution away from the valley by means of the primordial Helium signal.

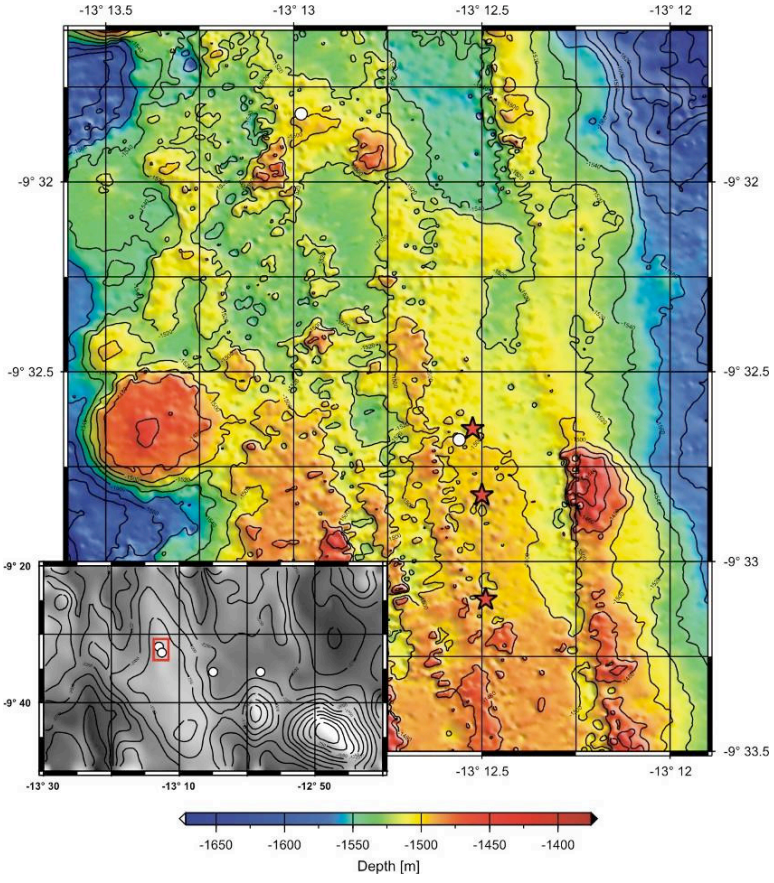

Fig. 1.34: Map of the 9°S working area. Red stars denote the vent sites, white dots classical CTD/LADCP stations. Map by O. Schmale.

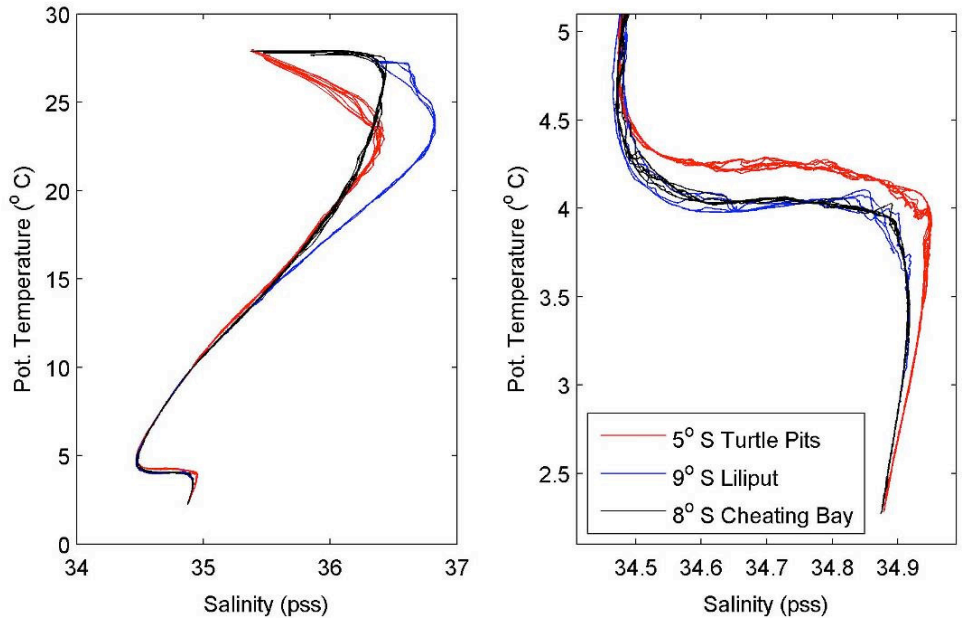

Fig. 1.35: Temperature-Salinity diagram of all three working areas. (Salinity values are preliminary).

8° S area (Nibelungen field, Cheating Bay)

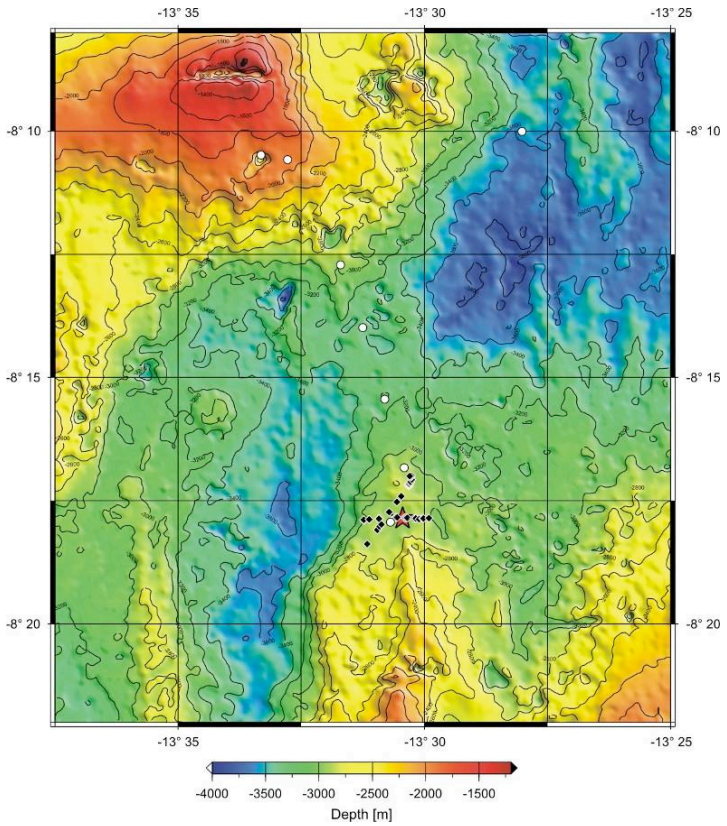

Fig. 1.36: Map of the 8°S working area. Red stars denote the vent sites, white dots classical CTD/LADCP stations and black diamonds water samples during tow-yo casts. Map by O. Schmale.

The part of the working area at 8°S named aptly “Cheating Bay” was subject to thorough hydrographic work during the Meteor cruise M62/5 in December 2004. Because of the complex current patterns and strong tidal variability, it had not been possible to detect the exact location of the vent site causing the observed hydrothermal plume signal.

The work in Cheating Bay started therefore with the reoccupation of the M62/5 station 1230 (43 CTD), which had shown the largest anomalies in turbidity and methane during that cruise. Again, large anomalies of those two parameters were found in the depth range between 2680 and 2750 m, with a second maximum between 2800 and 2900 m.

The two cores of the plume signal were already observed during M62/5; they are probably caused by the strong mixing in the region which is modulated in strength by the tidal cycle and affects the stratification at the vent site and hence the density horizon of the effluent layer.

The strong mixing in the form of internal wave breaking (which gives rise to the short-lived occurrence of density inversions and well-mixed layers) is also hampering the detection of temperature anomalies in this area, so plume mapping is restricted to turbidity and methane anomalies. Directly in the plume, there is a strong signal in the turbidity and only a somewhat heightened variability in T and S. The methane and hydrogen output of the Nibelungen field is rather strong (see Chapter 1.4.6. on Gases in hydrothermal fluids and plumes).

Two tow-yo casts (one -47 CTD- from S to N across the position of the large anomaly, the other -64 CTD- approximately in W-E direction on a line crossing the large anomaly position as well as the now known position of the source) confirmed the already suspected strong temporal variability of the plume spreading in Cheating Bay: During the first track (Fig. 1.37), the plume signal was clearly visible west of the now known position of the source (the black smoker ‘Drachenschlund’ at 8°17.865’S, 13°30.440’W). During the second cast, no anomaly could be traced at the location of the former large-anomaly position, but strong turbidity and methane signals were observed to the east of the source (Fig. 1.38). It is not clear yet whether these latter anomalies belong to the same source (Drachenschlund), or whether there is a second vent site located even farther to the east.

Despite the failure to find the source of the hydrothermal signal in the water column during M62/5, the horizontal spreading of the plume was satisfactory mapped in both along and across rift valley direction. Virtually no traces of elevated turbidity and methane were observed at the outer edges of the station grid, thus the calculation of inventories is possible.

To complete the mapping, and to compare the background flow condition to those in 2004, a transect of 4 CTD/LADCP/water sampling profiles (49-52 CTD) was measured across the rift valley at the shallow sill north of Cheating Bay.

As an attempt to measure the strength of the Drachenschlund vent and to complement the calculation of the output of the source by helium inventories, an ROV experiment was conducted with combined measurements of fluctuations of temperature and vertical velocities in the rising plume. The magnitude of the vertical velocities w was between 10 and 20 cm/s at heights between 5 to 20 m above the crater; several orders of magnitude larger than the typical w (10^{-7} m/s) in the ocean, and enough to lift the ROV considerably up.

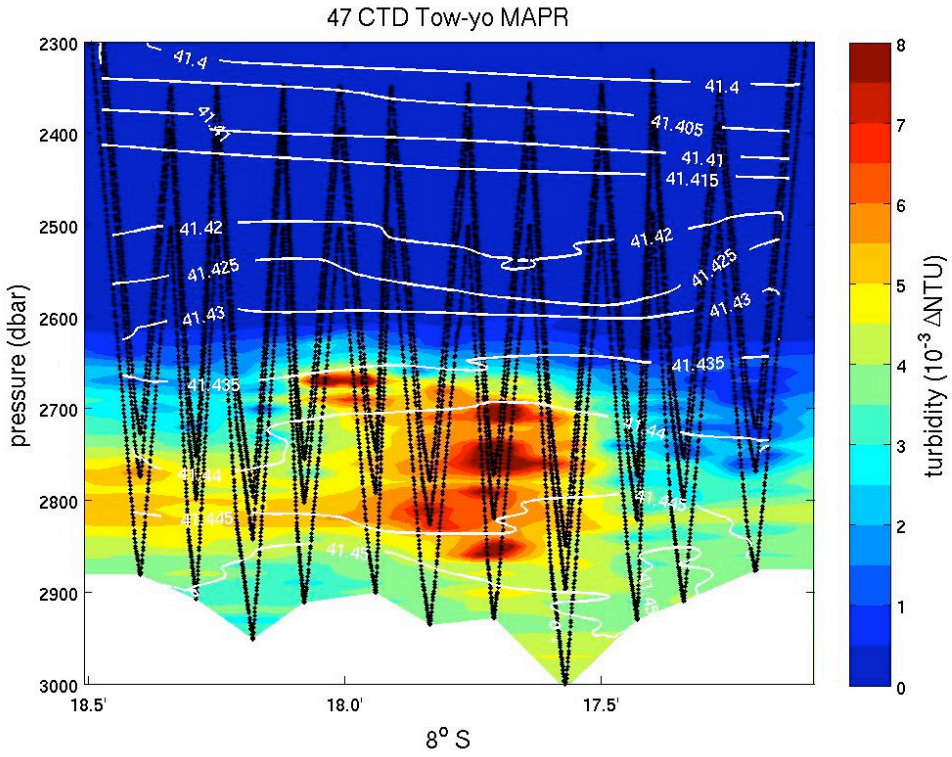

Fig. 1.37: Turbidity anomaly along a Tow-yo track with CTD and MAPR (Miniature Autonomous Plume Recorder) across the plume dispersion in S-N direction in the Nibelungen field.

The cause of this anomaly, the black smoker 'Drachenschlund' is situated at 8°17.9'S. Due to the hydrothermal output, the turbidity is enhanced in the whole region below a depth of 2500m. White lines represent isopycnal surfaces, black lines denote positions of the different instruments along the track. Data from MAPR in Δntu relative to background.

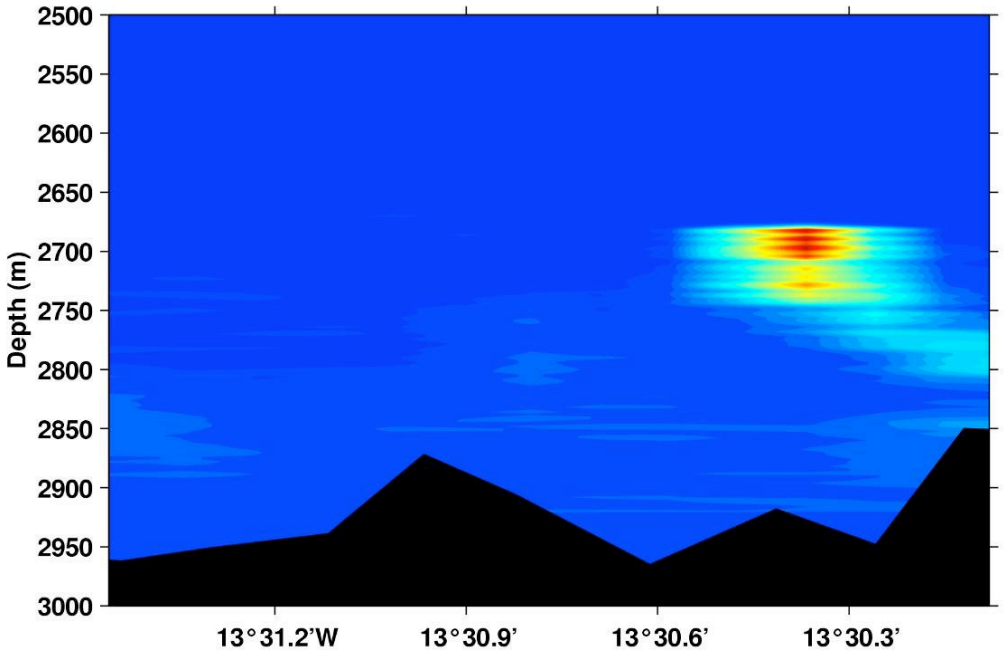

Fig. 1.38: Turbidity anomaly of a E-W Tow-yo (64 CTD) track from CTD and MAPR across the black smoker 'Drachenschlund', 8°17.865'S, 13°30.440'W. It is not clear whether this plume signal emanates from Drachenschlund or from an unknown vent to the east. Data from the CTD nephelometer in Δntu relative to background.

During M62/5, a methane maximum was observed at a depth of approximately 1900 m on the western wall of the rift valley at a latitude of 8°10'S. Since this was an isolated measurement and no further information about the (possibly hydrothermal) source of this was available, a repeat of this station was carried out, and two more CTD/water sampling profiles were taken at a submarine hill in the inside corner between segments A1 and A2 to localize the origin of the methane plume (59 CTD, 67 CTD, & 72 CTD). The signals found during the casts were small, but consistent (temperature and backscatter anomalies close to the seafloor at a depth of about 1900 m). However, there were no significant gradients, and the deep currents were variable, so no clear target could be identified.

Another CTD Tow-yo cast (45 CTD) in the 8°S area was done as a preparation for the AUV exploration at 7°57'S. This area was chosen as a potential target because it showed strong turbidity and accompanying temperature anomalies close to a terraced structure at the western rift valley in the TOBI/MAPR deployments of M62/5. This years' tow-yo data could indeed identify a distinct plume with its maximum turbidity anomaly lying directly above the terraces (Fig. 1.39). However, the subsequent AUV dives did not result in the clear localization of the hydrothermal source, and no further work was done in that area.

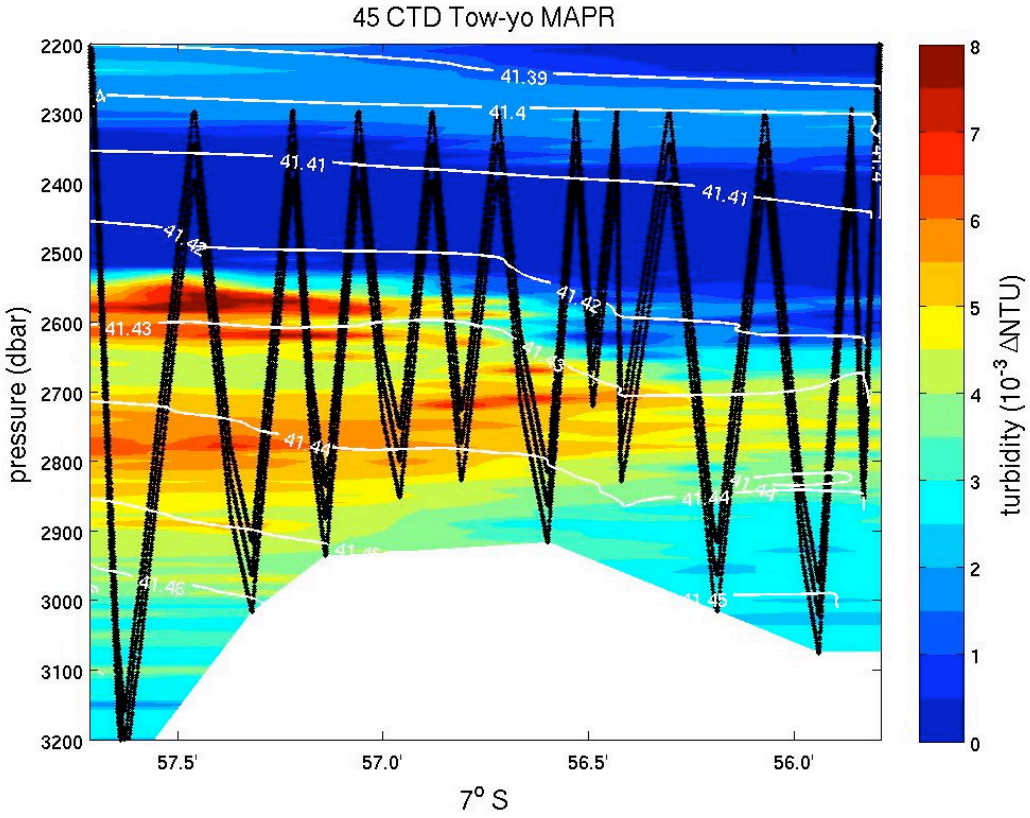

Fig. 1.39: Backscatter signal from MAPR LSS sensors along tow-yo track at 7°57' S. The turbidity anomaly was accompanied by an -albeit small- temperature anomaly, which indicates the presence of a hydrothermal source somewhere in the area. White lines represent isopycnals, black lines denote positions of the different instruments along the track. Data from MAPR in Δntu relative to background.

1.4.6 Gases in Hydrothermal Fluids and Plumes

(R. Keir, O. Schmale, R. Seifert, S. Weber)

Hydrothermal vents produce variable amounts of methane and hydrogen that depend on geological controls and on the temperature of the venting. These gases were measured on board during M68; the measurements were carried out on water column samples and on vent fluids obtained during the ROV dives. In addition, gas samples were conserved for subsequent carbon isotope analysis in the isotope laboratories at IFM-GEOMAR and at the University of Hamburg. Table 1.3 contains a list of the methane and hydrogen measurements carried out on these stations as well as on vent fluids collected during the ROV dives.

Table 1.3 a: Sample list for CTD-stations.

Station	Profile	Long. W	Lat. S.	CH_4	$\delta^{13}CH_4$	δDCH_4	H_2	δD
1CTD	001	12°23.022	4°48.804	20	20		18	
4CTD	002	12°22.414	4°48.554	14	14		11	
5CTD	003	12°22.60	4°47.28	14	14			
8CTD	004	12°19.514	4°51.297	16	16		14	
9CTD	005	12°21.479	4°52.010	16	16			
10CTD	006	12°23.36	4°53.0	16	16			
13CTD	007	Tow-yo		22	22		17	
16CTD	008	12°25.36	4°46.0	16	16			
17CTD	009	12°23.0	4°45.16	17	17			
18CTD	010	12°20.693	4°44.299	17	17			
19CTD	011	Tow-yo		10	10			
22CTD	012	Tow-yo		21	21			
27CTD	013	13°12.98	9°31.82	19	19		17	
29CTD	014	13°05.01	9°35.51	22	22		19	
34CTD	015	12°58.01	9°35.50	21	21			
37CTD	016	13°12.560	9°32.679	18	18		16	
43CTD	017	13°30.69	8°17.94	21	21		15	
45CTD	018	Tow-yo		22	22			
47CTD	019	Tow-yo		19	19		15	
49CTD	020	13°30.41	8°16.50	16	16		15	
50CTD	021	13°30.803	8°15.440	17	17		14	
51CTD	022	13°31.25	8°13.99	16	16		15	
52CTD	023	13°31.70	8°12.71	16	16		15	
59CTD	024	13°28.021	8°10.009	21	21		8	
64CTD	025	Tow-yo		22	22		21	
67CTD	026	13°33.316	8°10.484	15	15		14	
72CTD	027	13°32.78	8°10.58	17	17		8	

Table 1.3 b: Sample list for ROV-stations

Station	ROV	Purge ^ Trap CH_4	Vacuum Extraction CH_4	$\delta^{13}C$ CH_4	δD CH_4	H_2	δD H_2	Fluid
3	ROV	4	12	6		6	1	1
7	ROV	2	6	6	2	6		
12	ROV	1	3	3	1	4		
20	ROV	2	4	4	1	5		
24	ROV	2	6	6		5		
39	ROV		4	4		2		
41	ROV		12	6		6		
62	ROV	2	3	3	4	4	3	
69	ROV	2	2	2	2	4		
70	ROV		6	6		6		

1.4.6.1 Methods

In order to analyze methane and hydrogen by gas chromatography, the dissolved gases were extracted from the seawater sample by one of three techniques. The majority of the water samples obtained from the CTD casts were processed by the partial vacuum technique described by Rehder et al. (1999). Briefly, the water samples are drawn from the Niskin bottle into an evacuated 2-liter bottle, which is filled up to about 70%. During this time, much of the gas effervesces into the gas phase, which is then transferred to a gas burette. Two aliquots of the gas were then sampled from the burette with a gas-tight syringe. One was injected into a GC equipped with a flame ionization detector in order to analyze methane; the other aliquot was injected into a second GC equipped with a pulse discharge detector in order to analyze hydrogen. The remaining gas was then transferred to a pre-evacuated glass vial through a septum, which was sealed with silicone on the outside and a saturated salt solution on the inside. These gas samples will be analyzed for the $^{13}C/^{12}C$ ratio of methane in laboratories at IFM-GEOMAR and the University of Hamburg. This same procedure was used to analyze fluids obtained by the KIPS sampler on the ROV. In this case the fluid was drawn into evacuated 500 ml bottles, which were half filled. In total, about 800 and 600 individual measurements were performed for hydrogen and methane respectively.

Two additional methods of extracting the gas samples were applied to selected samples. Methane was stripped and concentrated using the purge and trap technique (Seifert et al., 1999). This gas was then released directly into a gas chromatograph equipped with a FID. Dissolved gasses were also extracted by applying high vacuum and ultrasound to the water sample while being heated up to the boiling point. As with the partial vacuum technique, aliquots of the gas were analyzed for hydrogen and methane on separate gas chromatographs.

The partial degassing method mentioned above does not extract 100% of the gas from the seawater, and therefore the concentration of dissolved methane in the fluid that is calculated on the basis of the gaseous mole fraction and the observed volume of extracted gas is systematically low. In order to investigate this effect, experiments were performed where variable volumes of

seawater were extracted from the same Niskin bottle, and the volume of gas and mole fractions of methane and hydrogen were measured. In addition, some of the sample flasks were treated with ultrasound and heated or were pre-loaded with salt in order to increase the extraction efficiency. These results are being compared to those obtained from the other two methods described above as an aid to correcting the final data.

1.4.6.2 Methane and Hydrogen in the Water Column

Twenty seven CTD stations and tow-yos were carried out during M68/1 (Table 1.3 a). Selected preliminary results are given below.

5°S

At 5°S, a series of stations and tow-yos bracketed vent sites located on the sill in the middle of this rift valley segment (Fig. 1.30). Despite the presence of these sources, methane concentrations in the surrounding water remained relatively low (Fig. 1.40). At depths greater than 1000m, methane concentrations are mostly about 0.5 nmol/L. A few samples exhibited higher concentrations of about 1 nmol/L in the vent plumes. In contrast, hydrogen increased sharply in the vent plumes at about 2800 to 3000m, with concentrations reaching 25 nmol/L. This contrast may be due to the nature of the venting in this area, some of which is characterized by extremely high temperature fluid in volcanic systems that produce high hydrogen to methane ratios. The highest methane (3.5 nmol/L) and hydrogen (25 nmol/L) in the water column were observed in a plume to the east of Red Lion (Fig. 1.41)

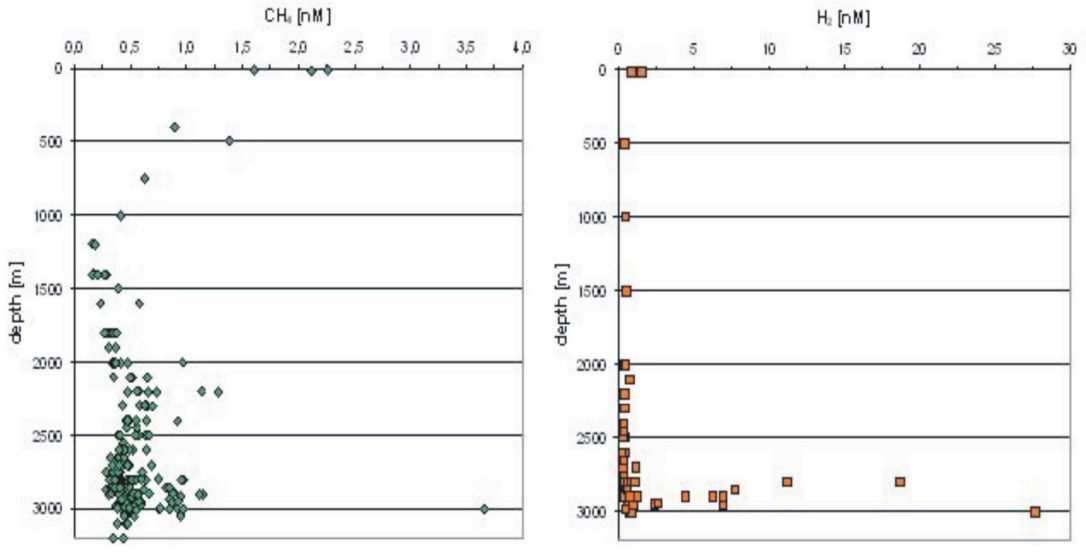

Fig. 1.40: Methane and hydrogen versus depth in 5°S area.

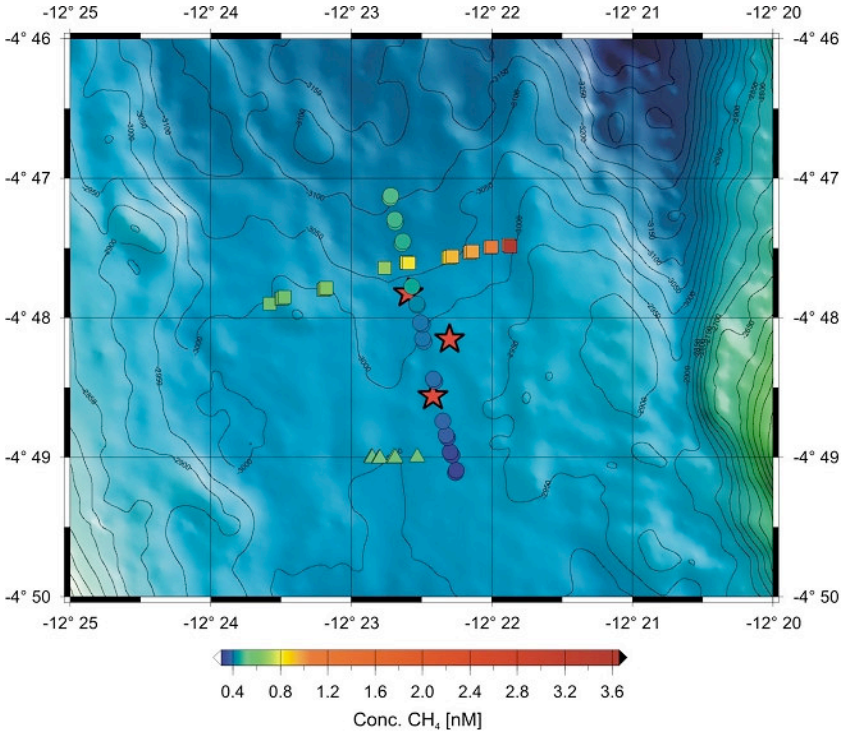

Fig. 1.41: Sampling positions of 5°S tow-yo stations with methane concentrations color-coded.

9°30'S

In this region, 4 CTD stations were conducted (Fig. 1.34). The two on-axis stations clearly showed an increase of methane and hydrogen in the bottom water. One of these stations was located near the Lilliput vent; the other was taken near an expired mussel bed observed during cruise M64. The presence of bottom methane and hydrogen in this area may indicate that venting may be taking place nearby (Fig. 1.42). The profiles at these stations indicate there may also be a weak plume signature at about 1000m depth.

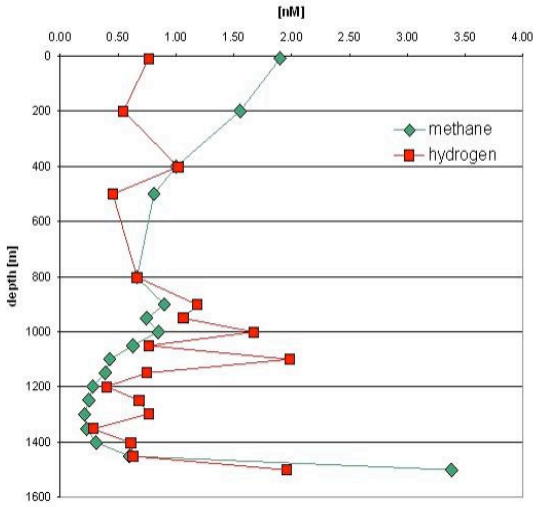

Fig. 1.42: Methane and hydrogen versus depth at 9°31.8'S, 13°13'W.

8°S

Several vertical CTD profiles were taken between 8°10'S and 8°20'S along the Mid-Atlantic Ridge, and 2 tow-yos were conducted across Cheating Bay at about 8°18'S (Fig. 1.36). We first re-occupied Station 1230 of M62/5, where a very strong methane anomaly had been observed in December, 2004. Once again, a methane plume containing about 50 nmol/L was observed at this position. Hydrogen concentrations reached 700 nmol/L in this plume (Fig. 1.43). A subsequent AUV dive discovered a black smoker about 650 meters to the east of this position ("der Drachenschlund"). It would appear that the very much higher fluxes of methane and hydrogen from this vent are responsible for plumes in the surrounding region that often contain on the order of 10 nmol/L CH_4.

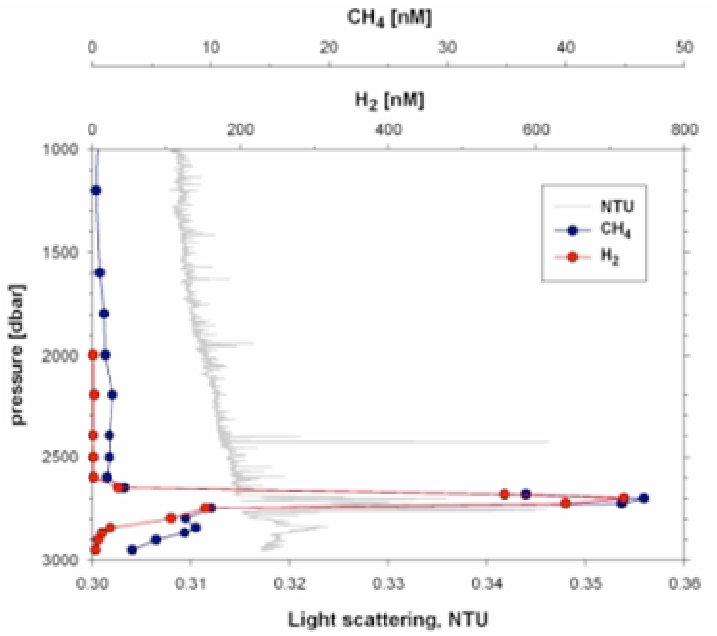

Fig. 1.43: Methane, hydrogen and optical backscatter at Station 43CTD (8°17.9'S, 13°30.7'W).

A subsequent tow-yo CTD from east to west over the "Drachenschlund" found a plume sitting to the east of this vent (Fig. 1.44). Whether the plume from the Drachenschlund shifted with the currents or whether it originated from a second vent located farther to the east is not known at this time.

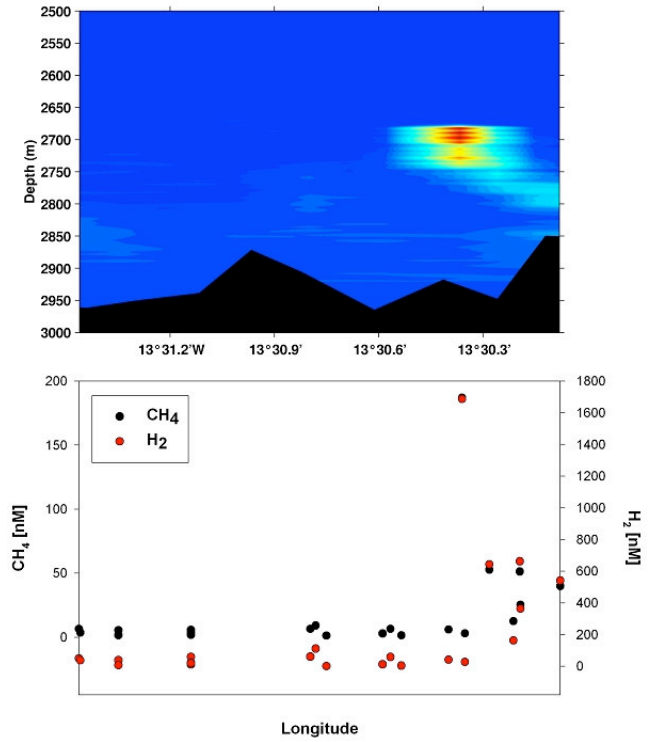

Fig. 1.44: Tow-yo (64CTD) from east to west across the "Drachenschlund" vent at 13°30.4'W. Upper section shows turbidity anomaly. The lower diagram shows methane and hydrogen concentrations of the discrete water samples as a function of position.

In Fig. 1.45, we show a diagram of hydrogen versus methane concentrations for all paired measurements on the same extracted gas samples. The good correlation between the measurements appears to be because of the trend found in Cheating Bay, which contained almost all of the higher gas concentrations measured in the water column. The ratio of hydrogen to methane increase appears to be about 14:1, which is about twice that observed in the Drachenschlund vent fluid. The reason for this is not known; this rather surprising result is subject to corrections that need to be made for incomplete gas extraction.

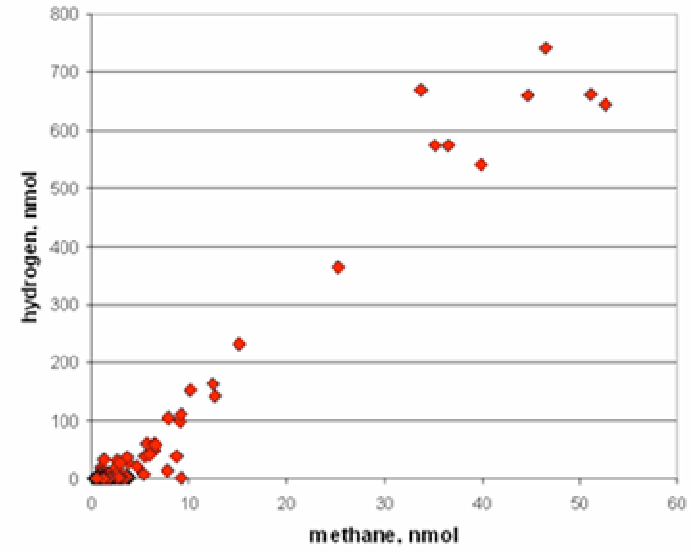

Fig. 1.45: Water column hydrogen versus methane for M68 stations.

Besides Cheating Bay, CTD stations were conducted in the rift valley and adjacent to the promontory located at 8°09'S, 13°34'W (Fig. 1.36). The latter stations were taken because a methane anomaly had been observed to the east, at 8°10'S, 13°28'W on previous cruise M62/5 as well as on the repeat station of this cruise (59CTD). As a first guess, two stations were placed on the ledge at the southeast corner of the promontory. The results of the hydrogen and methane measurements show that methane sharply increases to about 4 nmol/L in a 100 m thick layer above the bottom and that hydrogen increases by a small amount (Fig. 1.46). These results indicate that there is venting from near the top of the promontory at circa 2000m depth but that we were not in the immediate vicinity of the vent with our first attempts.

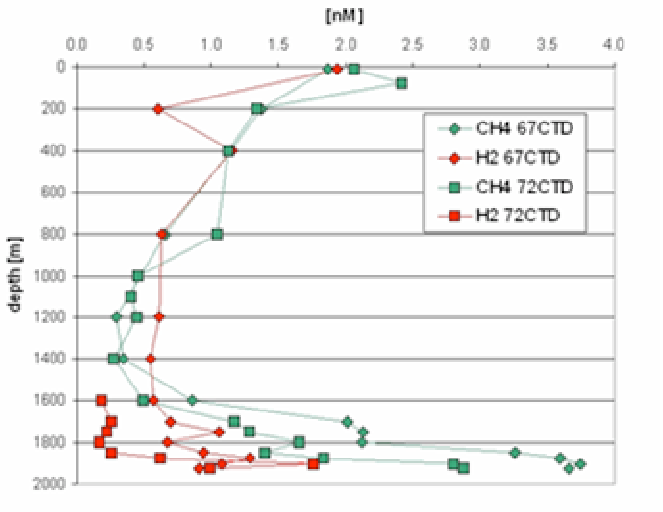

Fig. 1.46: Methane and hydrogen versus depth near 8°10'S, 13°33'W.

1.4.7 Metals and Other Compounds in Hydrothermal Fluids and Plumes

(D. Garbe-Schönberg, S. Sander, J. Mawick, M. Peters, A. Koschinsky)

1.4.7.1 Sampling and Analytical Methods

Hydrothermal fluids are characterized by their unique chemical and isotopic composition, which is significantly different from ambient seawater (e.g., von Damm, 2004). Scientific objectives for fluid chemical analyses, both on-board and subsequently in the home laboratories, include the detection of hydrothermal plumes in the water column, and a quantification of the chemical and isotopic composition of hydrothermal fluids discharging from the ocean crust via distinct vent sites - either through black smokers or diffuse venting.

Three different types of samples were collected for chemical and isotopic analyses: (i) vent fluid samples collected with the Kiel Pumping System (KIPS) by inserting a titanium sampling nozzle into the orifice of smoker structures; (ii) samples from discharging vent sites collected with three Niskin flasks (5 l volume), mounted at the front of the MARUM ROV QUEST; (iii) water column samples from the CTD/Rosette, equipped with 24 bottles à 10 l volume.

1.4.7.1.1 Sampling With the KIPS Fluid Sampling System

One pre-requisite for an accurate estimate of the composition of hydrothermal fluids venting at high-temperature Black Smokers or from diffuse mussel-field sites is sampling of the hydrothermal fluids without entrainment of ambient seawater which would cause immediate precipitation of sulphides and barite and, hence, loss of these compounds from solution. One important measure of the purity of the sampled hydrothermal fluid is temperature. Consequently, real-time *in-situ* measurement of the temperature helps to guide the tip of the sampling nozzle to the hottest region within the vent orifice where the purity of the venting fluid is highest and least diluted with seawater. Another pre-requisite is that all materials coming into contact with the sampled fluid are inert and have lowest adsorption coefficients preventing systematic errors introduced by either contamination or losses due to adsorption. Precipitation during cooling of the sampled fluid, however, cannot completely be avoided.

A fully remotely controlled flow-through system – the Kiel Pumping System (KIPS-3) - mounted on the ROV's starboard tool sled was used for this purpose (Garbe-Schönberg et al., 2006). The parts of the system getting into contact with the sample are entirely made of inert materials: perfluoralkoxy (PFA) and polytetrafluorethylene (PTFE, Teflon®), and a short tube of high-purity titanium (99.9 % Ti). Fluid enters via this titanium tube (50 cm length, 8 mm I.D., bent to 45°) - the nozzle – mounted to a T-handle which is guided by the ROV's ORION manipulator arm. Parallel to the titanium nozzle is a high-temperature sensor (see below) delivering real-time temperature data for the tip of the nozzle. Coiled PFA tubing (3/8" O.D., 3 m length) connects the nozzle to a remotely controlled multi-port valve (PETP/ PTFE) delivering the fluid to the respective sampling flask. The valve is driven by a stepper motor (electric actuator, Schilling Robotics, U.S.A.) with software fully integrated into the ROV control system (ROV Hub 2, port #26, software FluidCtrl V. 0.2.2.9, by Marum Soft, Bremen).

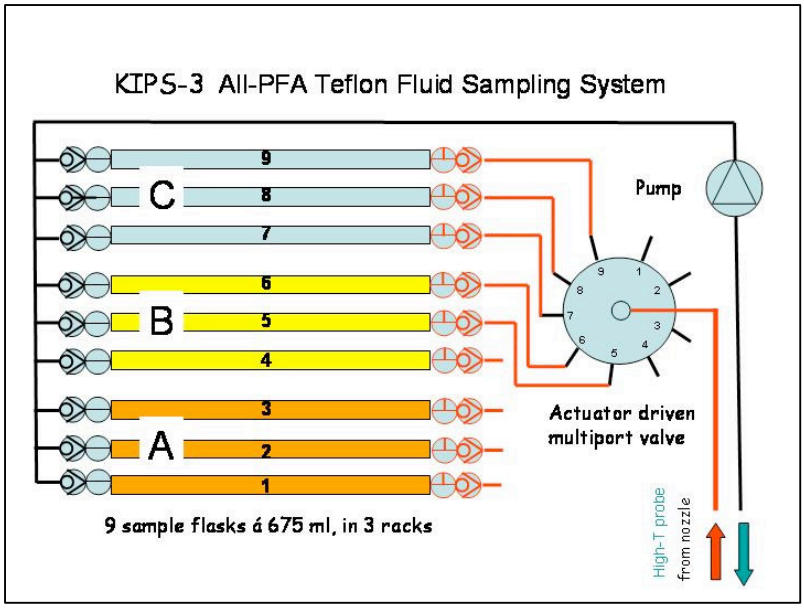

Fig. 1.47: Schematic configuration of the inert KIPS fluid sampling system (only tubing connections to flasks # 5 - # 9 are shown for clarity). Fluid entering the nozzle is distributed by a motorized multiport-valve to 9 PFA sample flasks of 675 ml, each with check valves and stopcocks. The pump is positioned downstream. Racks A, B, C with 3 flasks each can be quickly removed and sub-sampled in the lab.

The multiport valve has 9 ports connected to 9 single PFA flasks with 675 ml volume each (Nalgene, USA). Each bottle was equipped with a check valve at the outlet. The flasks are mounted in three racks A-C, with every rack containing three horizontally positioned bottles, allowing an easy transfer of the racks to the laboratory where sub-sampling was done. Flasks were pre-filled with ambient bottom seawater (North Atlantic Deep Water, NADW) obtained from CTD hydrocasts. A 24 V deep sea mechanical gear-pump is mounted downstream to the sample flasks, thus avoiding contamination of the samples. The pumping rate can be adjusted by the voltage applied from the ROV's dimmable port (Hub 2, port # 2); it was set to approx. 800 ml/ min at 26 VDC. The standard pumping time per sample was set to 4-5 min making sure that the flask volume was exchanged at least 4 times. The outlet of the KIPS system is located on the porch at the front-side of the ROV, where video control allows the observation of warm fluids leaving the system. In addition, a flow mobile was attached to the outlet tube.

Fig. 1.48: ROV "QUEST" with KIPS mounted on the starboard side of the tool sled

A high-precision thermistor temperature sensor (manufactured by H.-H. Gennerich, Bremen) inside a stainless steel pressure housing was attached parallel to the nozzle. The sensor is connected to the ROV's modified CTD-60_77 (Sea and Sun, Trappenkamp, Germany) using two channels for data handling: a broadband channel for temperatures < 100 °C, and a dedicated high-temperature channel for the range 100 – 450 °C. The 90% time constant of the sensor in water is better than 12 s. Two individual sensors were used during this cruise: sensor #2 during dives #86 - #89, and sensor #1 for all subsequent dives. Calibration coefficients used during the cruise are tabulated in Table 1.4. A pre-cruise calibration was performed by H.-H.Gennerich with the CTD-60_77 housing equilibrated to 2.4 °C water temperature, simulating *in-situ* conditions during the cruise.

Table 1.4: Coefficients used for calculation of (A) temperatures for sensor #1 and #2, and of (B) sensor resistance with CTD-60_77: (R = a * counts + b).

(A) **Calibration coefficients**		A_0	A_1	A_2	A_3
Sensor #1	**T <100 °C**	-7.1037E-03	2.6691E-03	-2.4547E-04	8.1721E-06
	T >100 °C	8.3036E-04	2.7073E-04	-1.0624E-05	7.7696E-07
Sensor #2	**T <100 °C**	-7.8705E-03	2.8902E-03	-2.6623E-04	8.8036E-06
	T >100 °C	9.8E-03	1.7E-03	8.8239E-06	3.5546E-07

(B) **Resistance CTD-60_77**		**a**	**b**
	T <100 °C	3.048780	-774.28
	T >100 °C	0.060769	-648.21

First on-board analyses showed that hydrothermal fluids at the Turtle Pits and Sisters Peak high-temperature Black Smoker sites could be sampled with high purity: the chlorinity of 285 mM of fluids from the Turtle Pits *Marker #2 Vent* was very close to the hydrothermal endmember value of 269 mM extrapolated from samples taken during M64/1 in 2005.

1.4.7.1.2 Sampling of the Hydrothermal Plume With CTD Rosette Sampler

Subsamples from vertical CTD casts and CTD tow-yo stations were taken from the Niskin bottles of the rosette water sampler for the purpose of total dissolvable Fe and Mn analysis in plume and non-plume water layers. The non-filtered samples were filled in 100 ml acid-cleaned PE bottles and acidified with 100 µl of Suprapure HCl (30%) to pH ≤2. The samples were partly analyzed onboard and partly stored for on-shore analysis.

1.4.7.1.3 Sub-sampling and Sample Preparation

Immediately after recovery of the ROV on deck, KIPS sample racks were transferred to the laboratory. Usually, 3-5 flasks were filled at each site. Two ml for the analysis of dissolved Mg as a measure for hydrothermal fluid purity were taken from every flask. For subsequent analyses of dissolved ions the complete volume of one flask was transferred to a N_2-flushed FEP bottle, homogenised, and then sub-sampled for the different analytes. Another flask was dedicated for the analysis of dissolved gases and isotopic composition, the sampling technique is described elsewhere in the respective gas chemistry chapter. An overview scheme of sub-samples taken is given in Table 1.5.

Table 1.5: Overview of sub-samples taken and analytical parameters determined on-board and, later, to be determined in the home laboratories.

Analysis on-board	diss. Oxygen (Winkler)	filtered/ not filtered acidified	Filtered/ not filtered not acidified		Ligand titration	Fe, Mn, Zn, Cu (ASV)	Eh, pH, sulphide, Cl, Mg		C1-C4 HC	H2, CH4			Sulphide		
Analysis on-shore		REE, trace metals, major elements (CAU-KI)	Anions (CAU-KI)	Mg, Majors (CAU-KI)	Organic complexation (Uni Otago-NZ)	Trace metals, major and minor elements (IUB-HB)	Anions (IUB-HB)	Amino acids (IUB-HB)		C and H isotopes CH4 (Uni-HH)	H2 isotopes; organic compounds (Uni-HH)	S and O isotopes in dissolved sulfate (Uni-MS)	S isotopes in dissolved sulfide (Uni-MS)	O and H isotopes of water (Uni-MS)	DIC-C isotopes (Uni-MS)
Volume (ml)	10	100	20	2	100	100	50	200	120	250	250	2	600	5	20
	Bottle 1								Bottle 2			Bottle 3			

Dissolved Oxygen. Only warm diffuse fluids were analysed for dissolved oxygen by titration, hot sulfide-rich fluids would massively precipitate sulfides after treatment with KOH.

Dissolved Mg. From each KIPS sample flask 2 ml original sample were taken and acidified with two drops of subb. HNO_3. This sample will be used for calculation of the purity of the hydrothermal fluid contained in each KIPS bottle assuming that pure fluid has no Mg.

Dissolved Sulfate. 1 ml of a fluid sample was acidified with two drops of hydrochloric acid (25%) and treated with 0.5ml of a barium chloride solution (8.5%) to precipitate the dissolved sulfate as barium sulfate. At the University of Münster, sulfur and oxygen isotopic measurements will be carried out by masspectrometer (Finnigan Mat 251).

Dissolved Sulfide. Next to sulfide fixation with a zinc actetate gelatine solution and on-board measurement of the sulfide concentration (see below), 3ml of a fluid sample were taken to be treated with 1ml of a Monobromobiman solution to fix the sulfide and other thiols. The concentration of the different sulfur species will be determined by HPLC at the BGR, Hannover.

Dissolved Inorganic Carbon. 20ml of a fluid sample were taken and poisoned with two drops of $HgCl_2$ to determine the isotopic composition of the inorganic carbon fraction at the University of Münster.

Major, minor, and trace elements. Hot hydrothermal fluids emerging from black smokers containing some precipitates formed during cooling were not filtered but acidified with 1-5 ml subb. HNO_3. Warm diffuse fluids emerging in mussel fields were pressure filtrated (99.9990 nitrogen) through 0.2 µm Nuclepore PC membrane filters in Sartorius filtration units and acidified with 1 ml subboiled concentrated nitric acid per 125 ml. Acidified samples are stored in 125 ml PFA bottles until analysis. Procedural blanks were processed in regular intervals. All work was done in a class 100 clean bench (Slee, Germany) using all-plastic labware (HDPE; PC, FEP, PFA). Rinse water was ultrapure (>18.2 Mohm) dispensed from a Millipore Milli-Q system. After return to the home labs in Kiel samples will be analysed for major and minor

element composition (Na, K, Ca, Mg, Sr, Ba, B, Fe, Mn, Cu, Zn) by means of ICP-optical emission spectrometry (Ciros SOP; Spectro), and trace elements (e.g., I, Br, B, Li, Al, Ti, Cs, Ba, Sr, Y-REE, Fe, Mn, Cr, V, Cu, Co, Ni, Pb, U, Mo, As, Sb, W) by ICP-mass spectrometry using both collision-cell quadrupole (7500 cs, Agilent), and high resolution sector-field based instrumentation (PlasmaTrace 2, Micromass). At IUB in Bremen, complementary analyses on major, minor and trace elements will be carried out by ICP-OES (Ciros, Spectro) and by ICP-MS (Perkin Elmer).

Anions. Aliquots of hot hydrothermal fluids with precipitate were pressure-filtrated through 0.2 µm PC membrane filters (Nuclepore), warm diffuse fluids were taken as original sample without further treatment and stored in LDPE bottles until analysis for Cl, Br, I, SO_4, SiO_2.

Amino acids and other organic compounds. Sub-samples for organic analyses, either filtered or non-filtered, were immediately frozen (-20°C) as 100 ml aliquots in acid-cleaned PE bottles, or poisoned with $HgCl_2$ in 100 ml glass bottles, which were acid-cleaned and pre-combusted at 480°C before use.

Particles from fluid samples. Filters (see above) from filtration of the KIPS fluid samples and partly also from the Niskin samples of the ROV were kept in plastic dishes for later inorganic analysis, or frozen for later organic analysis, in addition to organic analyses of the fluids.

1.4.7.1.4 Analytical Procedures On-board

pH and Eh Measurements. For all samples collected with the CTD/Rosette, the Niskin flasks and the Kiel Fluid Pumping System (KIPS), pH and Eh measurements were performed on unfiltered sample aliquots immediately after sampling. Measurements were carried out with WTW electrodes (Ag/AgCl reference electrode).

Winkler Titration of Dissolved Oxygen. Immediately after sample recovery, dissolved oxygen was determined in hydrothermal fluids from diffuse vent sites only. The procedure followed the standard procedure as outlined in Grasshoff (1999) with the exception that 10 ml volumetric flasks were used. The detection limit is approx. 0.5 ml/l O_2, precision is in the range of ± 0.1 ml/l O_2. Concentrated hydrothermal fluids from black smokers were not titrated.

Chloride Titration. In order to determine whether or not phase separation affected the chemical composition of the hydrothermal fluids, respective fluid samples collected during ROV dives, either with Niskin bottles or with KIPS, were subjected to chloride concentration analysis. Measurements were performed as titration with 0.1 mM $AgNO_3$-solution, using fluorescene-sodium as the indicator. For reference, samples from a water column profile were also analyzed. Concentrated hydrothermal fluids from black smoker vents were outgassed prior to analysis.

Photometric Determination of Dissolved Inorganic Silica. Silica tends to be enriched in hydrothermal fluids (e.g., van Damm, 2004). Hence, fluid samples and selected CDT/Rosette water column samples were analyzed for their abundance of dissolved silica. The analysis of dissolved silicon compounds in seawater and hydrothermal fluids is based on the formation of α-silicomolybdic acid via complexation of the dissolved silica with ammoniumheptamolybdate (e.g., Grasshoff et al., 1999). Concentration measurements were performed with a Biochrom Libra S12 spectral photometer at an extinction of 810 nm.

Photometric Determination of Iron Concentrations. The principle of this method is the determination of an orange-red ferroin complex, which is formed by Fe(II) ions in the fluid

sample with 1,10-phenantroline in a pH range of 3-5. In addition to a quantification of Fe(II), it is also possible to measure the Fe_{tot} fraction in the sample by reducing all Fe with ascorbic acid. Fe(III) is determined as difference between Fe_{tot} and Fe(II). Analyses were carried out with a Biochrom Libra S12 spectral photometer and the absorption was measured at 511 nm. Fe concentrations were measured only in filtered samples of hydrothermal fluids. The detection limit is about 0.1 ppm. Samples with concentrations above 100 ppm were measured in diluted samples.

Chemoluminescence Determination of Iron(II). Fe(II) was determined by flow injection analysis using a modified Fe-chemilumenescence method described by Croot and Laan (2002). The unfiltered samples taken with he KIPS sampling system or the Niskin bottles attached to the ROV were diluted with aged seawater, acidified to pH 1 (1% HCL s.p.) to avoid a conversion of redoxspecies of iron. The dilution factor depended on the actual Fe(II)-concentration. Seawater from the ship seawater supply was stored at neutral pH for at least 24h in the dark to have all Fe present as Fe(III), which dos not interfere with the very specific Fe(II) determination. Standards from 50 to 500 nM were prepared in acidified aged seawater and resulted in a nonlinear calibration curve. For the actual measurement the sample is in the detector cell with Luminol (5-amino-2,3-dihydro-1,4-phthalazine-dione, 1mM) adjusted to pH 12, resulting in a pH of 10.2 of the detector cell effluent, which allows optimal chemiluminescence for seawater. The resulting luminescence signal was measured by a home-made flow injection system with a HC-135 photon counter linked to a laptop computer running a homemade software for data acquisition.

Photometric Determination of Sulfide. As sulphide is volatile and oxidizes quickly in contact with the atmosphere, it has to be either analyzed immediately after sample recovery, or have to preserved by precipitation as ZnS by addition of Zn acetate solution. On board, detection was carried out photometrically by forming a complex of hydrogen sulphide with dimethyl-p-phenylene-diamine that transforms to leucomethylene blue. This is then oxidized to methylene blue by ferric iron. The solution is measured in 5 cm cuvettes at 660 nm 1 hour after the reagents have been added. For the calibration curve, a stock solution of 80 mM sulphide was used to prepare a fresh 10 ppm standard for every run. For each calibration curve, which covered a range between 0.2 and 3 ppm sulfide, a small aliquot of the standard was preserved with Zn acetate to determine the factor of the solution later in the home laboratory.

A slightly different method (Marc Peters, University of Münster) uses a zinc acetate gelatine solution to fix the sulfide of the sample. This solution keeps the precipitated zinc sulfide in a colloidal state. The homogeneous distributed sulfide reacts with N,N´-dimethyl-1,4-phenylene-diamine-dihydrochloride to colourless leucomethylene blue. This component is oxidized by Fe^{3+} ions of an iron chloride solution to methylene blue. Methylene blue absorbs light with a wavelength of 660nm. One hour after the reagents have been added the solution is measured photometrically. Before the photometric determination, a calibration curve is constructed by the measurement of different calibration solutions, each with a certain sulfide concentration. For the production of the calibration solutions a fresh stock solution with a sulfide concentration of 5,8mmol/L is used. The exact sulfide concentration of the stock solution is determined by titration with a 0,02N thiosulfate solution.

Titrimetric Determination of Calcium and Magnesium. Mg^{2+} concentrations in the fluids can be used to extrapolate to the endmember concentrations of the hydrothermal fluid, based on the fact the Mg in seawater is constant at 54 mM and Mg in the pure fluid is 0 mM. First, Ca^{2+} is

determined in a solution containing 10 ml deionized water and 1 ml of sample, and the pH is adjusted with NaOH to pH ≥12. After addition of Murexid buffer, the solution is titrated with 0.01 M EDTA from orange to purple. From the titration result, the content of Ca^{2+} is calculated. For the determination of the sum of Ca^{2+} and Mg^{2+}, 10 ml deionized water and 1 ml sample are mixed with an ammonium buffer of pH 10 and Eriochrome-black T is added as indicator. The titration is carried out with 0.01 M EDTA, and from the resulting concentration of titrated ions, the Ca^{2+} value is subtracted to calculate the Mg^{2+} concentration.

Voltammetric Determination of Fe, Mn, Zn, Cu, Cd, and Pb by CSV/ASV. For on-board trace metal concentration analyses, the electrochemical method of voltammetry was used. Voltammetry is able to differentiate between different redox species and (in combination with UV digestion of the water samples) free and complexed forms of ions in solution and is highly sensitive. All the voltammetric measurements were performed using either a Metrohm system comprising a 757 VA Computrace run with a standard PC, an 813 Compact Autosampler and two 765 Dosimats or a system consisting of an EcoChemie Autolab II, an IME interface and a Metrohm 663 VA stand. In both cases the three-electrode configuration consisted of the multi-mode electrode (MME) as the working electrode, an Ag/AgCl reference electrode (3 mol l^{-1} KCl), and a platinum wire as the auxiliary electrode. Filtered aliquots were submitted to a digestion process in a UV Digestor (Model 705, Metrohm), which contains a high pressure mercury lamp (500 W), decomposing organic metal complexes. After 1 hour of UV irradiation, the total content of Fe and Mn in all samples and of Zn, Cu, Cd, and Pb in selected samples were determined by the standard addition method. For Fe, the highly sensitive cathodic stripping voltammetric method of Obata and van den Berg (2001) using 2,3-dihydroxinaphthalene as complexing agent was applied in samples with low Fe concentrations, while photometry was used for samples with high Fe concentrations (>0.1 ppm). Mn concentrations were determined using anodic stripping voltammetry in an alkaline ammonia buffer solution (Locatelle and Torsi, 2001). For Cu, Pb, Cd, and Zn analyses samples were buffered at pH 4.6 with 1 M acetate buffer solution and measured by ASV (Application Bulletin Metrohm 231/2).

Ligand titration. Cu^{2+}-binding ligand concentration ($[L_{Cu}]$) and conditional stability constant (K''_{CuL}) were measured using the competing-ligand-equilibration cathodic-stripping-voltammetry (CLE-CSV) technique with salicylaldoxim (SA) as the competing ligand (Sander et al., 2004). The theory behind this technique is described elsewhere (Sander et al., 2004). The Gerringa (Gerringa et al., 1995) method was used to receive numerical values for $[L_{Cu}]$ and K''_{CuL}. In general, the metal ligand titrations were performed by measuring the voltammetric peak current i_p of separate aliquots of the sample to which different concentrations of copper standard solution were added. The titration aliquots were prepared in Teflon^R vials with increasing concentrations of copper added depending on the expected ligand concentration, which was roughly determined before. One hour after the addition of copper SA was added to a final concentration of 20 M. The aliquots were left for a minimum of 6h, usually overnight to allow equilibration of metal with metal-binding ligands and than measured using DP-CSV.

1.4.7.2 First Results

1.4.7.2.1 *In-Situ* Temperatures and Chemistry of Black Smoker Hydrothermal Fluids

A dedicated high-precision thermistor-based temperature sensor integrated within the KIPS fluid sampling system and mounted parallel to the sampling nozzle was used for our temperature measurements of hydrothermal fluids. It has to be kept in mind that fluids emerging at the top of a 12 m tall chimney may have already cooled or mixed with seawater inside the chimney structure. Moreover, vigorous venting involves turbulent mixing of hydrothermal fluids with seawater leading to a highly chaotic temperature distribution within the orifice. It becomes evident that temperature measurements under these conditions and with a ROV difficult to hold in position within a few millimetre for some 10s seconds are at best a rough estimate of the real temperature of the hydrothermal fluid. However, quite constant temperature readings could be obtained for some high-temperature vents including the Marker #2 vent at Turtle Pits where we measured with T_{max} = 408.3 °C the highest temperature ever obtained for a fluid on the seafloor worldwide. Boiling of the emerging fluids could be observed visually and was video-recorded. This temperature at a depth of 2986 m coincides with the experimentally determined temperature for the critical point of seawater (Bischoff and Rosenbauer, 1988) where vapour phase and fluid cannot be discriminated anymore. This suggests that the phase-separated hydrothermal system at Turtle Pits and Sisters Peak (T_{max} = 400.3 °C) might react under supercritical conditions. In contrast, non-phase-separated fluids emerging at the Mephisto and Tannenbaum vents in the Red Lion hydrothermal system - in only 1 nm distance to Sisters Peak - both have temperatures of 347 and 349 °C, respectively (Table 1.6). The following Figs. 1.49 through 1.56 illustrate the conditions during our fluid sampling of the high-temperature black smoker chimneys.

Table 1.6: Measured temperatures of venting hydrothermal fluids.

Area	*Site*	*Station*	T_{max} [°C]	*Average ± 1σ* [°C]	*Sample No.*
MAR 5° S					
Turtle Pits	Marker #2 Vent	12 ROV	408.7	405.7 ± 1.1	3 ROV-10/11 12 ROV-4/ -8
Comfortless Cove	Sisters Peak	24 ROV	400.3	395.4 ± 2.2	20 ROV-4/ -7
Red Lion	Mephisto	7 ROV	346.3	345.6 ± 0.3	7 ROV-3/ -5
Red Lion	Tannenbaum	7 ROV	349.0	348.0 ± 1.5	not sampled
Red Lion	Shrimp Farm	7 ROV	193.0	191.8 ± 1.5	7 ROV-9/ -11
Wideawake	Wideawake mussel field	3 ROV	19.2	17.4 ± 1.9	3 ROV-1/ -4
Comfortless Cove	Marker # 6 mussel field	24 ROV	10.0	9.4 ± 0.4	24 ROV-1/ -3
Comfortless Cove	Golden Valley mussel field	24 ROV	3.6	3.4 ± 0.1	24 ROV-6/ -8
MAR 9° S					
Lilliput area Limtoc	Mussel field 180	39 ROV	17.3	16.3 ± 0.6	39 ROV-3/ -5

	m S Lilliput				
Main Lilliput	Mussel field between pillows	41 ROV	4.9	4.7 ± 0.1	41 ROV-3/ -5
Main Lilliput	Mussel field with cloudy water	41 ROV	6.5	6.3 ± 0.2	41 ROV-6/ -8
Main Lilliput	Northern border of ABE map	41 ROV	6.8	6.6 ± 0.2	41 ROV-10/ -12
MAR 8° S					
Nibelungen	Dragon Throat	62 ROV	192	153 ± 27	62 ROV-5, -9/ -10

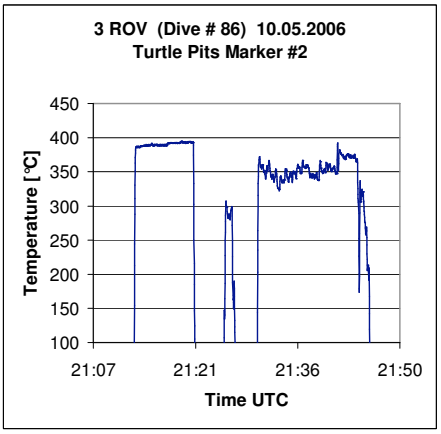

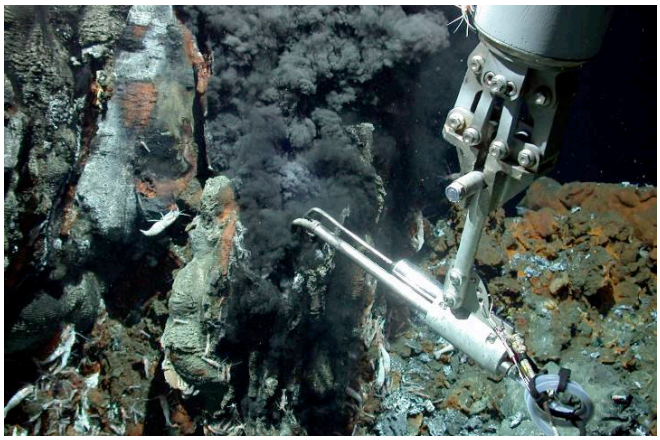

Fig. 1.49: Measured in-situ temperatures during fluid sampling with KIPS at ***Marker #2 Vent***, Turtle Pits, in an orifice approx. 1 m above ground. Maximum temperature measured was 395.1 °C (note unstable temperature readings, compare to Fig.1.53), at a water depth of 2986 m. Samples 3 ROV-10 and -11 were taken from 21:30 – 21:45 UTC.

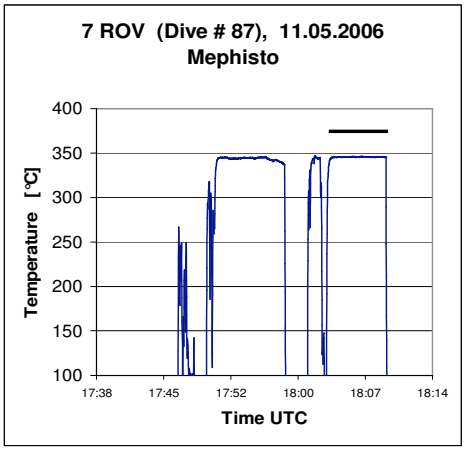

Fig. 1.50: Measured in-situ temperatures during fluid sampling with KIPS at *Mephisto Ven,* Red Lion, orifice on top of the chimney. Maximum temperature measured was 346.3 °C, at a water depth of 3098 m. Samples 7 ROV-1 to -3 were taken from 7:50 – 18:08 UTC.

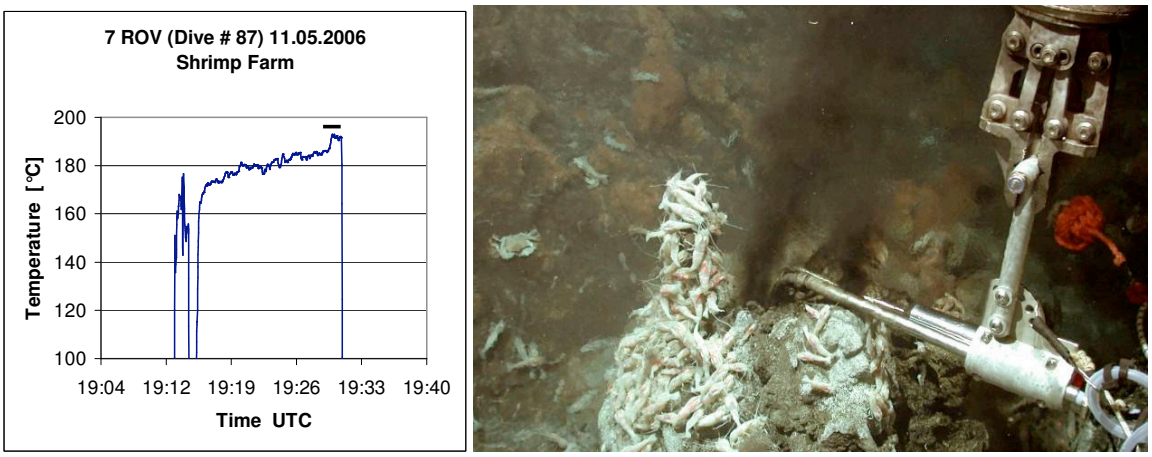

Fig. 1.51: Measured in-situ temperatures during fluid sampling with KIPS at ***Shrimp Farm Vent***, Red Lion, orifice on top of the flange structure. Maximum temperature measured was 193.0 °C, at a water depth of 2986 m. Samples 7 ROV-1 to -3 were taken from 19:16 – 19:30 UTC.

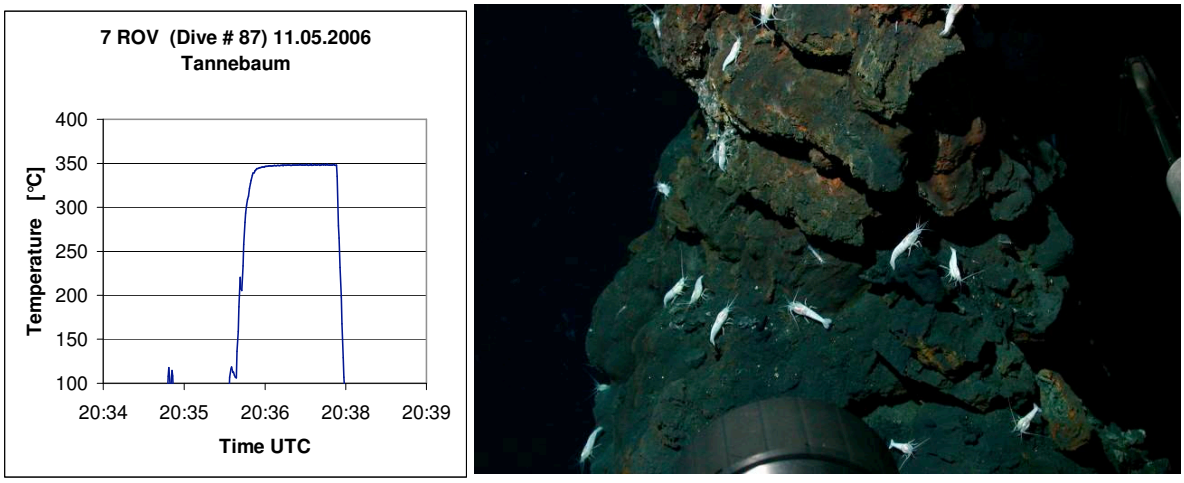

Fig. 1.52: Measured in-situ temperatures at ***Tannenbaum*** *Vent,* Red Lion, orifice on top of the chimney. Maximum temperature measured was 349.0 °C, at a water depth of 3044 m. No samples were taken.

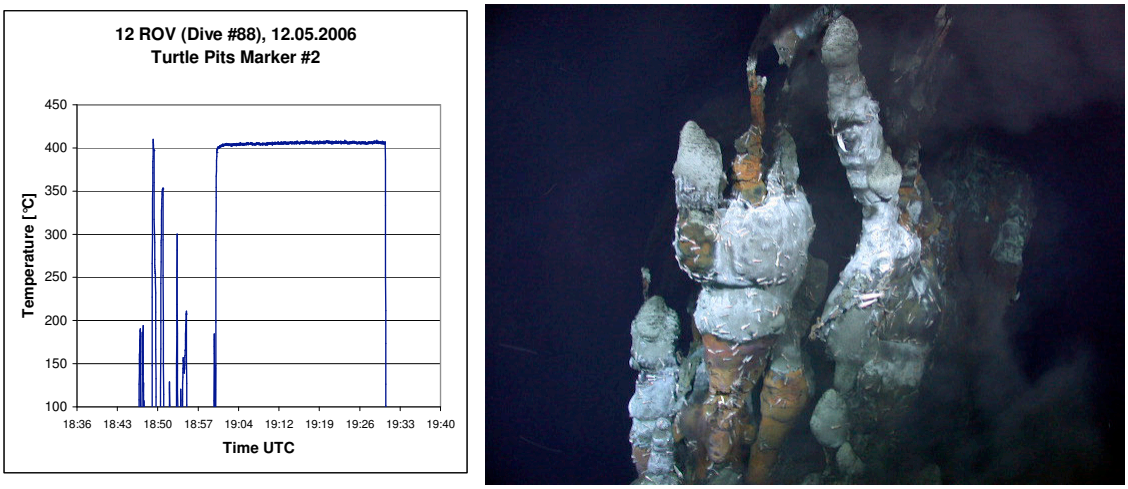

Fig. 1.53: Measured in-situ temperatures during fluid sampling with KIPS at ***Marker #2 Vent***, Turtle Pits in the same orifice approx. 1 m above ground already sampled during 3 ROV. Maximum temperature measured was 408.7 °C, at a water depth of 2988 m. Samples 12 ROV-4 to -8 were taken from 19:01 – 19:30 UTC.

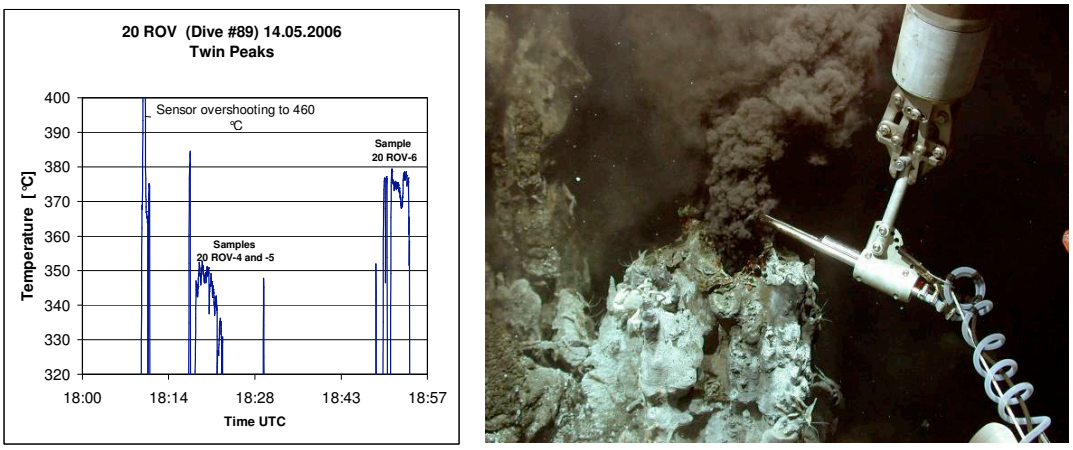

Fig. 1.54: Measured in-situ temperatures during fluid sampling with KIPS at ***Sisters Peak***, orifice on the top of the chimney 12 m above ground. Maximum temperature measured was 379.3 °C (note unstable temperature readings), at a water depth of 2988 m. Samples 20 ROV-4 to -6 were taken from 18:11 – 18:54 UTC.

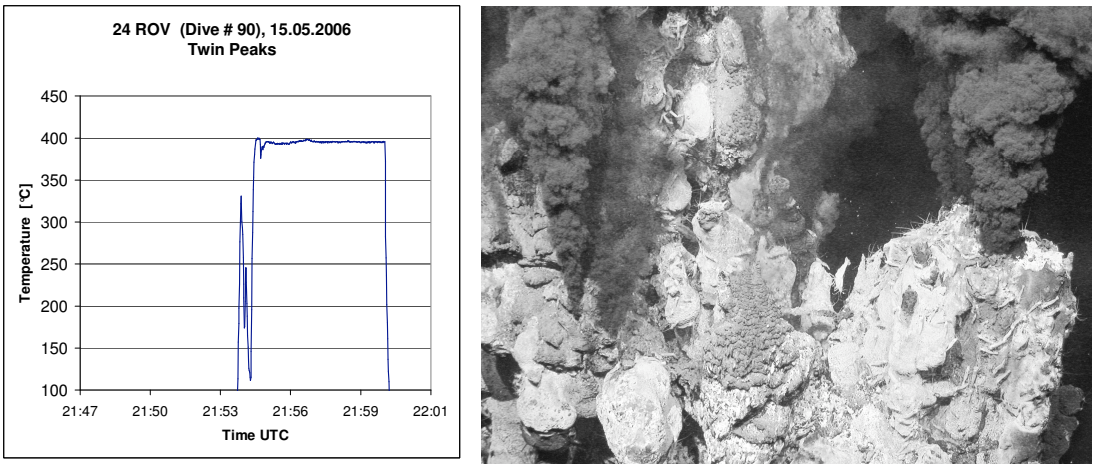

Fig. 1.55: Measured in-situ temperatures at ***Sisters Peak***, at the same orifice on the top as 20 ROV. Maximum temperature measured was 400.3 °C, at a water depth of 2988 m. No samples taken.

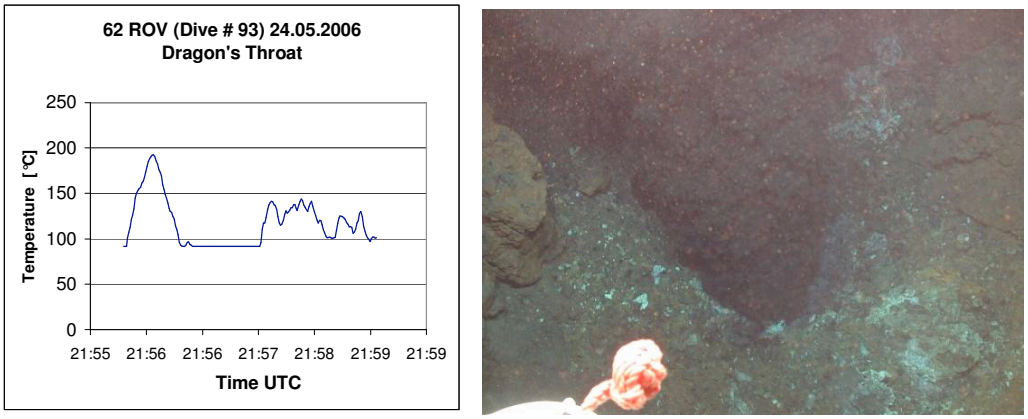

Fig. 1.56: Measured in-situ temperatures at ***Dragon's Throats,*** but nozzle could not be correctly inserted into orifice. Maximum temperature measured was 192 °C, at a water depth of 2910 m. Samples 62 ROV-5 and -9/-10 taken from 20:08 until 20:18 UTC.

Onboard analysis of the fluid samples recovered by the ROV revealed a large spectrum of fluid compositions from samples of different fields. The 407°C hot smoker Two Boats at Turtle Pits, which was discovered last year, is still characterized by phase separation und emanation of a salt-depleted vapour phase (Fig. 1.53) with high concentrations of hydrogen, iron, and copper. The pH is as low as 3.1. The hot vent Sister Peak in the Comfortless Cove field between Turtle Pits and Red Lion shows basically the same chemistry, and although boiling could not directly be observed, depleted chlorinity (the samples are on the same mixing line of fluids and seawater as the Turtle Pits ones, Fig. 1.57) and high metal concentrations indicate a common fluid source of the two vents. In contrast, in the Red Lion field NW of Comfortless Cove the four different smokers display cooler temperature (between 193°C for Shrimp Farm and 349°C for Mephisto and Tannenbaum) and show no phase separation. This indicates that these fluids have never been as hot as the Turtle Pits and Sisters Peak ones and that this is probably a separate vent system.

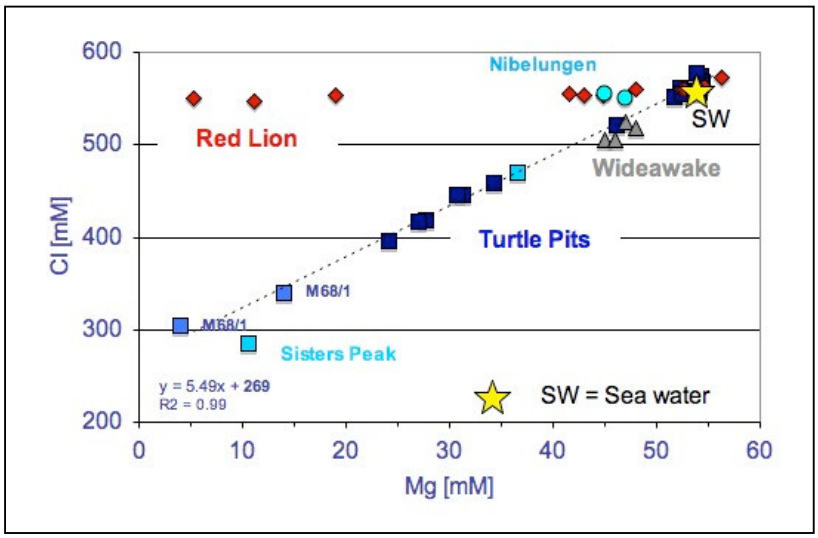

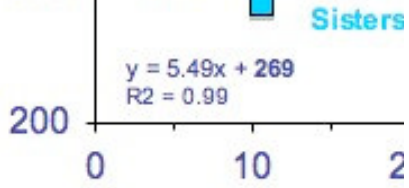

Fig. 1.57: Plot of chlorinity versus Mg concentrations with data from M64/1 and M68/1. Pure seawater has a Mg concentration of ca. 54 mM, while the hydrothermal endmember is assumed to have Mg = 0 mM. Turtle Pits and Sisters Peak fluids area clearly phase-separated, while Red Lion and Nibelungen fluids are not.

While the fluids at 5°S are clearly a result of water-rock interaction in a basaltic system, the vent crater "Drachenschlund" at Nibelungen indicates fluid reactions with mantle rocks, i.e. serpentinization reactions. Besides the very high gas concentrations (see chapter 1.4.6), high Fe and Cu contents confirm this assumption. The high H_2/CH_4 ratio (see chapter 1.4.6) and the extremely high Cu concentrations indicate an endmember fluid temperature in the range of 360-400°C, because Cu precipitates as chalcopyrite at temperatures <350°C. The fluids are probably not hotter than 400°C, because at the depth of the field the boiling point would be around 400°C and phase separation is not apparent from the chlorinity data (Fig. 1.57).

Table 1.7: Comparison of the geochemistry of high temperature vents and diffuse flow mussel fields.

	$T_{in\ situ}$ (°C)	pH	Eh (mV)	O_2 (ml/l)	S^{2-} (µM)	Cl^- (mM)	Si (µM)	Mg^{2+} (mM)	Ca^{2+} (mM)	Fe_{ges} (µM)	Fe^{2+} (µM)	Fe^{2+} (µM)	Cu^{2+} (nM)	Zn^{2+} (nM)	Pb^{2+} (nM)
(A) High Temperature Vents															
5°S															
Turtle Pits & Comfortless Cove															
min	*350*	*3.1*	*-304*		*5.7*	*285*	*231*	*4.0*	*7.5*	*9.4*	*4.0*	*0.3*	*2.8*	*111*	*0*
max	*407*	*7.9*	*70*		*957*	*540*	*5925*	*36.5*	*12.0*	*3675*	*3240*	*6498*	*1622*	*938*	*4.1*
median	*395*	*4.1*	*-212*		*217*	*325*	*840*	*12.3*	*8.3*	*1564*	*1665*	*2096*	*82*	*648*	*0.7*
Red Lion															
min	*186*	*5.5*	*-289*		*37.8*	*555*	*267*	*41.5*	*9.0*	*1.78*	*1.1*	*7.0*			
max	*346*	*7.3*	*-47*		*1027*	*560*	*1416*	*55*	*12.0*	*888*	*26.6*	*130*			
median	*345*	*6.2*	*-182*		*343*	*555*	*767*	*48.5*	*11.0*	*49.3*	*15.9*	*83*	*29.9*		
Nibelungen															
min	*30*	*6.4*	*-357*		*0.6*	*550*	*86*	*45*	*13.0*	*11*	*3.2*	*2.3*	*60.8*	*1158*	
max	*90*	*7.9*	*-90*		*7.0*	*555*	*2263*	*47*	*14.0*	*843*	*796*	*930*	*5693*	*8700*	
median	*90*	*7.1*	*-236*		*3.0*	*553*	*1175*	*46*	*13.5*	*121*	*71*	*50*	*435*	*5446*	
(B) Diffuse Flow Mussel Fields															
5°S															
min	*30*	*6.4*	*-357*		*0.6*	*550*	*86*	*45*	*13.0*	*11*	*3.2*	*2.31*	*60.8*	*1158*	
max	*90*	*7.9*	*-90*		*7*	*555*	*2263*	*47*	*14.0*	*843*	*796*	*930*	*5693*	*8700*	
median	*90*	*7.1*	*-236*		*3*	*553*	*1175*	*46*	*13.5*	*121*	*71*	*50*	*435*	*5446*	
Liliput															
min	*4.8*	*6.0*	*-190*	*< 0.5*	*4*	*550*	*57*	*52.5*	*10.0*	*0*	*0*	*0.15*	*8.04*	*140*	*0*
max	*15.8*	*7.9*	*42*	*5.27*	*341*	*555*	*1082*	*55.5*	*10.0*	*43*	*42*	*25*	*76.5*	*650*	*1.9*
median	*6.8*	*6.7*	*-89.5*	*3.12*	*22.5*	*550*	*114*	*55.0*	*10.0*	*2.7*	*2*	*5.4*	*20.1*	*272*	*0.4*

Note: Mg not corrected for interference by Fe(II)

1.4.7.2.2 Mussel Fields in Areas with Diffuse Hydrothermal Fluid Flow

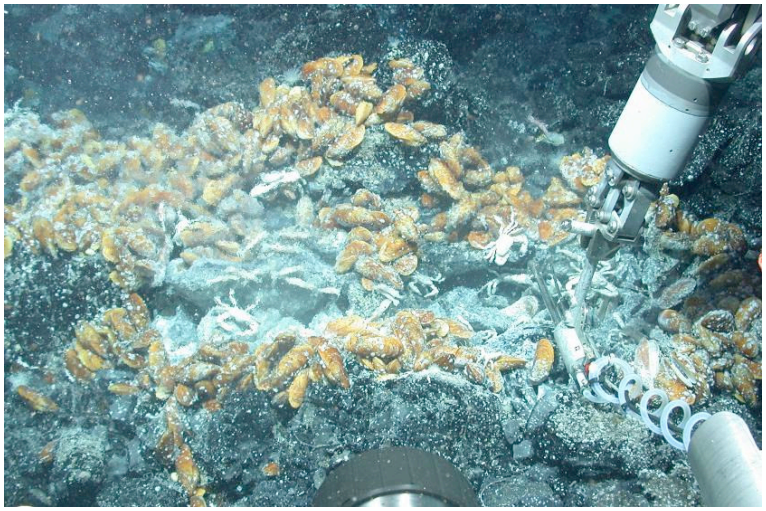

Fig. 1.58: Area 5° S, Wideawake mussel field, abundant shrimps and crabs in the pond, T = 16.7 °C, KIPS samples 3 ROV-1 to -4.

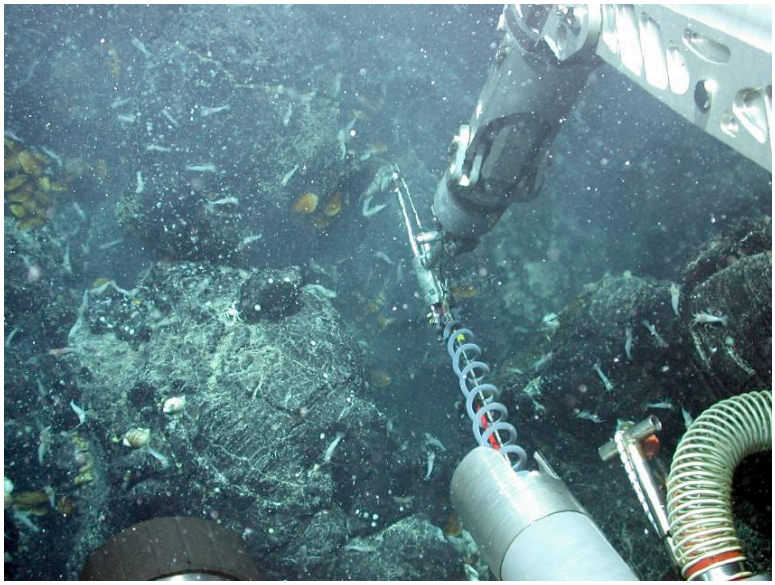

Fig. 1.59: Area 5° S, Marker #6 site, turbid water from diffuse vents along cracks, abundant shrimps, T = 10 °C, KIPS samples 24 ROV-1 to -3.

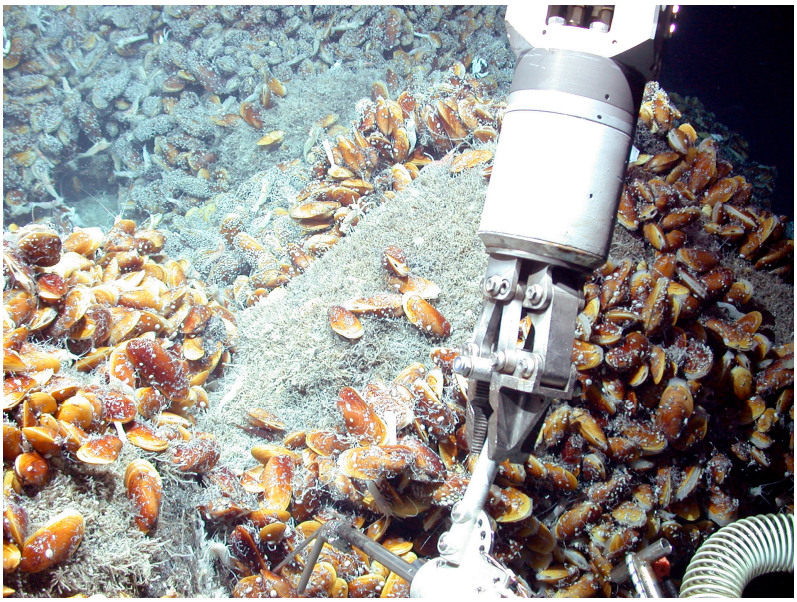

Fig. 1.60: Area 5° S, Golden Valley mussel field, dense *Bathymodiulus*, filamentous bacteria, shrimps, T = 3.6 °C, KIPS samples 24 ROV-6 to -8.

Fig. 1.61: Lilliput area 9° S, 180m S Lilliput, small crack w/ abundant mussels, bacterial mats, and shrimps, T = 16.7 °C, KIPS samples 39 ROV-3 to -5.

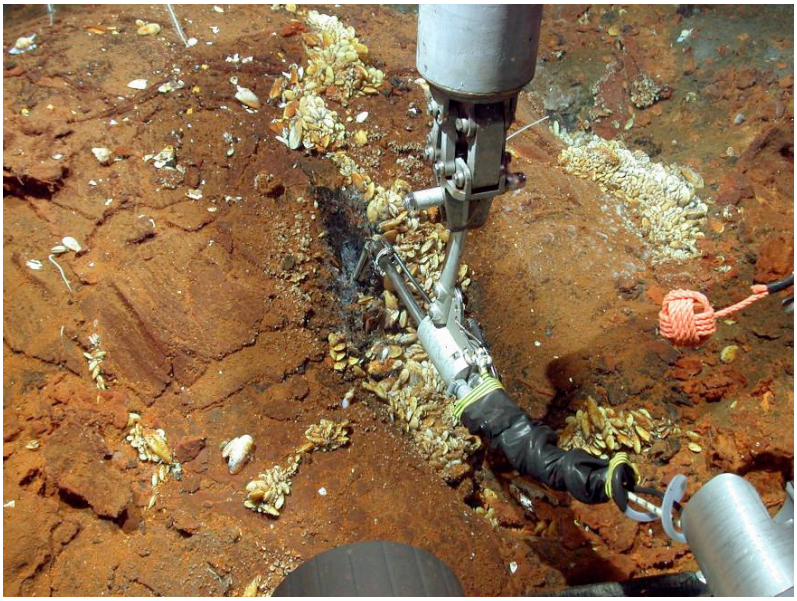

Fig. 1.62: Lilliput area 9° S, S Lilliput, small outlet in between oxidized pillows w/ filamentous bacteria, mussels, T = 4.8 °C, KIPS samples 41 ROV-3 to -5.

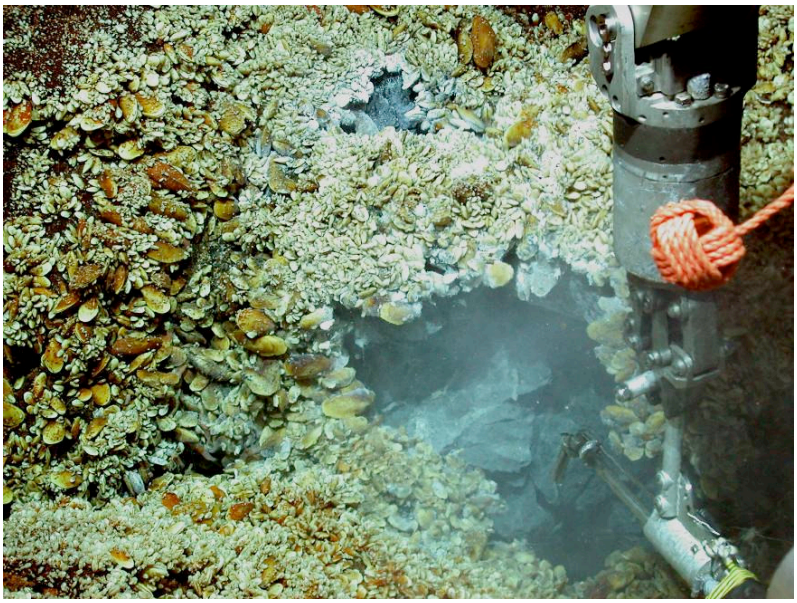

Fig. 1.63: Lilliput area 9° S, w/ dense mussel kindergarten, cloudy water, T = 6.6 °C, KIPS samples 41 ROV-6 to -8.

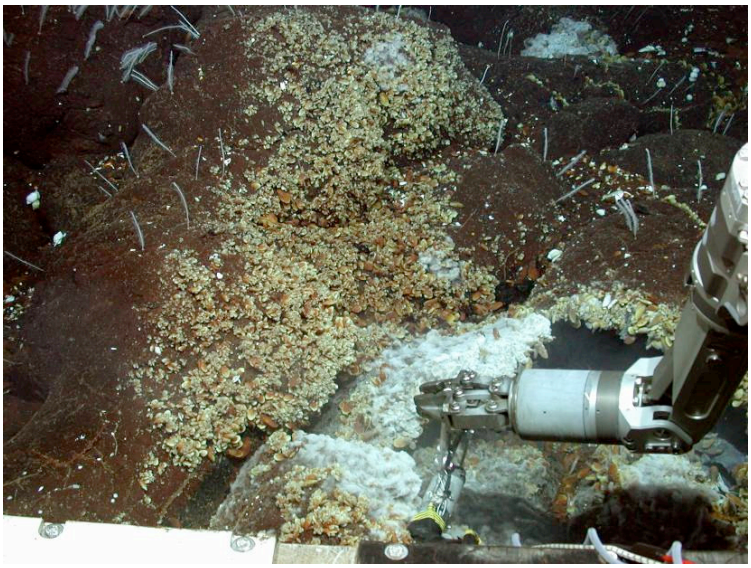

Fig. 1.64: Lilliput area 9° S, Northern border of ABE map, small crack w/ abundant mussels, bacterial mats, and shrimps, T = 6.8 °C, KIPS samples 41 ROV-10 to -12.

All individual on-board fluid chemistry data from the diffuse fluids is listed in Table 1.8 and further parameters will be measured once the samples have returned to the home lab. However, since a large uncertainty is attached to the on-board magnesium values, the extrapolation to calculate endmember: seawater ratios in these samples is not allowing many interpretation of the data yet.

Eh, in contrary to the pH, is a good indicator for the hydrothermal influence of the samples as reducing compounds such as free dissolved sulphide, hydrogen and methane, produced during the hydrothermal process The correlation shown in Fig. 1.65 indicates, that in the diffuse hydrothermal samples the strongly reducing character, mirrored by a negative Eh is mainly caused by free sulphide, which is present in a much higher concentration than methane and hydrogen.

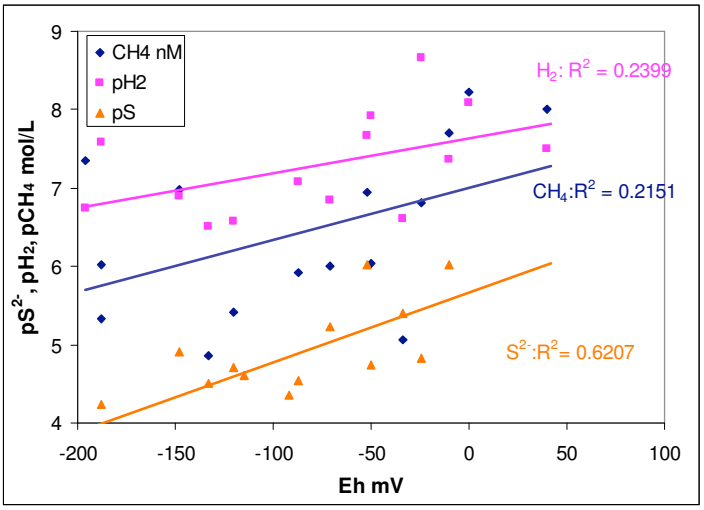

Fig. 1.65: Correlation of the measured Eh with reducing components in the diffuse hydrothermal fluid samples taken during M68/1. (Note that the concentrations of sulphide, methane and hydrogen have been plotted as the negative logarithm. Methane and hydrogen data from R. Seifert and S. Weber).

Table 1.8: On-board fluid chemistry data from samples taken at diffuse hydrothermal sites.

ID	T (ºC)	pH	Eh (mV)	O_2 (ml/l)	S^{2-} (µM)	CH_4 nM	H_2 nM	Cl^- (mM)	Si (µM)	Mg^{2+} (mM)	Fe_{ges}*(µM)	Fe^{2+}* (µM)	Fe^{2+}** (µM)	Cu^{2+} (nM)	Zn^{2+} (nM)
5ºS Widewawake mussle field															
3 ROV-5 N1		7.8	0			6	8	560			10.3	4.7	0	34.8	128
3 ROV-1/2 b1,	17.5	6.7	-188	1.77	59.1	959		550			12.5	7.8	4.3	218	396
12 ROV-10 N3		7.8	-196		115	44	180						0.43	1.49	379
24 ROV-3 b7	9.6	7	-148	5.16	12.2	104	126	550	338	52.5	1.43	0.71	1.71	10.7	421
24 ROV-4 N1		7.9	40			10	31		39				0	12.1	650
24 ROV-4N2	3.2	7.9	-10		0.94	20	42		32	54	0	0	0	3.28	33.6
24 ROV-8 b4	3.6	7.7	-52	5.1	0.94	113	21	550	25		4.64	1.25	2.25	6.49	365
Lilliput south															
39 ROV-8 N1		7.8	42										1.154	8.04	253
39 ROV-8 N2		7.8						550					0.198		
39 ROV-3 b9	15.8	6.2	-190					550							
39 ROV-4 b8	15.8	6.3	-188	0	341	4600	26	555		52.5	15	15	16	11.4	140
70 ROV-2 b2	8.5	5.9	-34		4	8865	250		256	55			25	22.7	650
70 ROV-5 b4	10	6.5	-133		31	13878	313		285	54.5			16.7	76.5	177
70 ROV-9 N1		7.6	-71		6	1007	143		57	55.5			0.15	37.6	247
70 ROV-10 N2		7.3	-120		20	3918	263		93	55			0.37	28.9	148
Lilliput center and north															
41 ROV-5 b7	4.8	7.2	-24	5.27	15	155	2				3.2	1.4	1.38	17.4	479
41 ROV-6 b6	6.6	6.5	-87	3.12	29	1188	84	550			6.8	7.5	13.8	14	454
41 ROV-8 b1	6.3	6.5	-115		25								6.02		
Cadelabrum Meadow north of Lilliput															
41 ROV-10 b3	7	6.6	-50		18	926	12	555					4.69	32.8	291
41 ROV-12 b4	6.5	6.9	-92		45						3.6	3.4	8.7	9	421

* Fe redox speciation measured photometrically

** Fe^{2+} measured by chemiluminescence

H_2 and CH_4 data from R. Seifert and S. Weber (see Chapter 1.4.6)

1.4.7.2.3 Organic Complexation of Copper in Hydrothermal Vent Samples

The complexation of copper and other heavy-metals with free inorganic sulphides in hydrothermal waters is considered to dominate their chemical speciation and bioavailability (Edgcomb et al., 2004; Luther III et al., 2001). However, recent studies on the effect of heavy metals on *Bathymodiolus azoricus* a deep-sea Mytilid bivalve very common in the Mid Atlantic Ridge (MAR) hydrothermal vent fields showed that these organisms in combination with their methanotroph and thiotroph symbiotic bacteria have mechanisms to protect themselves from heavy metal toxification including the production of metallothioneines and antioxidants (Bebianno et al., 2005; Company et al., 2004; Cosson and Vivier, 1997).

It is now also well established that in the ocean at large, the biological availability of all essential or toxic metal ions are controlled by the formation of strong complexes with natural organic matter ligands of which many are presumed to be of biological origin, produced either to acquire metal-ions (e.g. Fe^{3+} (Van den Berg, 1995)) or to reduce their toxicity (e.g. Cu^{2+} (Dupont et al., 2004; Moffett and Brand, 1996)). However, the link between these detoxification mechanisms and possible metal binding ligands released into the hydrothermal vent environment as conditioning reagents for the local hydrothermal bio-community has not been made yet by other researchers and a first study in samples from the Logatchev field and the Kermadec Arc had shown that organic copper binding ligands can be found in hydrothermal vent fluids.

The goal of the present study was:

A. To confirm that the presence of organic copper binding ligands in samples from deep-sea hydrothermal vent systems can be generalised. Therefore a large number of samples has been measured to obtain the ligand concentration [L_{Cu}].

B. To determine the conditional stability constant $K''_{CuL,Cu2+}$ (salinity 35, pH 7.8) and compare them with values of ambient seawater.

C. To gain information about the selectivity of L_{Cu} (i.e. in competition with other heavy metals such as Zn, Pb, Cd, and Fe).

D. To collect sample material for structural and stable isotope analysis with the focus to find out if L_{Cu} is produced biotically and abiotically.

Except for sample 7ROV-11 bottle6, it can be seen that all hot vent samples either had no ligand present in an excess of total dissolved copper, or the samples developed fluffy brown or white precipitate upon readjusting the pH of the acidic and sulphide free solution to normal sea water pH. We will remeasure those samples in the home lab at their original pH and or after dilution. (see Table 1.9).

Sample 7ROV-11 bottle6 had an in-situ temperature of 186 ºC and was taken at Shrimp farm vent, an orifice on top of a flange structure, site which is characterised by abundant shrimps which also gave it its name.

All other samples where copper binding ligands were found are diffuse vent sites, with emanation temperatures below 20 ºC and abundant biological activity. Fig. 1.66 shows all data from diffuse sites sorted by sampling areas.

In some cases, when samples were taken directly above or even from inside a cave with mussel growth and a second a bit further above (e.g. sample pairs 3ROV-1 / 3ROV-5, and 39ROV-8 / 39ROV-4) the gradient with distance can also be seen in the ligand concentrations found. This is a clear evidence that copper binding ligands are produced within the hydrothermal field; the coincidence with the presence of dense biological activity also indicates that they are of biotic origin.

Pictures of sampling sites are shown in 1.4.7.2.1.

Table 1.9: Results for the copper binding ligand measurements in venting hydrothermal fluids.

Area	Station	sample	bottle	T(°C)	Cu^{2+} (nM)	L_{Cu} (nM)	$logK_{CuL, Cu2+}$
WA	3 ROV	5	N1		34.8	60.95	13.31
WA	3 ROV	1/2	b1, b2	17.5	218	637.7	12.93
TP, M2	3 ROV	10	b5	395	1622	< $[Cu^{2+}]$	
RL, Me	7 ROV	4	b2	345		precipitation	
RL, Me	7 ROV	5	b3	345		precipitation	
RL, Sf	7 ROV	11	b6	186	29.9	482.8	12.52
RL, Tb	7 ROV	13	N1	346		precipitation	
WA	12 ROV	10	N3		1.49	407.3	12.59
TP, M2	12 ROV	*	b8		9.5	precipitation	
TP, M2	12 ROV	5	b2	405	8.5	precipitation	
TP, M2	12 ROV	8	b5	407	2.8	precipitation	
TwP	20 ROV	5	b2	350	154	precipitation	
TwP	20 ROV	6	b3	380	341	precipitation	
M7	20 ROV	8	N1		3.65	< $[Cu^{2+}]$	
DF	24 ROV	3	b7	9.6	10.7	repeat	
GV	24 ROV	4	N2	3.2	3.28	689	13.00
GV	24 ROV	8	b4	3.6	6.49	67	12.64
LI-S	39 ROV	8	N1		8.04	109	12.62

Ll-S	39 ROV	4	b8	15.8	11.4	234	12.50
Ll	41 ROV	5	b7	4.8	17.4	repeat	
Ll-N	41 ROV	6	b6	6.6	14.0	45	12.90
CM	41 ROV	10	b3	7	32.8	repeat	
CM	41 ROV	12	b4	6.5	9.0	repeat	
Nb	62 ROV	3	N2		5693	< $[Cu^{2+}]$	
Nb	62 ROV	4	N1		435	< $[Cu^{2+}]$	
Nb	62 ROV	5	b1	30	60.8	< $[Cu^{2+}]$	
Nb	62 ROV	9	b2	90	409	precipitation	
Nb	62 ROV	10	b3	90	692	precipitation	
Ll-S	70 ROV	2	b2	8.5	22.7	195	12.42
Ll-S	70 ROV	5	b4	10	76.5	1770	12.40
Ll-S	70 ROV	10	N2		28.9	353	12.82

< $[Cu^{2+}]$: no ligand could be found in excess of Cu present in the sample;
Precipitation: the sample developed precipitates during equilibration, probably hydrous ferric oxides;
Repeat: the titration was somehow faulty and a result could not be obtained although there might be a ligand present. Measurements will be repeated with frozen samples in the home lab.
For area descriptions see the main table on fluid chemistry.

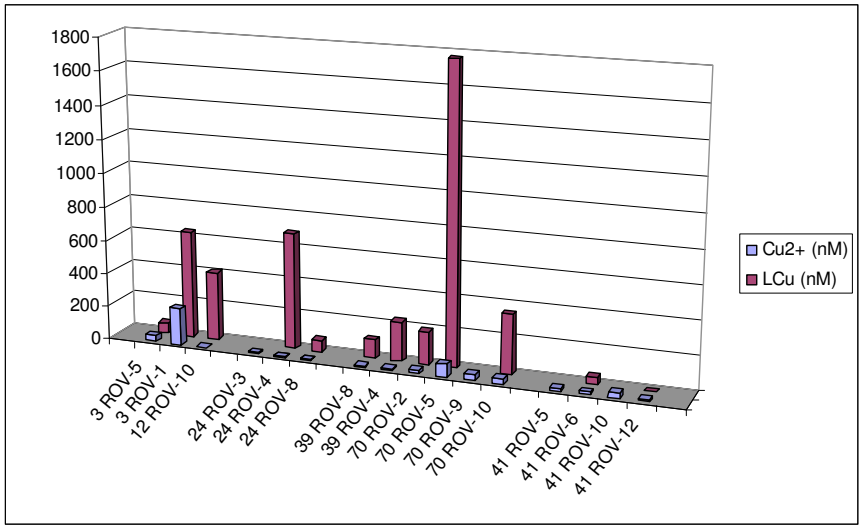

Fig. 1.66: Total dissolved copper concentrations [Cu_T] and Cu-binding ligand concentrations [L_{Cu}] in diffuse hydrothermal fluid samples taken during M68/1 cruise.

Cu-ligand measurements in samples 24ROV-3, 41ROV-5, 41ROV-10 were troublesome and, although there seems to be a ligand present, the data did not allow a calculation of [L_{Cu}] and logK''_{CuL}

1.4.8 Hydrothermal Symbioses

(N. Dubilier, F. Zielinski)

Our main goal for this cruise was to investigate the transfer of energy from vent fluids to the dominant members of the faunal community at many of the Southern MAR vent sites, the mussels *Bathymodiolus* sp. These mussels have greatly reduced guts, and their main source of nutrition is symbiotic bacteria that live in their gills. Two types of symbionts coexist in the gill cells: thiotrophic bacteria that use reduced sulfur compounds such as sulfide as an energy source and fix CO_2 as a carbon source, and methanotrophic bacteria that use methane as both an energy and a carbon source. The energy sources for the mussel symbioses are delivered by the hydrothermal fluids that carry high concentrations of sulfide, methane, hydrogen, and other reduced compounds. The concentrations of these energy sources vary over time and space and play a major role in determining the biomass, activity and productivity of the vent community. We have defined these interactions between hydrothermal and biological processes as the geobiological coupling between vent fluids and symbiotic primary producers.

During this cruise, we contributed to our ongoing studies of geobiological coupling at MAR vents by:

1) Identifying the energy sources used by the mussel symbionts
2) Comparing the rates at which different energy sources are used by the symbionts
3) Comparing how consumption rates of different energy sources are related to their concentrations at vent sites

To collect geochemical data at a scale relevant to the mussel community, we worked in close collaboration with the fluid and gas chemistry groups, and on board analyses of hydrogen and methane uptake were in collaboration with Richard Seifert and Stefan Weber.

Mussels were collected using the ROV manipulator arm in nets (40 cm length with a 20 cm diameter opening, mesh size 1000 µm) at different sites in the Wideawake, Comfortless Cove (Sisters Peak and Golden Valley), and Lilliput vent fields (Table 1.10).

Table 1.10: Mussel collection sites at Southern MAR vent sites

Sample	Station Number	Site	Coordinates
1	3 ROV-6	Wideawake (Marker 1)	4° 48,6404 S 12° 22,3634 W
2	12 ROV-9	Wideawake (Marker 1)	4° 48,6404 S 12° 22,3634 W
3	20 ROV-1	Sisters Peak (Marker 5)	4° 48,188 S 12° 22,301 W
4	24 ROV-5	Golden Valley (no marker?)	4° 48,166 S 12° 22,271 W
5	39 ROV-6	Lilliput South (no marker?)	9° 32,955 S 13° 12,531 W
6	70 ROV-8	Lilliput South (no marker?)	9° 32,9606 S 13° 12,5339 W

On board, the mussels were dissected and prepared for morphological and molecular analyses in the home laboratory. For on board analyses of uptake rates of energy sources, gill tissues (that contain the bacterial symbionts) were incubated in methane, sulfide, and hydrogen and the decrease of these energy sources over time was measured in the head space or fluid of the incubation vial. Carbon fixation rates were determined radioactively, using $^{14}CO_2$ for sulfide and hydrogen, and $^{14}CH_4$ for methane. Vials with mussel foot tissue (that is symbiont free) or with only sea water were used as controls.

Although not all results from our onboard experiments were available at the time of writing this report, some first results can be summarized at this point. No uptake of methane was measured, neither in the labeled nor the unlabled experiments. This result was unexpected because at least one mussel specimen collected from the Wideawake vent site in the previous year, contained methane-oxidizing symbionts. Possibly, methane concentrations were too low in the incubation (< 30 µM), as other authors were only able to show significant $^{14}CH_4$ uptake at methane concentrations above 50 µM.

Sulfide is clearly used as an energy source by the mussel symbionts, based on experiments showing a much greater decrease of sulfide in vials containing mussel gill tissues than in the controls with foot tissue or seawater (Fig. 1.67). In correspondence to the linear decrease in sulfide, $^{14}CO_2$ fixation rates increased linearly until sulfide concentrations apparently became too low for further $^{14}CO_2$ fixation (Fig. 1.67).

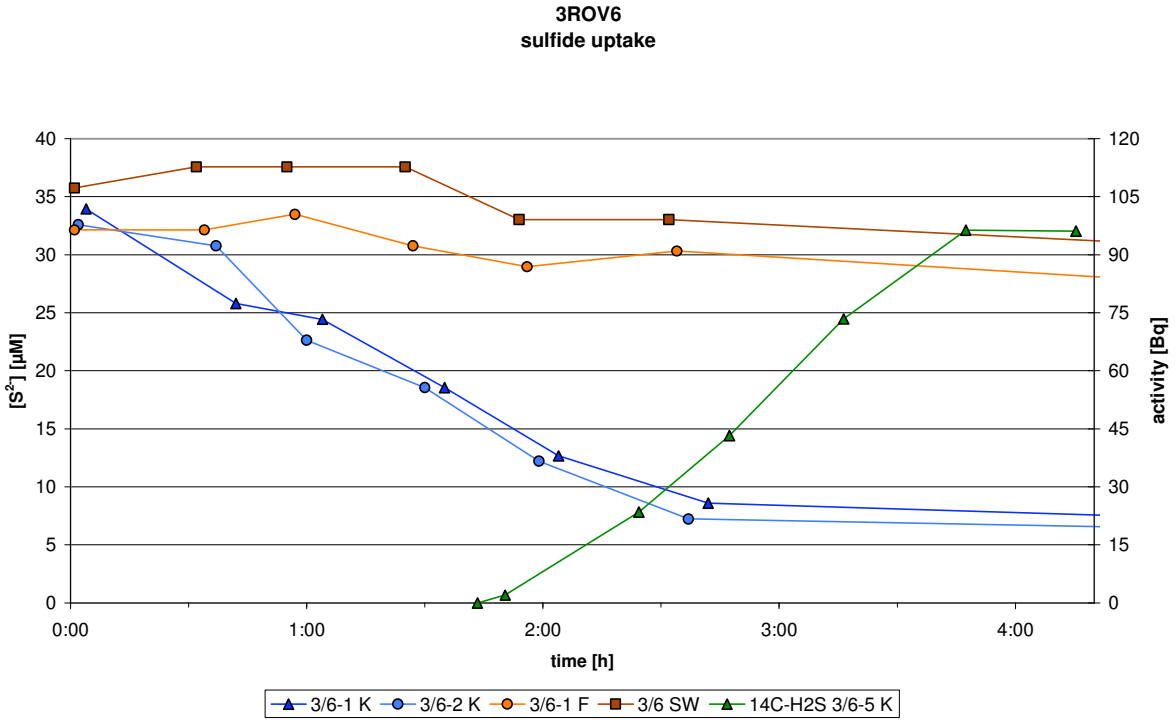

Fig. 1.67: Decrease of sulfide in symbiont-containing gill tissues from 2 mussel individuals (blue lines) is linear until approx. 8 µM sulfide, while almost no decrease of sulfide was observed in seawater (orange line) and symbiont-free foot tissue (burgundy line). Fixation of $^{14}CO_2$ (green line) increased linearly, but leveled off at the end of the experiment, in correspondence to the leveling off of sulfide uptake rates.

Sulfide consumption rates were significantly higher in mussels collected from Wideawake than in those collected from Lilliput. Intriguingly, sulfide concentrations in Wideawake diffuse fluids were higher at 80 – 750 µM than those in Lilliput at 31 – 36 µM, indicating a possible correlation between sulfide concentrations in the mussel environment and symbiotic activity.

Hydrogen was also used as an energy source, although at much lower rates than sulfide. Fixation rates of $^{14}CO_2$ were correspondingly lower for hydrogen than for sulfide. This corresponds well with the concentrations of these two energy sources at the collection sites on Southern MAR vent fields, where hydrogen concentrations were at least 100-fold lower than those of sulfide.

In summary, our first results indicate that both sulfide and hydrogen can be used as energy sources by mussel symbionts, and that the rates at which these energy sources are used are dependent on their concentrations in the mussel environment. This result is surprising given that the oxidation of hydrogen provides the bacteria with more energy than the oxidation of sulfide and needs to be confirmed in further experiments and during the following cruises.

1.4.9 The Hydrothermal Vent Fauna in SMAR – a Characterization of Three Communities

(O. Giere)

Summary

The faunistic communities encountered during M68/1 are characterized and related to their specific environment. The mussel (*Bathymodiolus*) populations, dominating at several vent sites, are diverging in their size-frequency distribution and the potential reasons are discussed. The absence of the typical vent macro- and even meiofauna in the surroundings of the smoker "Drachenschlund" is striking. In their general structure and composition, the populations at the SMAR vents do not seem to differ from those at NMAR, but deviations at lower taxonomic levels will certainly occur.

Faunistic sampling was performed for several scientific goals:

a) Sampling for a taxonomical characterization as a comparison to the vent sites north of the equator (various museum specialists),
b) Fixing for revealing the population genetics of species at various sites (T. Shank, USA),
c) Freezing material for isotopic analyses as a contribution to food web analyses
d) Fixing for ultrastructural investigations, especially in symbiotic animals.

On the basis of the numerous samples taken, a picture of three different communities can be drawn:

Mussel beds at diffuse venting sites (Wideawake, 5° S, and Lilliput, 9° S)

The diffuse vent sites sampled (Wideawake, 5° S, and Lilliput, 9° S) are dominated by dense thickets of *Bathymodiolus* of a quite different size distribution. While at Wideawake larger mussels dominated (80% >8 cm), the fields in the Lilliput area were dominated by smaller specimens (only 1.5 % >6.5 cm, post-settlement stages prevailing). Size-frequency plots illustrate this discrepancy (Fig. 1.68 a,b).

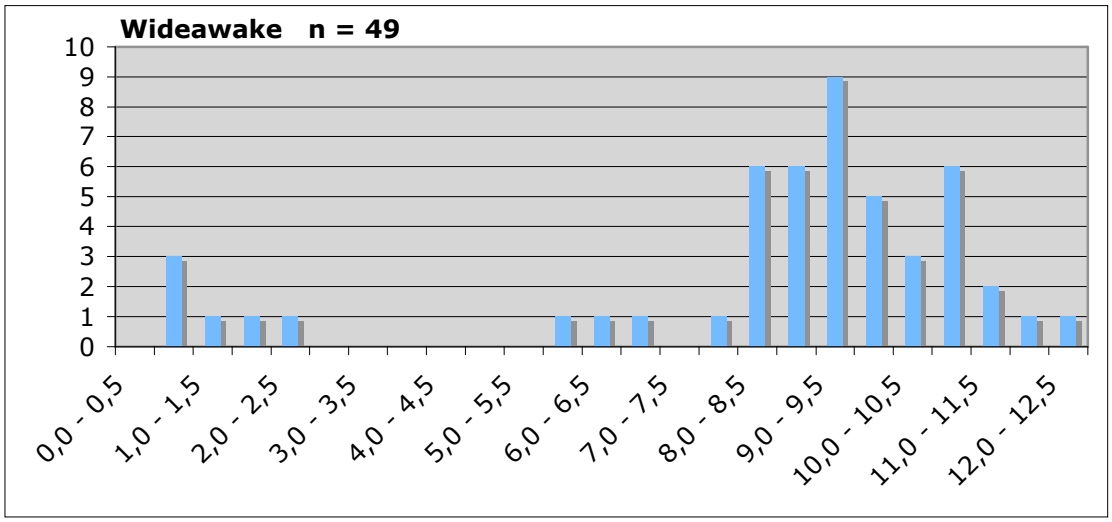

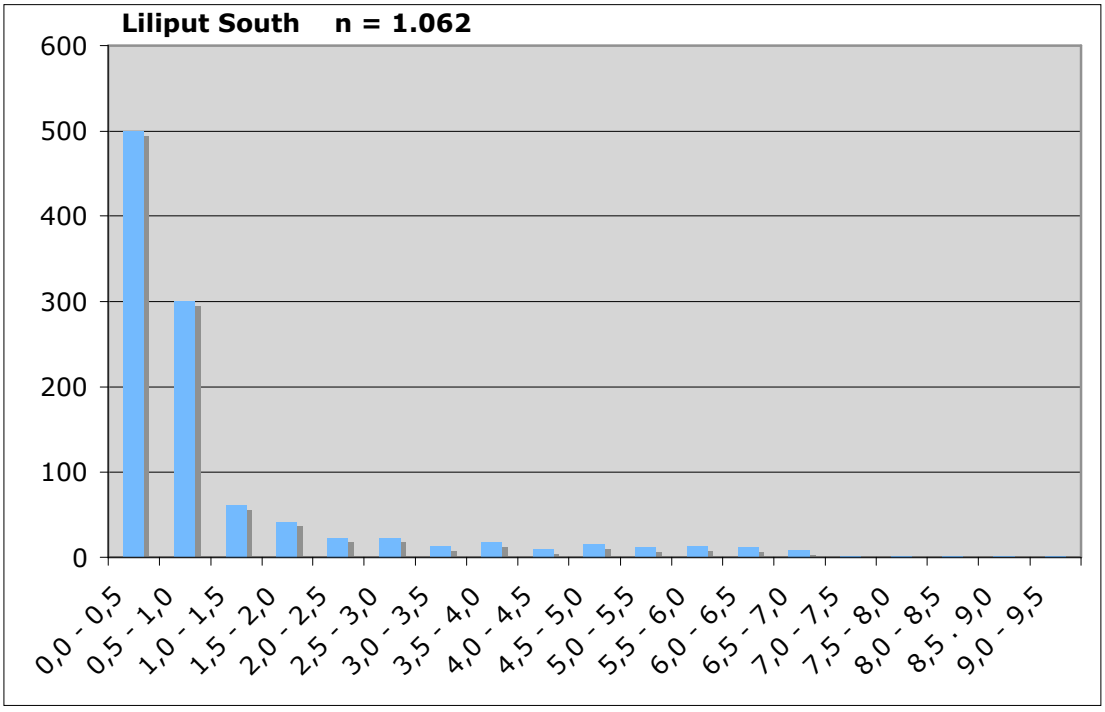

Fig. 1.68 a, b: Comparison of size-frequency distributions of *Bathymodiolus* sp. at 5° S (Wideawake) and 9° S (Lilliput).

It was observed that most of the mussels at 9° S were more elongate and thinner-shelled than those at 5° S. However, these differences occurred also within the Lilliput populations (Fig. 1.69), ruling out the possibility that they might relate to different age groups.

Fig. 1.69: Different shell shapes of *Bathymodiolus* sp. from the Lilliput South mussel field.

The species identity of this key taxon is presently clarified by a specialist, since the external shape is subject to much variation. Muscle and shell scar preparations have been already made to support the taxonomist's work. We will perform age determinations on the basis of micro-increments in the shell structure which can yield a picture of the settlement history of the respective vents. The wide distribution of this genus can be explained by its planktotrophic and widely dispersing larvae and its ecological flexibility: A bacteria-symbiotic specialist, the mussel can also switch (for a while?) to filter feeding sustaining itself on bacterial flocks suspended in the inhaled water current.

At the vertical walls of hot smokers, *Bathymodiolus* is represented at selected sites in smaller patches only. At the Wideawake mussel sites, usually somewhat apart from the mussel thickets, one could occasionally find a rarity in the Atlantic, the white clam *Calyptogena* sp. Only one specimen could be retrieved at M68/1, and will be studied ultrastructurally and genetically. In contrast to the Pacific vents, Calyptogena from the MAR lacks detailed description and investigation.

The notorious commensal of these mussels, the polychaete *Branchipolynoe* sp. (Fig. 1.70) was to be found in the northern fields in almost each specimen, while the southern mussel populations were only little infested. Also here, the species affiliation needs to be identified.

Fig. 1.70: Commensalic polychaete *Branchipolynoe*, living in *Bathymodiolus* sp., length 1.5 cm.

In order to efficiently evaluate the fauna in the mussel thickets, the sample has been washed out and the remainder sieved. By far most frequent were the molluscs: small gastropods (probably *Lirapex*) dominated in the southern fields, several kinds of limpets (Lepetodrilids and Fissurellids) at the northern sites. The limpets preferably attach themselves to the shells of live mussels. These molluscs are typical grazers feeding on the bacterial films on all substrates around vents. In the richly structured mussel beds they have an effective shelter against predators. All limpets are under identification by the Swedish specialist, the material probably contains some new species.

Predators are represented by various polychaete worm groups (Aphroditidae, see Fig. 1.71, Polynoidae, Phyllodocidae).

Other, more frequently occurring polychaetes belong to the feeding guild of deposit feeders/detritivores. A terebellid (cf. *Amathys*) is particularly frequent. It builds its small tubes of fine particles, often fluffy precipitates and debris, probing the sediment in its environment with its numerous head tentacles. The spionid polychaetes found have the same feeding strategy. In a community with abundant life, the consumers of dead or moribund animals have an important ecological role. Among the larger of these scavengers is the crab (cf. *Segonzacia*) which occurs frequently both in mussel fields and at hot smokers. Another conspicuous scavenger occurring in singular specimens among the mussels is the large conid snail *Phymorhynchus*. It is necrophagous, taking up freshly dead or moribund animals.

Fig. 1.71: Representative of the predacious polychaete family Aphroditidae.

Especially near the "hot spots" with outflows of shimmering water, some shrimps can be observed climbing over the surface of the mussels: *Rimicaris* exoculata (white shrimp, Fig. 1.72) and occasionally also a smaller, reddish caridid, cf. *Mirocaris fortunata* (Lilliput area). According to recent information from a specialist, this is not M. fortunate, perhaps a new species.

The nutritive basis of *Rimicaris* is disputed; the species probably combines bacterial food cultivated on especially formed mouth parts and inner carapace surfaces with bacterial films scraped off the surfaces in the environment using its mouth parts. *Mirocaris* is necrophagus, living on dead or moribund *Rimicaris*.

The bizarre looking and regularly occurring sea spider *Sericosura heteroscela* (Pantopoda, Pycnogonida, Ammotheidae, Fig. 1.73) has piercing and sucking mouth parts. Their food basis in mussel fields is not clear, probably small sea anemones, soft corals or hydroid colonies.

Frequent members of the meiofauna are the representatives of cyclopoid copepods of a reddish colour. Living on the surface of the thicket of byssus threads and mussel shells, they also make short excursion into the water, only to return immediately to their substrate. Cyclopoids are known to be micro-predators. Their food basis in the vent mussel community is unknown. Some suspension feeders can usually be found in direct vicinity of the mussel fields, filtering the flow of venting water: soft corals (gorgonians), hydrozoan colonies (e.g. *Candelabrum*), small actiniarians attach themselves preferably to exposed sites (top of lava blocks) where they filter the vent fluids rich in particle suspensions.

Comparable to blue mussel beds in shallow waters, the thickets of vent mussel shells and byssus threads are populated by a well definable community of invertebrates of various size and trophic groups. They differ in their food basis, at the vents the chemosynthetic free-living or symbiotic bacteria, in shallow waters the photosynthetically driven phytoplankton. As for their production, the deep-sea communities are comparable to their shallow-water counterparts (Giere et al., 2003), and, thus truly represent oases of life in the sparsely populated deep-sea.

Fig. 1.72: Typical shrimps (white: *Rimicaris exoculata*, red: *Mirocaris fortunata*) from the chimneys of black smokers (length of Rimicaris: 7 cm).

Fig. 1.73: A pantopod (Pycnogonida, Ammotheidae) from mussel beds, size: 1 cm.

The fauna at the Black Smoker sited at 5° S

The hydrothermal fauna in the vicinity or on the walls of black smokers is less clearly definable and more varying than that of the mussel beds at diffuse venting fields. Amazingly close to the vent outlets with their hot fluids aggregate rich populations of the key species, the white vent shrimp *Rimicaris exoculata* (see Fig.1.72). The often thick clumps of their bodies remind of a "swarming" behaviour in insects. In contrast, on the cooler surfaces the shrimps are regularly

dispersed, keeping a certain distance and actively moving their mouthparts in a sweeping mode over the rock surfaces. A relation to the activity of the smoker was indicated at the smoker "Shrimp Farm" whose flanges in 2005 were densely covered by huge populations of shrimps, while in 2006 this smoker was less active and the shrimp populations were much reduced, concentrated in small patches only. In contrast, at the neighbouring "Mephisto", a reversed process could be observed; it now had a white appearance due to its dense cover with shrimps. Whether this switch in the population centre is due to increased settlement of young recruits due to more attractive vent conditions, remains open since the settlement cues and the growth curves of these shrimps are as yet, undetermined.

The mussel *Bathymodiolus* sp. is regularly, but patchily, found attached to crevices and even vertical walls of the smokers. But the small size classes seem to be absent here. This species has its centre of occurrence certainly at the diffuse vent sites. On a smaller scale, the mussel thickets are populated by essentially the same community of small fauna as in the mussel beds. Among the numerous shrimps climb many crabs (*Segonzacia sp*) searching for suitable moribund animals. In the surroundings and at the base of the smokers there occur suspension feeders such as actiniarians or gorgonians. In the sheltered crevices of rocks, terebellid detritus feeders (cf. *Amathys*) extend their tentacles out of their small tubes. Occasional gastropods (cf. *Lirapex*) can also be encountered. Summarizing, the fauna at the hot smokers, although spectacular in their close contact to the hot effluents, has a lower diversity than that of the vent mussel fields and is clearly dominated by the white shrimps.

The fauna around the crater vent "Dragon's Throat, 8° S

The surroundings of the powerful smoker were devoid of the typical vent fauna except for numerous parchment-like, flexible tubes of chaetopterid polychaetes of unknown identity (Fig. 1.74) which were attached to the loose alterated rocks and sand of the crater walls. Some 15 specimens have been removed from their tubes and fixed for genetic and taxonomical studies. The absence of all vent-related macrofauna might reflect difficulties for larvae to settle on fairly loose sediment, but the complete absence of meiofauna in the voids of the sand points to other hostile environmental conditions, such as high concentrations of toxic heavy metals bound as sulfides (Fig. 1.75).

This report does not mention singular findings of isolated species. All the material has been adequately fixed and has been sent to the various taxonomic specialists in the museums.

In comparison, the M68/1 studies of fauna communities in the MAR hydrothermal fields south of the equator show essentially the same taxonomic composition and ecological structure as those in the north (Gebruk et al., 1997). Despite some taxonomic differences, this overall correspondence could not be anticipated considering the huge Romanche Fracture Zone which might have been a barrier restricting or at least filtering dispersal of vent animals. The data of M68/1 so far underline the conclusion drawn from the results of M64/1 that delineation of a separate zoogeographical province (see Van Dover et al., 2002) for the South Atlantic vent sites near the equator is not required.

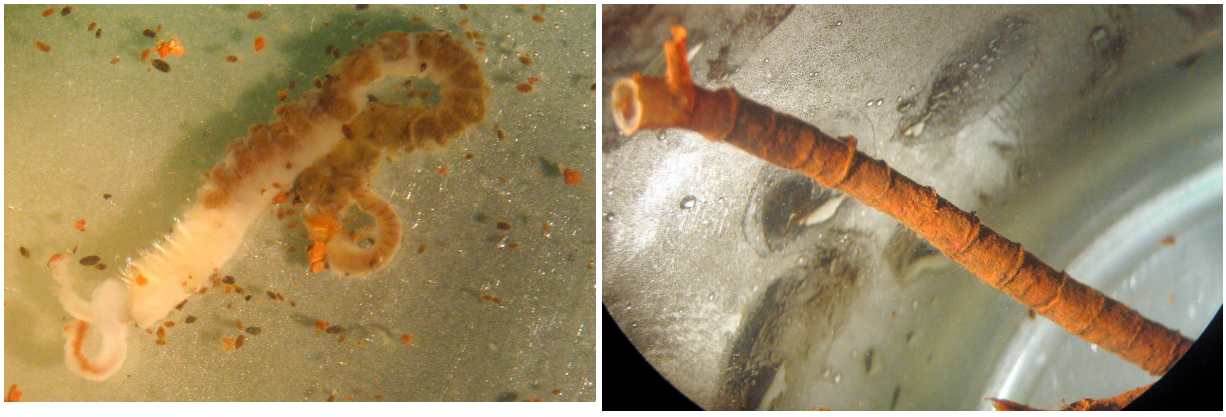

Fig. 1.74 a, b: A chaetopterid polychaete and its annulated tube from the crater walls of the smoker "Drachenschlund"

Fig. 1.75: A microscopic view of a sulfidic hydrothermal sand rich in heavy metals

1.5 Weather Conditions

METEOR left the port of Bridgetown in the forenoon of April 27. The weather situation was characterized by an easterly to northeasterly trade wind of Bft 4 to 5, a broken sky and short shower activity associated with head easterly swell up to 2.5 m.

On May 02 the northern limit of the Intertropical Convergence Zone (ITCZ) was met near 05° North 38° West with easterly to northeasterly winds of 5 to 6 Bft and shower squalls of Bft 7. The wind decreased not before May 05 and became easterly force 3 to 4.

On the following day, shortly before crossing the equator near 25° West, METEOR left the ITCZ. The number and intensity of clouds got less, the wind veered easterly to southeasterly and decreased to 2 to 3 Bft.

The cruise to the first area of investigation near 04,8°S 12,3°West, arriving there on May 09 in the evening, was affected by southeasterly trade winds caused by a Southatlantic high between 40° and 45° South.

METEOR remained in the region of southesterly trade winds during the whole time of research. The range of wind speed was 2 to 4 Bft with a sea of 1.5m and mostly scattered

clouds. This situation continued from May 17 in the second area of investigation near 09,5°South 13,5° West.

The third area was situated more northwesterly near 08,3° South 13,5° West.

This point was reached on May 20. One day later in the evening an intensive shower activity began with easterly gusts up to Bft 7.

Since the ridge of the subtropical high expanded northerly the wind from east to southeast increased to Bft 5 or 6, with gusts up to 7. The height of the sea and swell increased to 2,5 and 3 m, in some cases of converging swell more than 3m. On May 05 the wind and sea decreased slowly. The wind became southeasterly of 4 to 5 Bft.

The scientific investigations ended on May 28 at noon and METEOR headed for Recife, sailing south of Ascenion.

During this transit, the southeasterly trade wind came with a force of about 4 Bft, accompanied by sea and swell of about 2m. The cloud conditions were mostly broken. The voyage ended in the morning of June 02 in the container harbour of Suape, south of Recife.

1.6 Acknowledgments

We would like to thank Captain Kull and his crew on R/V Meteor for their professionalism and excellent cooperation during cruise M68/1, which was a major contribution to the success of the expedition.

Furthermore, we acknowledge the professional patronage of the German Ministry of Foreign Affairs as well as of Captain Berkenheger at the "Leitstelle Meteor".

We wish to thank the German Science Foundation (DFG) for funding the cruise and the subsequent scientific work in the framework of the priority program SPP 1144 “From Mantle to Ocean: Energy-, Material-, and Life Cycles at Spreading Axes”.

1.7 References

Bebianno, M.J. et al., 2005. Antioxidant systems and lipid peroxidation in Bathymodiolus azoricus from Mid-Atlantic Ridge hydrothermal vent fields. Aquatic Toxicology, 75(4): 354.

Bischoff, J.L. and Rosenbauer, R.J., 1988. Liquid-vapor relations in the critical region of the system NaCl-H2O from 380 to 414°C: A refined determination of the critical point and two-phase boundary of seawater. Geochimica et Cosmochimica Acta, 52: 2121-2126.

Company, R. et al., 2004. Effect of cadmium, copper and mercury on antioxidant enzyme activities and lipid peroxidation in the gills of the hydrothermal vent mussel Bathymodiolus azoricus. Marine Environmental Research, 58(2-5): 377.

Cosson, R. and Vivier, J.-P., 1997. Interactions of metallic elements and organisms within hydrothermal vents. Cah. Biol. Mar., 38: 43-50.

Croot, P.L., Laan, P., 2002. Continuous shipboard determination of Fe(II) in polar waters using flow injection analysis with chemiluminescence detection. Analytica Chimica Acta 466: 261–273.

Devey, C.W., Lackschewitz, K.S., and E. Baker, 2005. Hydrothermal and volcanic activity found on the southern Mid-Atlantic Ridge. EOS 86, 209 and 212.

Dupont, C.L., Nelson, R.K., Bashir, S., Moffett, J.W. and Ahner, B.A., 2004. Novel copper-binding and nitrogen-rich thiols produced and exuded by Emiliania huxleyi. Limnol Oceanography, 49(5): 1754-1762.

Edgcomb, V.P. et al., 2004. Sulfide Ameliorates Metal Toxisity for Deep-Sea Hydrothermal vent Archea. Applied and Environmental Michrobiology(April): 2551-2555.

Garbe-Schönberg D, Koschinsky A, Ratmeyer V, Jähmlich H, and Westernströer U (2006) KIPS – A new Multiport Valve-based all-Teflon Fluid Sampling System for ROVs. *EGU General Assembly, Vienna, April 2006*

Gerringa, L.J.A., Herman, P.M.J. and Poortvliet, T.C.W., 1995. Comparison of the linear Van den Berg/Ruzic transformation and a non-linear fit of the Langmuir isotherm applied to Cu speciation data in the estuarine environment. Marine Chemistry, 48: 131-142.

Gebruk, A.V., Galkin, S.V., Vereshchaka, A.L., Moskalev, L.I. and Southward, A.J. (1997): Ecology and biogeography of the hydrothermal vent fauna of the Mid-Atlantic Ridge.

Adv. Mar. Biol., 32: 93-144.

Giere, O., Borowski, C. and Prieur, D. (2003): Biological Productivity in Hydrothermal Systems. In: Energy and Mass Transfer in Marine Hydrothermal Systems (P.E. Halbach, V. Tunnicliffe & J.R. Hein, eds.), Dahlem Workshop, Berlin, October 14-19, 2001, Dahlem Univ. Press, Berlin, 211-233.

Grasshoff, K., Ehrhardt, M. and Kremling, K., 1983. Methods of Seawater Analysis. Verlag Chemie, Weinheim.

Luther III, G.W. et al., 2001. Chemical speciation drives hydrothermal vent ecology. Nature (London), 410(12 April): 813-816.

Moffett, J.W. and Brand, L., 1996. Production of strong, extracellular Cu chelators by marine cyanobacteria in response to Cu stress. Limnology and Oceanography, 41: 388-395.

Rüth, C., Well, R., Roether, W., (2000). Primordial 3He in South Atlantic deep waters from sources on the Mid-Atlantic Ridge. Deep-Sea Research I 47, 1059–1075.

Sander, S., Kim, J.P., Anderson, B. and Hunter, K.A., 2004. Effect of UVB irradiation on Cu2+-binding organic ligands and Cu2+ speciation in alpine lake waters of New Zealand. Environmental Chemistry, submitted.

Sander, S. G., Koschinsky, A., Massoth, G., Stott, M and Hunter, K. A., 2006. Organic complexation of copper in deep-sea hydrothermal vent systems. Geophysical Research Letters, in press.

Sültenfuß, J, Roether W., Rhein M., (2006), The Bremen Mass Spectrometric Facility for the Measurement of Helium Isotopes, Neon, and Tritium in Water, International Symposium on Quality Assurance for Analytical Methods in Isotope Hydrology, IAEA CN 119/7, in press

Van den Berg, C.M.G., 1995. Evidence for organic complexation of iron in seawater. Marine Chemistry, 50: 139-157.

Van Dover, C.L., German, C.R., Speer, K.G. & Parson, L.M. (2002): Evolution and biogeography of deep-sea vent and seep invertebrates. Science, 295: 1253-1257.

Van Dover, C.L. (2000): *The ecology of hydrothermal vents.* Princeton University Press, Princeton New Jersey.